AD-A138 900 NUMERICAL AERODYNAMIC ANALYSIS OF A FREE FALLING AUTOROTATING PLATE(U) AIR FORCE INST OF TECH WRIGHT-PATTERSON AFB OH SCHOOL OF ENGINEERING 1/2

UNCLASSIFIED C R GALLAWAY OCT 83 AFIT/DS/AA/83-2 F/G 1/2 NL

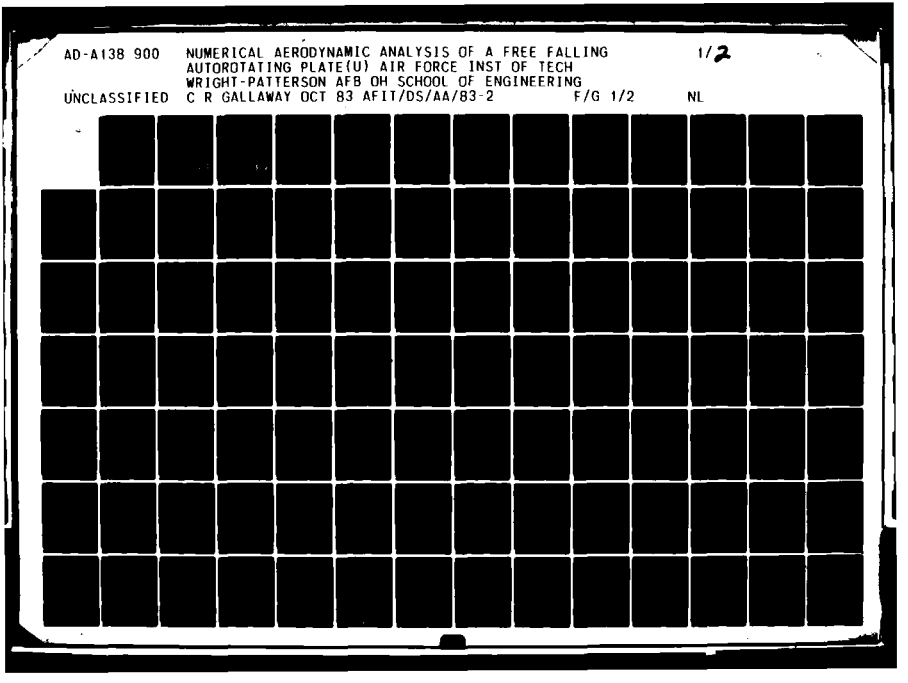

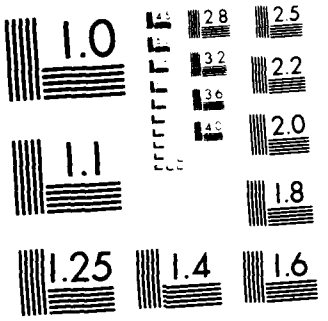

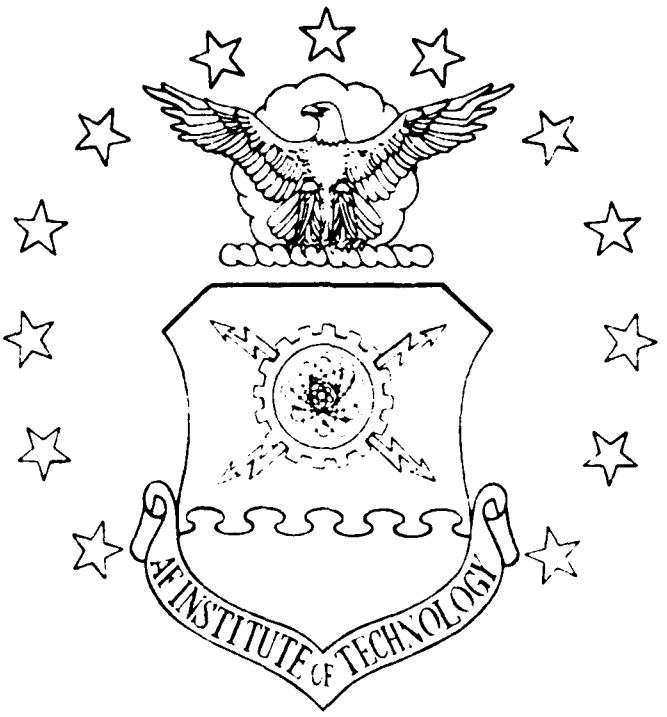

AD A138900

NUMERICAL AERODYNAMIC ANALYSIS OF A FREE FALLING AUTOROTATING PLATE

DISSERTATION

AFIT/DS/AA/83-2

Charles R. Gallaway

DEPARTMENT OF THE AIR FORCE
AIR UNIVERSITY (ATC)
AIR FORCE INSTITUTE OF TECHNOLOGY

Wright-Patterson Air Force Base, Ohio

AFIT/DS/AA/83-2

NUMERICAL AERODYNAMIC ANALYSIS OF A FREE FALLING AUTOROTATING PLATE

DISSERTATION

AFIT/DS/AA/83-2 Charles R. Gallaway

Approved for public release; distribution unlimited

AFIT/DS/AA/83-2

NUMERICAL AERODYNAMIC ANALYSIS OF A FREE FALLING AUTOROTATING PLATE

DISSERTATION

Presented to the Faculty of the School of Engineering
of the Air Force Institute of Technology
Air University
in Partial Fulfillment of the
Requirements for the Degree of
Doctor of Philosophy

by

Charles R. Gallaway, B.S., M.S.

AFIT/DS/AA/83-2

NUMERICAL AERODYNAMIC ANALYSIS OF A FREE FALLING AUTOROTATING PLATE

by

Charles R. Gallaway, B.S., M.S.

Approved:

B. E. Franke — 1 Nov 1983
Chairman

John Jones Jr — 1 Nov 1983

Michael Smith — 1 Nov 1983

Willy Hankey — 2 Nov 1983

James H. Holt — 2 Nov 1983

Accepted:

J. S. Przemieniecki — 3 Nov 1983
Dean, School of Engineering

ACKNOWLEDGEMENTS

I would like to thank the members of my committee from AFIT, Dr. Milton Franke, my committee chairman; LTC Michael Smith; and Dr. John Jones Jr. for their assistance and guidance throughout my AFIT studies. I am thankful to Capt James Hodge for his assistance and for acting as the Dean's representative to my committee.

I would like to express my most sincere appreciation to Dr. Wilbur L. Hankey, Jr., adjunct AFIT professor and Technical Manager of the Computational Aerodynamics Group, for conceiving the idea for this study and guiding me through this research. I would like to thank the other members of the Computational Aerodynamics Group for their support.

I am grateful to the management of the Foreign Technology Division, particularly Mr. James Bartley, for allowing me the opportunity to pursue this degree under the Long Term Full Time Training program. I would like to extend a word of thanks to Lt. William Shelton Jr. for proof reading the final document.

Finally, but certainly not least, I am very thankful to my wife, Deborah, for providing encouragement and unwavering moral support throughout this endeavor. In addition I would like to thank her for her assistance in preparing the final document.

CONTENTS

LIST OF FIGURES

LIST OF TABLES

NOTATION

SYMBOL	
ACOEF	Adam-Bashforth coefficients
c	Chord of the plate
C_c	Constant for variable time step
C_D	Drag coefficient
C_x	Exponential stretching coefficient in x direction
C_y	Exponential stretching coefficient in y direction
D	Aerodynamic drag
D'	Flow field dilatation or divergence
e	Base of natural logarithm
F_{xp}	Pressure force in x direction
F_{xv}	Viscous force in x direction
F_{yp}	Pressure force in y direction
Fyv	Viscous force in y direction
g	Gravitational constant
i	Counter
$\underline{i}$	Unit vector in the x coordinate direction
$\underline{i}'$	Unit vector in the x' coordinate direction
I_y	Mass moment of inertia
IMAX	Numerical designator for the maximum number of ξ lines
j	Counter
$\underline{j}$	Unit vector in the y coordinate direction
$\underline{j}'$	Unit vector in the y' coordinate direction
J	Jacobian of the grid transformation
JMAX	Numerical designator for the maximum number of η lines

L	Aerodynamic lift
L_x	Nondimensional distance to outer boundary in x direction
L_y	Nondimensional distance to outer boundary in y direction
M	Aerodynamic moment about center of gravity
m	Mass
n	Summation index or designates the nth time step
p	Static pressure variable
p^*	Current value of the fluid static pressure obtained from the finite difference equation
$\hat{p}$	Nondimensional static pressure, $p-p_\infty/U_\infty^2$
q	Rotational velocity
Re	Freestream Reynolds number, $\rho U_\infty c/\mu$
t	Time variable
$\hat{t}$	Nondimensional time, tU_∞/c
t'	Nondimensional time in rotating axis system
u	Variable which denotes the local x component of flow field velocity
u_b	Boundary condition velocity on the body in the x direction
u_n	Velocity derivative normal to the surface
u^*	Current value of the u component of velocity obtained from the finite difference equation
$\tilde{u}$	Contravariant velocity in x' direction
$\hat{u}$	Variable which denotes the nondimensional local x component of flow field velocity
U_∞	Magnitude of the freestream velocity
V_{cg}	Velocity of center of gravity of plate
v	Variable which denotes the local y component of the flow field velocity

v_b	Boundary condition velocity on the body in the y direction
v^*	Current value of the v velocity component obtained from the finite difference equation
$\bar{v}$	Contravariant velocity in y' direction
$\hat{v}$	Variable which denotes the local nondimensional y component of flow field velocity
W	Weight of plate
x	Coordinate in the physical plane
x'	Coordinate in the rotated physical plane
x_{min}	Minimum grid spacing in x direction
x_o	Location of origin of rotating axis system in inertial plane
$\hat{x}$	Nondimensional coordinate
y	Coordinate in the physical plane
y'	Coordinate in the rotated physical plane
y_{min}	Minimum grid spacing in y direction which is also the thickness of the plate
y_o	Location of origin of rotating axis system in inertial plane
$\hat{y}$	Nondimensional coordinate
α	Geometric angle of attack
α'	Grid transformation coefficient $x_\eta^2 + y_\eta^2$
β'	Grid transformation coefficient $x_\xi x_\eta + y_\xi y_\eta$
γ	Glide path angle
γ'	Grid transformation coefficient $x_\xi^2 + y_\xi^2$
η	Coordinate in the computational plane
Ω	Angular velocity
θ	Rotation angle
$\dot{\theta}$	Nondimensional rate of rotation

$\ddot{\theta}$	Nondimensional rotational acceleration
μ	Dynamic viscosity coefficient
ν	Kinematic viscosity μ/ρ
ξ	Coordinate in the computational plane
ρ	Fluid density
σ	Grid transformation coefficient
τ	Grid transformation coefficient
τ'	Shear stress
Φ	Acceleration paramenter for pressure iteration defined as $2\ \omega_{pb} J^2 / ((\alpha'+\gamma')\ t)$
Ψ	Inviscid stream function
ω	Local acceleration parameter
ω_p	Acceleration parameter for the field pressure finite difference equations
ω_{pb}	Acceleration parameter for the surface pressure iteration
ω_{uv}	Acceleration parameter for the u and v velocity component finite difference equations

Subscript

b	Denotes a location on the body surface
i	Denotes the ξ coordinate location in the computational plane for finite difference equations
j	Denotes the η coordinate location in the computational plane for finite difference equations
max	Denotes the maximum values of a variable
min	Denotes the minimum values of a variable
o	Denotes initial condition

t	Denotes differentiation with respect to time
x,xx	Denote differentiation with respect to x
$x',x'x'$	Denote differentiation with respect to x'
y,yy	Denote differentiation with respect to y
$y',y'y'$	Denote differentiation with respect to y'
$\eta,\eta\eta$	Denote differentiation with respect to η
$\xi,\xi\xi$	Denote differentiation with respect to ξ
$\underline{\ }$	Denotes a vector quantity

Superscript

$*$	Denotes a quantity in the transformed plane
$\hat{}$	Denotes a temporary nondimensional variable
s	Iteration number in the successive-over-relaxation iteration procedure
η	Pertaining to η contours
ξ	Pertaining to ξ contours
$\tilde{}$	Denotes a transformed nondimensional variable
$\cdot$	Denotes differentiation with respect to time

Prefix

d	Derivative operator
D	Substantial derivative operator ($D/Dt = \partial(\cdot)/\partial t + \underline{v} \cdot \nabla(\cdot)$)
Δ	Increment
Σ	Summation

ABSTRACT

A computational method coupling the three degrees of freedom flight mechanics equations and the two dimensional Navier-Stokes equations was developed which could be used to predict the flight path of a free falling, autorotating, two dimensional flat plate. The two dimensional incompressible Navier-Stokes equations were cast in a body fixed coordinate system. The corresponding velocities were cast in an inertial reference system. The equations were represented by backward-time-central-space finite differences and solved using a successive-over-relaxation iteration technique. The resulting aerodynamic coefficients were entered into the three degrees of freedom flight mechanics equations. The system of ordinary differential equations was solved using an Adams open formula to predict the movement of the plate. New boundary conditions for the Navier-Stokes equations solver were derived from the movement of the plate. The process was repeated to advance the solution in time.

The computational method was used to calculate the flow field around a flat plate forced to rotate at nondimensional angular velocities of 1.0, 2.0, and 4.0. A calculation was performed for a plate with one degree of freedom (rotation) which simulated a plate mounted on a frictionless bearing in a wind tunnel. The plate was found to undergo pinned autorotation at a mean nondimensional rotational velocity of 1.58. Finally, the flight path of a free falling autorotating plate was predicted using the computational procedure. The validity of the overall approach was demonstrated by comparison with experiment.

SECTION I

INTRODUCTION

The USAF has lost hundreds of millions of dollars worth of aircraft to accidents which were attributed to aircraft departure during stall which resulted in a spin (Ref 1). Examination of the accident statistics for a large number of NATO combat aircraft showed that approximately 20 percent of the aircraft losses in combat training were caused by stall departure and spinning accidents (Ref 2). Many of the accidents may have been prevented if the spin characteristics of the aircraft had been better understood. However, predicting the characteristics of a spinning aircraft is very involved. Conventional wind tunnel testing of aircraft models does not accurately simulate spin. Experience has indicated aircraft spin can be investigated safely and at a comparatively moderate cost by testing small dynamic models in a vertical wind tunnel (Ref 3). However, because of the many variables in a spin, interpretation of the results for application to a corresponding airplane is difficult and may only show general trends. Ultimately, it is necessary to turn to full scale flight testing which is extremely expensive. One is inclined to turn to numerical techniques to analyze aircraft spin because the per unit computing costs are decreasing rather than increasing. Unfortunately, the numerical aerodynamic analysis of an aircraft during spin is extremely complex.

The flight condition of a "spinning" aircraft was defined by Bairstow (Ref 4) as a steady spiral descent with the mean angle of attack of the wing greater than stalling. This latter element infers

there is unsteady, separated flow about the aircraft which makes it difficult to mathematically predict the spin characteristics of the aircraft. Quasi-steady techniques developed to predict aircraft spin are incapable of correctly defining the true dynamics of the flow field (Ref 5). Only solutions of the Navier-Stokes equations can accurately predict unsteady, separated flow fields.

To mathematically investigate aircraft spin, a six degrees of freedom trajectory program should be combined with a three dimensional Navier-Stokes program. The large computer memory requirements and long run times make this task impractical on today's computers (Ref 6). While one awaits larger computers to precisely calculate aircraft spin, one can search for a simpler problem which can be accurately solved on present computers. Developing and demonstrating a procedure to solve a simpler problem which incorporates the essential elements of a spinning aircraft will be a step towards solving the complete aircraft spin problem.

The free falling, autorotating, flat plate incorporates the essential elements (unsteady aerodynamics, flight mechanics, and autorotation) of a spinning aircraft. When a rectangular piece of paper (e.g. a computer card) is dropped, it falls obliquely as shown in Figure 1a and not vertically as might be expected. The flow field around the free falling flat plate is unsteady and separated. Based on experimental observations, the autorotating flat plate can be modeled in two dimensions (Ref 7). The author feels the flight path of a free falling, autorotating, flat plate can be numerically predicted using

present computers.

The purpose of this research was to develop and apply a method for solving the three degrees of freedom flight mechanics equations. These equations could be used to predict the flight path of a free falling, autorotating, two dimensional object. The three degrees of freedom are vertical translation, horizontal translation, and rotation. The unsteady, nonlinear aerodynamic forcing functions (lift, drag, and moment) in the flight mechanics equations were simulaneously calculated by solving the two dimensional incompressible Navier-Stokes equations. Past attempts failed to predict the flight path of a free falling, autorotating, flat plate because the aerodynamic forces were linearized and assumed to be quasi-steady (Ref 7). The method of solution was validated by predicting the flight path of a free falling flat plate and comparing it to experimental data. To the author's knowledge, this was the first attempt to use an unsteady, nonlinear aerodynamic prediction method to calculate the aerodynamic forces included in the three degrees of freedom flight mechanics equations. This research will assist in the future analysis of the complete aircraft spin problem.

SECTION II

BACKGROUND

This section briefly outlines the history of the phenomenon of the free falling, autorotating, flat plate. The phenomenon was first described in the middle of the last century, but early investigators were unable to explain the autorotating plate for two primary reasons. First, detailed experimental data, being difficult to obtain, were not available. Secondly, scientists attempted to calculate the flow field around the flat plate using linear, quasi-steady techniques. This led to erroneous conclusions because the autorotating phenomenon was caused by the neglected unsteady, nonlinear effects. Fortunately, in the past few years, detailed experimental data and accurate nonlinear, unsteady aerodynamic prediction techniques have aided in satisfactorily explaining autorotation of free falling flat plates.

Maxwell (Ref 8), in a brief theoretical study written in 1854, was probably the first person to attempt to describe the phenomenon of an autorotating rectangular plate falling through the air. Maxwell's explanation of autorotation, although inaccurate, is summarized with the aid of Figure 1a. At position 1, the plate is parallel to the flight path which corresponds to the least drag. The plate has its maximum drag at postion 3 because it is normal to the flight path. The plate therefore has a higher velocity at position 2 than at position 4. Since a plate always tends to place itself normal to the flight path, the torque at position 2 is in the direction of rotation and the torque at postion 4 is opposite to the direction of rotation. Hence, the torque

at postion 2 which supports rotation is larger than the adverse torque at postion 4 which resists rotation. Even though Maxwell's explanation of the phenomenon was inaccurate, several French and German papers written between 1880 and 1900 essentially restated it (Ref 7). They assumed the total torque could be divided into a quasi-steady part which always acted in the direction of rotation and a quasi-steady part which always acted opposite to the direction of rotation.

It was not until around 1905 that Rianbouchinskiy realized Maxwell's quasi-steady theory would not account for a flat plate autorotating about a fixed axis (Ref 7). This may have suggested to him Maxwell's theory was not valid for the free falling plate either. He recognized Maxwell's assumption that, in position 1, the movement of the flat plate was faster than it was in position 3, which was not valid for a flat plate autorotating about a fixed axis. Riabouchinskiy (Ref 9) explained, that in position 1, the streamlines at the retreating edge of the plate are more curved than in position 3, thus, due to the higher suction effect, the torque favorable to rotation was greater. It was not until several years later that he realized the moment of inertia must be large enough to overcome the period of adverse torque (Ref 7).

In 1941, Dupleich (Ref 10) published the first experimentally obtained trajectories of free falling plates in air and water. Dupleich's explanation of autorotation was adopted from Maxwell and depended on the incorrect idea that the influence of rotation on the total torque was always opposite to the direction of rotation.

A.M.O. Smith (Ref 11) in 1953 published the first accurate explanation of the free falling flat plate. He realized the asymmetry due to rotation was the key to explaining the autorotation and this asymmetry was caused by hysteresis during acceleration. Smith explained that at position 2, as shown in Figure 1b, the plate was at a large angle of attack, producing a force R. This force R causes a nose up moment which tended to increase the angle of attack. Rotation was rapid; consequently the boundary layer was thinner than it would have been for the steady state condition and the stall was delayed to high values of lift coefficient. At position 3, the plate was probably completely stalled. At position 4, it continued to be stalled. However, between positions 4 and 5, attached flow over the trailing edge was established. Reattachment was delayed to angles below the static stall angle because the thick wake was a retarding influence. Hence the downward lift impulse was less than the upward lift impulse. The clockwise rotation impulse, and the inertia of the plate, carried it past the region of retarding impulse. The motion from 5 to 9 was essentially a repetition of that from 1 to 5.

In the late 1960's Bustamante and Stone (Ref 12) experimentally investigated autorotation of flat plates at subsonic and hypersonic speeds. They found, although not conclusively, that plates could autorotate in hypersonic flow. They suggested that autorotation of wings with a symmetric cross section is due to a large vortex shed from the retreating face of the wing. Iversen (Ref 13) was able to show the same result theoretically in 1969.

In 1970, E.H. Smith (Ref 14) published the first detailed experimental data on the lift, drag, moment, angular acceleration, and angular velocity as a function of time for a flat plate autorotating about a fixed axis in a wind tunnel. Smith studied the corresponding flow patterns using smoke and tufts. He also experimentally investigated free falling wings. He found, for Reynolds numbers above 4000, the average lift and drag coefficients were comparable to those observed in the fixed axis tests.

In 1974, Kry and List (Ref 15) experimentally determined the range of autorotation in which a quasi-steady technique could be applied to rotating oblate spheroids. They found, if the Reynolds number was less than 150,000, the moment predicted for the oblate spheroid was valid for rotation rates about the major axis equivalent to Strouhal numbers less than 0.04. Under their conditions, the moment acting on an oblate spheroid in a steady flow differed by less than 10% from the moment acting on a free spheroid with the same instantaneous orientation. List actually computed rates of autorotation by means of the quasi-steady approach.

In 1978, Lugt (Ref 7) numerically predicted the autorotation of a thin elliptic cylinder rotating about a fixed axis. Lugt transformed the elliptic cylinder from the physical plane to a computational plane where he solved the Navier-Stokes equations. The equations which were valid for laminar, incompressible, two dimensional flow were formulated in terms of vorticity and the stream function. The initial conditions consisted of the potential flow solution and a vorticity sheet

distributed along the surface of the cylinder to model a no slip condition. Lugt significantly reduced the computer time necessary to arrive at a solution by assuming the cylinder autorotated at a constant angular velocity. He predicted the autorotation of the elliptic cylinder and showed autorotation was caused by a complicated interplay of vortex shedding, boundary layer hysteresis, and vorticity generation around the edges. Autorotation and the aerodynamic forces on the ellipse predicted by Lugt correlated very well with the high Reynolds number and three dimensional experimental data obtained by E.H. Smith (Ref 14).

Researchers attempted to explain the free falling, autorotating, flat plate as early as 1854. It was not until 1953 that A.M.O. Smith was able to explain the phenomenon. To the author's knowledge, no one has been able to accurately predict the flight path of a free falling, autorotating, flat plate. In this study a computational method was developed which coupled the three degrees of freedom flight mechanics equations with the two dimensional Navier-Stokes equations. This numerical method was used to predict the flight path of a free falling, autorotating, flat plate.

SECTION III

NAVIER-STOKES EQUATIONS SOLVER

A numerical two dimensional incompressible Navier-Stokes equations solver was developed to calculate the aerodynamic characteristics of a flat plate. The flow field was modeled by a finite number of points. The finite difference representation of the Navier-Stokes equations was solved at each of these points to obtain an x velocity component, a y velocity component, and a static pressure. The aerodynamic characteristics of the plate were obtained by integrating the forces around the plate.

A. Grid Description

The aerodynamic forces acting on the plate were obtained by solving the Navier-Stokes equations using a finite difference technique. This required the flow field to be modeled by discrete points. An incompressible flow field should have an infinite outer boundary because each point in the flow field influences every other point in the flow field. An infinite outer boundary is not feasible nor is it necessary in numerical modeling of a flow field. Previous researchers (Refs 16 and 17) found placing the outer boundary 10 chords away from the body closely approximated an infinite boundary. Therefore the outer boundary was placed at 10 chords throughout this study.

The Navier-Stokes equations were solved over a rectangular physical domain in this study. The domain was modeled by IMAX points distributed horizontally in the x direction and JMAX points distributed vertically

in the y direction. The grid points in the physical plane were clustered near the plate where large velocity and pressure gradients were anticipated. The grid point clustering was arranged so it did not favor any particular flow direction because the freestream velocity could originate from any direction. In addition, the points were distributed so they could be transformed into a computational domain with uniform grid spacing in both directions.

Many investigators used wrap around grid systems when solving the Navier-Stokes equations over airfoils. A wrap around grid system (O-Grid) was not used in this study because it could present numerical difficulties at sharp edges. Hodge (Ref 16) found the large leading edge radius on an airfoil did not present any difficulty whereas the sharp trailing edge was a constant source of numerical difficulty. Similar difficulties were anticipated on the edges of the flat plate investigated in this study.

Hodge (Ref 18) found an exponentially stretched grid inferior to an optimized grid in solving the flow field around an airfoil. The optimized grid minimized the truncation error assuming steady Blasius profiles. In addition, Hodge also found the maximum grid spacing near the outer boundary necessary to obtain acceptable accuracy was approximately one chord. However, combining an exponentially stretched grid with a very small spacing near the plate, and a maximum grid spacing of approximately one chord on the outer boundary required many grid points.

A stretched Cartesian coordinate system was selected as a compromise. It avoided the numerical difficulties of a wrap around grid system. It was unnecessary to accurately resolve the boundary layer on the plate during this study because the pressure forces produced by the large eddy structure were expected to dominate the problem (Ref 19). Therefore it was decided to distribute the grid points to more accurately resolve the large eddy structure. An adaptive grid is another approach to optimizing the grid, however, that is beyond the scope of this study.

The Cartesian grid simplified the transformation metrics because each variable in the computational domain was a function of only one variable in the physical plane as seen in equations (1) and (2).

$$x = x(\xi) \tag{1}$$

$$y = y(\eta) \tag{2}$$

The grid was generated with analytic functions. This presented the option of calculating the transformation metrics with numerical or analytical derivatives. Both types of derivatives were investigated and are discussed in Section VI.

The thickness of the plate was used to determine the minimum grid spacing in the y direction. It would have been computationally prohibitive to accurately model this mimimum thickness. The minimum grid spacing was selected to produce a grid with an outer spacing of approximately one chord and a total number of points which permitted the

problem to be solved on a CYBER 750 computer. The actual thickness of the plate was not felt to be a key feature of autorotation.

A patched exponential stretching scheme of the following form was used to smoothly distribute the grid points in the physical plane

$$y = L_y \frac{(e^{C_y \eta_j} - 1)}{(e^{C_y} - 1)} \quad \text{for } j = 1, JMAX/2 \tag{3}$$

where C_y is the stretching coefficient in the y direction (Ref 20). The remaining variables are illustrated in Figure 2.

Equation (3) was rearranged to give an implicit equation for the stretching coefficient.

$$C_y = \frac{1}{\Delta\eta} \ln\left(1 + \frac{y_{min}}{L_y}(e^{C_y} - 1)\right) \tag{4}$$

Equation (4) was iteratively solved to determine the stretching coefficient in the y direction. An algorithm which combined a linear interpolation, an inverse quadratic interpolation, and a bisection was used to accelerate the iterative scheme (Ref 21). The minimum grid spacing used in equation (4) was the thickness of the plate.

A similar minimum grid spacing was used along the complete length of the plate in the x direction. The respective forms of equations (3) and (4) were solved to obtain the stretching coefficient in the x direction. This coefficient was used to exponentially stretch the grid from the minimum grid spacing at the ends of the plate to approximately one chord at the outer boundary. The finite difference grid in the

physical plane is shown in Figure 3 while an expanded view in Figure 4 shows the grid near the plate. The corresponding computational domain is shown in Figure 5.

B. Equations of Motion

The Navier-Stokes equations could have been formulated in several reference systems. The reference system was selected to simplify the overall approach to the problem. Two reference systems looked appealing for application to this problem. The first was a rotating reference system attached to the plate. The second formulation used a mixed reference system based on an inertial system.

The flow field was calculated using the two dimensional time dependent incompressible Navier-Stokes equations in primitive variables (Refs 22 and 23). The problem was formulated in a body fixed coordinate system which has proven to be a powerful tool in applying numerical methods to practical boundary value problems involving partial differential equations (Ref 6). The surface of the plate was represented as coordinate lines which reduced the difficulties associated with numerically specifying boundary conditions in finite difference methods. Formulating the mathematical problem in a coordinate system fixed to a body undergoing time dependent motion conveniently eliminated the time dependent grid transformation terms.

The velocities used in the Navier-Stokes equations can be cast in several reference systems (Ref 24). In most formulations the velocities are cast in the rotating system which means the velocities appear as if

one is moving with the body (Ref 25). Hegna (Ref 26) used this approach in his pitching airfoil problem. Alternately, the velocities can be cast in an inertial reference system while the coordinates are in the rotating system. This formulation is called a "mixed" system in this study.

The two velocity formulations were equally appealing at the beginning of this study. A rotating reference system fixed to the plate was found to be unsatisfactory because the solution diverged at fast rotation rates as outlined in Appendix A. The other classical reference system is a purely inertial system in which the plate moves within the computational domain. The inertial system presents several difficulties. First, the boundary conditions imposed on the plate no longer coincide with the location of grid points. This increases the required computing time and decreases the accuracy because the boundary conditions must be interpolated. Second, the grid points are no longer properly clustered to resolve the large velocity gradients near the plate. Finally, with enough time, the plate will exit the computational domain.

The Navier-Stokes equations were formulated in a "mixed" system. The spatial coordinates were formulated in a reference system attached to the plate (Ref 27). The "mixed" system retained the advantage of the body fixed system of calculating the grid only one time and having it properly stretched throughout the calculation. The flow velocities were calculated in an inertial system to avoid the large velocities introduced by the body fixed system. There was no flow near the outer

boundary in the "mixed" system. The velocities used in the "mixed" system, called contravariant velocities (Ref 28), were the components of the inertial velocities in the direction of the coordinate reference system fixed to the plate. This system avoided the difficulty of the plate exiting the computational domain usually encountered in an inertial reference system.

The time dependent, two dimensional, incompressible Navier-Stokes equations cast in primitive variables in an inertial reference system are given by (Ref 29):

$$u_t + uu_x + vu_y = -\frac{p_x}{\rho} + \nu(u_{xx} + u_{yy}) \tag{5}$$

$$v_t + uv_x + vv_y = -\frac{p_y}{\rho} + \nu(v_{xx} + v_{yy}) \tag{6}$$

$$u_x + v_y = 0 \tag{7}$$

The body gravity forces were neglected even though the aerodynamic forces involved in this problem were very small. The classical arguments for neglecting the body gravity forces were still valid (Ref 30). The changes in pressure acting on the plate caused by differences in height were insignificant compared to the other forces acting in the problem.

The following nondimensional variables are introduced:

$$\hat{x} = \frac{x}{c} \tag{8}$$

$$\hat{y} = \frac{y}{c} \tag{9}$$

$$\hat{u} = \frac{u}{U_\infty} \tag{10}$$

$$\hat{v} = \frac{v}{U_\infty} \tag{11}$$

$$\hat{p} = \frac{p-p_\infty}{\rho U_\infty^2} \tag{12}$$

$$\hat{t} = \frac{tU_\infty}{c} \tag{13}$$

The nondimensional variables were substituted into equations (5) through (7) resulting in the following set of equations:

$$u_t + uu_x + vu_y = -p_x + \frac{1}{Re}(u_{xx} + u_{yy}) \tag{14}$$

$$v_t + uv_x + vv_y = -p_y + \frac{1}{Re}(v_{xx} + v_{yy}) \tag{15}$$

$$u_x + v_y = 0 \tag{16}$$

The nondimensional symbols are understood and omitted for simplicity.

The equations are transformed from an inertial (unprimed) to a rotating coordinate system (primed) using the following transformations:

Transformed Coordinates

$$\underline{i} = \underline{i}' \cos \theta(t') - \underline{j}' \sin \theta(t') \tag{17}$$

$$\underline{j} = \underline{i}' \sin \theta(t') + \underline{j}' \cos \theta(t') \tag{18}$$

$$x = x_o(t') + x' \cos \theta(t') - y' \sin \theta(t') \tag{19}$$

$$y = y_o(t') + x' \sin \theta(t') + y' \cos \theta(t') \tag{20}$$

Inverse Transformed Coordinates

$$\underline{i}' = \underline{i} \cos \theta(t) + \underline{j} \sin \theta(t) \tag{21}$$

$$\underline{j}' = - \underline{i} \sin \theta(t) + \underline{j} \cos \theta(t) \tag{22}$$

$$x' = (x - x_o(t)) \cos \theta(t) + (y - y_o(t)) \sin \theta(t) \tag{23}$$

$$y' = - (x - x_o(t)) \sin \theta(t) + (y - y_o(t)) \cos \theta(t) \tag{24}$$

The transformed coordinates and inverse transformed coordinates in the inertial axis and rotating body axis are shown in Figure 6.

The chain rule was used to transform equations (5) through (7) from the purely inertial reference system into the rotating body inertial axis system given below:

$$\begin{aligned} & t'_t u_{t'} + x'_t u_{x'} + y'_t u_{y'} + u(t'_x u_{t'} + x'_x u_{x'} + y'_x u_{y'}) \\ & + v(t'_y u_{t'} + x'_y u_{x'} + y'_y u_{y'}) = - (t'_x p_t + x'_x p_x + y'_x p_{y'}) \\ & + \frac{1}{Re} (\cos^2\theta \, u_{x'x'} - 2 \sin\theta \cos\theta \, u_{x'y'} + \sin^2\theta \, u_{y'y'} \\ & + \sin^2\theta \, u_{x'x'} + 2 \sin\theta \cos\theta \, u_{x'y'} + \cos^2\theta \, u_{y'y'}) \end{aligned} \tag{25}$$

$$\begin{aligned} & t'_t v_{t'} + x'_t v_{x'} + y'_t v_{y'} + u(t'_x v_{t'} + x'_x v_{x'} + y'_x v_{y'}) \\ & + v(t'_y v_{t'} + x'_y v_{x'} + y'_y v_{y'}) = - (t'_y p_{t'} + x'_y p_{x'} + y'_y p_{y'}) \\ & + \frac{1}{Re} (\cos^2\theta \, v_{x'x'} - 2 \sin\theta \cos\theta \, v_{x'y'} + \sin^2\theta \, v_{y'y'} \\ & + \sin\theta \, v_{x'x'} + 2 \sin\theta \cos\theta \, v_{x'y'} + \cos^2\theta \, v_{y'y'}) \end{aligned} \tag{26}$$

$$t'_x u_{t'} + x'_x u_{x'} + y'_x u_{y'} + t'_y v_{t'} + x'_y v_{x'} + y'_y v_{y'} = 0 \tag{27}$$

The transformation derivatives, calculated from equations (17) through (24), are:

$$t'_t = 1 \tag{28}$$

$$x'_t = y'\dot{\Theta} - \dot{x}_o \cos\Theta - \dot{y}_o \sin\Theta \tag{29}$$

$$y'_t = -x'\dot{\Theta} + \dot{x}_o \sin\Theta - \dot{y}_o \cos\Theta \tag{30}$$

$$t'_x = 0 \tag{31}$$

$$x'_x = \cos\Theta \tag{32}$$

$$y'_x = -\sin\Theta \tag{33}$$

$$t'_y = 0 \tag{34}$$

$$t'_y = \sin\Theta \tag{35}$$

$$y'_y = \cos\Theta \tag{36}$$

The dot over a term denotes differentiation with respect to time.

The transformation metrics were substituted into equations (25) through (27) and the equations simplified yielding:

$$u'_t + [(y'\dot{\Theta} - \dot{x}_o \cos\Theta - \dot{y}_o \sin\Theta) + u\cos\Theta + v\sin\Theta]u_{x'} + [(-x'\dot{\Theta} + \dot{x}_o \sin\Theta - \dot{y}_o \cos\Theta) - u\sin\Theta + v\cos\Theta]u_{y'} = -(\cos\Theta\, p_{x'} - \sin\Theta\, p_{y'}) + \frac{1}{Re}(u_{x'x'} + u_{y'y'}) \tag{37}$$

$$v'_t + [(y'\dot{\Theta} - \dot{x}_o \cos\Theta - \dot{y}_o \sin\Theta) + u\cos\Theta + v\sin\Theta]v_{x'} + [(-x'\dot{\Theta} + \dot{x}_o \sin\Theta - \dot{y}_o \cos\Theta) - u\sin\Theta + v\cos\Theta]v_{y'} = -(\sin\Theta\, p_{x'} + \cos\Theta\, p_{y'}) + \frac{1}{Re}(v_{x'x'} + v_{y'y'}) \tag{38}$$

$$\cos\Theta\, u_{x'} - \sin\Theta\, u_{y'} + \sin\Theta\, v_{x'} + \cos\Theta\, v_{y'} = 0 \tag{39}$$

The contravariant velocity components defined as follows:

$$\tilde{u} = u \cos\Theta + v \sin\Theta \tag{40}$$

$$\tilde{v} = -u \sin\Theta + v \cos\Theta \tag{41}$$

were substituted into equations (37) through (39) giving:

$$\tilde{u}_{t'} + \tilde{u}\tilde{u}_{x'} + \tilde{v}\tilde{u}_{y'} = -p_{x'} + \frac{1}{Re}(\tilde{u}_{x'x'} + \tilde{u}_{y'y'}) + A \tag{42}$$

$$\tilde{v}_{t'} + \tilde{u}\tilde{v}_{x'} + \tilde{v}\tilde{v}_{y'} = -p_{y'} + \frac{1}{Re}(\tilde{v}_{x'x'} + \tilde{v}_{y'y'}) + B \tag{43}$$

where

$$A = \dot{\Theta}\tilde{v} - (y'\dot{\Theta} - (\dot{x}_o \cos\Theta + \dot{y}_o \sin\Theta))\,\tilde{u}_{x'} - (-x'\dot{\Theta} - (\dot{x}_o \sin\Theta + \dot{y}_o \cos\Theta))\,\tilde{u}_{y'} \tag{44}$$

$$B = -\dot{\Theta}\tilde{u} - (y'\dot{\Theta} - (\dot{x}_o \cos\Theta + \dot{y}_o \sin\Theta))\,\tilde{v}_{x'} - (-x'\dot{\Theta} - (\dot{x}_o \sin\Theta + \dot{y}_o \cos\Theta))\,\tilde{v}_{y'} \tag{45}$$

The tildes and primes are omitted after this point for simplicity.

Terms A and B are similar to the source terms which are destabilizing in the rotating formulation as described in Appendix A. However, all but one of the individual terms from A and B will be moved to the left hand side of the equations. There they will be added to the coefficients of the velocity derivatives and will be upwind differenced improving the convergence of the implicit iteration scheme.

Calculating pressure in the primitive variable formulation was difficult because pressure did not appear in the continuity equation nor was there a time derivative of pressure in the governing equations. Two approaches have been extensively used to compute the pressure which employed the velocity divergence, $\nabla.\underline{V}=D'$, as a correction factor. The

first method, introduced by Chorin (Ref 31), computed pressure using an iterative procedure with D' as the correcting term. The expression is

$$p^{(s+1)} = p^{(s)} - \phi D' \tag{46}$$

where s denotes the iteration number. The second method used a Poisson equation for pressure derived from the divergence of the momentum equations expressed in equations (25) and (26) (Refs 16, 32, and 33). The simplified incompressible Poisson pressure equation is

$$D'_t + (uD')_x + (vD')_y + u_x^2 + 2v_x u_y + v_y^2 + uD'_x + vD'_y$$
$$= \frac{1}{Re}(D'_{xx} + D'_{yy}) - (p_{xx} + p_{yy}) \tag{47}$$

This equation contains both spatial and time derivatives of the velocity divergence as well as the fluid velocities and pressure. Further simplifications occurred when small variations in the velocity divergence are assumed. In this case, the spatial derivatives of D' were set to zero in equation (47) and the result becomes

$$D'_t + (u_x^2 + 2v_x u_y + v_y^2) = -(p_{xx} + p_{yy}) \tag{48}$$

This equation is identical to the one used by Hodge (Ref 18) for his nonrotationg calculations. The Poisson pressure equation technique was used to calculate the interior flow field because of the increased coupling which occurred in the finite difference representation. The pressure on the plate was calculated using the iterative technique of equation (46). Conservation of mass was imposed directly and the difficulty of evaluating the Laplacian of pressure on the plate was avoided.

The following expressions taken from equations (37), (42), (43), and (48) became the system used for the solution of a plate rotating in an incompressible viscous two dimensional flow:

$$u_t + (u + y\dot{\theta} - (\dot{x}_o \cos\theta + \dot{y}_o \sin\theta))\, u_x + (v - x\dot{\theta} - (-\dot{x}_o \sin\theta + \dot{y}_o \cos\theta))u_y = - p_x + \frac{1}{Re}(u_{xx} + u_{yy}) + \dot{\theta}v \tag{49}$$

$$v_t + (u + y\dot{\theta} - (\dot{x}_o \cos\theta + \dot{y}_o \sin\theta))\, v_x + (v - x\dot{\theta} - (-\dot{x}_o \sin\theta + \dot{y}_o \cos\theta))v_y = - p_y + \frac{1}{Re}(v_{xx} + v_{yy}) - \dot{\theta}u \tag{50}$$

$$D'_t + u_x^2 + 2v_x u_y + v_y^2 = - (p_{xx} + p_{yy}) \tag{51}$$

$$D' = u_x + v_y \tag{52}$$

The governing equations were transformed to a computational plane. The corresponding governing equations, transformed using the relationships described by Hodge, become:

$$u_t + \frac{(u + y\dot{\theta} - (\dot{x}_o \cos\theta + \dot{y}_o \sin\theta))}{J}(y_\eta u_\xi - y_\xi u_\eta) + \frac{(v - x\dot{\theta} - (-\dot{x}_o \sin\theta + \dot{y}_o \cos\theta))}{J}(x_\xi u_\eta - x_\eta u_\xi) + uD'$$
$$= - \frac{1}{J}(y_\eta p_\xi - y_\xi p_\eta) + \frac{1}{Re}\left\{\frac{(\alpha' u_{\xi\xi} - 2\beta' u_{\xi\eta} + \gamma' u_{\eta\eta})}{J^2} + u_\eta\left(\frac{\sigma}{J^2}\right) + u_\xi\left(\frac{\tau}{J^2}\right)\right\} + \dot{\theta}v \tag{53}$$

$$v_t + \frac{(u + y\dot{\theta} - (\dot{x}_o \cos\theta + \dot{y}_o \sin\theta))}{J}(y_\eta v_\xi - y_\xi v_\eta)$$

$$+ \frac{(v + x\dot{\theta} - (\dot{x}_o \sin\theta + \dot{y}_o \cos\theta))}{J} (x_\xi v_\eta - x_\eta v_\xi) + vD'$$

$$= -\frac{1}{J}(x_\xi p_\eta - x_\eta p_\xi) + \frac{1}{Re}\{\frac{(\alpha' v_{\xi\xi} - 2\beta' v_{\xi\eta} + \gamma' v_{\eta\eta})}{J^2} + v_\eta (\frac{\sigma}{J^2})$$

$$+ v_\xi (\frac{\tau}{J^2})\} - \dot{\theta}u \qquad (54)$$

$$D'_t + \frac{1}{J^2}\{(y_\eta u_\xi - y_\xi u_\eta)^2 + 2(y_\eta v_\xi - y_\xi v_\eta)(x_\xi u_\eta - x_\eta u_\xi)$$

$$+ (x_\xi v_\eta - x_\eta v_\xi)^2\} = -\{\frac{(\alpha' p_{\xi\xi} - 2\beta' p_{\xi\eta} + \gamma' p_{\eta\eta})}{J^2}$$

$$+ p_\eta (\frac{\sigma}{J^2}) + p_\xi (\frac{\tau}{J^2})\} \qquad (55)$$

$$D' = (y_\eta u_\xi - y_\xi u_\eta) + (x_\xi v_\eta - x_\eta v_\xi) \qquad (56)$$

where

$$\alpha' = x_\eta^2 + y_\eta^2 \qquad (57)$$

$$\beta' = x_\xi x_\eta + y_\xi y_\eta \qquad (58)$$

$$\gamma' = x_\xi^2 + y_\xi^2 \qquad (59)$$

$$\sigma = [y_\xi (\alpha' x_{\xi\xi} - 2\beta' x_{\xi\eta} + \gamma' x_{\eta\eta}) - x_\xi (\alpha' y_{\xi\xi} - 2\beta' y_{\xi\eta} + \gamma' y_{\eta\eta})]/J \qquad (60)$$

$$\tau = [x_\eta (\alpha' y_{\xi\xi} - 2\beta' y_{\xi\eta} + \gamma' y_{\eta\eta}) - y_\eta (\alpha' x_{\xi\xi} - 2\beta' x_{\xi\eta} + \gamma' x_{\eta\eta})]/J \qquad (61)$$

At this point the equations were valid for an arbitrary transformation. In the exponential transformation described in Section III-A, each spatial coordinate in the computational plane was a function of only one spatial variable in the physical plane. Therefore, x_ξ and y_η were both set to zero which significantly simplified the governing

equations.

A backward-time-central-space finite difference method similar to the one developed by Hodge (Ref 16) was used to solve equations (53) through (56). The implicit method consisted of a linearization of the equations and the application of finite differences to these equations (Refs 34 and 35).

Standard finite difference expressions were used to approximate equations (53) through (56) (Ref 36). First order accurate backward differences were used for the time derivatives. The first derivatives of pressure were approximated with second order accurate central differences. Second order central difference expressions were used for the second derivatives of velocity in the viscous terms. Second order accurate upwind differencing was used for the velocity first derivatives in the convective terms. Three point, one sided, backward or forward finite differences were used for the velocity first derivatives in the viscous terms. First order upwind differences were used next to the plate and the outer boundary. The grid spacing near the plate was small, as were the velocity gradients near the outer boundary. In both cases the artificial viscosity induced by first order upwind differencing had a negligible effect. The transformation derivatives were evaluated analytically or with second order central differences. The velocity derivatives in the velocity divergence forms were evaluated using central differences.

Difference equations were written in the following convention used

by Hegna (Ref 36). Terms which contained unknowns at location (i,j) are fully subscripted. The subscripts, i and j, and superscript, n, are assumed when omitted. Equation 53, the x momentum equation, becomes:

$$\frac{u_{ij}^{n} - u_{ij}^{n-1}}{\Delta t} + (3\,u_i - 4\,u_{i\pm1} + u_{i\pm2}) \left| \frac{y_\eta}{J} (u + y\dot{\theta} - (\dot{x}_o \cos\theta + \dot{y}_o \sin\theta)) \right| + (3\,u_j - 4\,u_{j\pm1} + u_{j\pm2}) \left| \frac{x_\xi}{J} (v - x\dot{\theta} - (-\dot{x}_o \sin\theta + \dot{y}_o \cos\theta)) \right|$$

$$+ uD' = -\frac{y_\eta}{2J} (p_{i+1} - p_{i-1}) + \frac{1}{Re} \{ \frac{\alpha'}{J^2} (u_{i+1} - 2\,u_{ij} + u_{i-1}) + \frac{\gamma'}{J^2} (u_{j+1} - 2\,u_{ij} + u_{j-1}) - (3\,u_i - 4\,u_{i\pm1} + u_{i\pm2}) \left| \frac{-\tau}{2J^2} \right| -$$

$$(3\,u_j - 4\,u_{j\pm1} + u_{j\pm2}) \left| \frac{-\sigma}{2J^2} \right| \} + \dot{\theta} v \qquad (62)$$

where the direction of the upwind differencing is determined by the sign of the coefficient multiplying the term. This equation is written to provide an expression for u_{ij}.

$$u_{ij}^{n} = \{u_{ij}^{n-1} + \Delta t[-\frac{y_\eta}{2J} (p_{i+1} - p_{i-1}) + (4u_{i\pm1} - u_{i\pm2}) \left| \frac{y_\eta}{J} (u + y\dot{\theta} - (\dot{x}_o \cos\theta + \dot{y}_o \sin\theta)) \right| + (4u_{j\pm1} - u_{j\pm2}) \left| \frac{x_\xi}{J} (v - x\dot{\theta} - (-\dot{x}_o \sin\theta + \dot{y}_o \cos\theta)) \right| - uD' + \frac{1}{Re}$$

$$[\frac{\alpha'}{J^2} (u_{i+1} + u_{i-1}) + \frac{\gamma'}{J^2} (u_{j+1} + u_{j-1}) + (4u_{i\pm1} - u_{i\pm2}) \left| \frac{-\tau}{2J^2} \right| + (4u_{j\pm1} - u_{j\pm2}) \left| \frac{-\sigma}{2J^2} \right|] + \dot{\theta} v] \} /$$

$$\{ 1 + \Delta t[3(\left| \frac{y_\eta}{J} (u + y\dot{\theta} - (\dot{x}_o \cos\theta + \dot{y}_o \sin\theta)) \right| + \left| \frac{x_\xi}{J} (v - x\dot{\theta} - (-\dot{x}_o \sin\theta + \dot{y}_o \cos\theta)) \right| + \left| \frac{-\tau}{2J^2} \right|$$

$$+\left|\frac{-\sigma}{2J^2}\right|)+\frac{2}{ReJ^2}(\alpha'+\gamma')\}$$ (63)

In an analogous manner, the transformed y momentum equation is written for v_{ij}.

$$v_{ij}^n = \{v_{ij}^{n-1} + \Delta t[-\frac{x_\xi}{2J}(p_{j+1}-p_{j-1})+(4v_{i\pm1}-v_{i\pm2})$$

$$\left|\frac{y_\eta}{J}(u+y\dot{\theta} - (\dot{x}_o\cos\theta+\dot{y}_o\sin\theta))\right| +(4v_{j\pm1}-v_{j\pm2})$$

$$\left|\frac{x_\xi}{J}(v-x\dot{\theta} -(-\dot{x}_o\sin\theta+\dot{y}_o\cos\theta))\right| -vD' +$$

$$\frac{1}{Re}[\frac{\alpha'}{J^2}(v_{i+1}+v_{i-1}) + \frac{\gamma'}{J^2}(v_{j+1}+v_{j-1})+(4v_{i\pm1}-v_{i\pm2})$$

$$\left|\frac{-\tau}{2J^2}\right| + (4v_{j\pm1}-v_{j\pm2})\left|\frac{-\sigma}{2J^2}\right|] + \dot{\theta}u]\} \;/$$

$$\{1+\Delta t[3(\left|\frac{y_\eta}{J}(u+y\dot{\theta} - (\dot{x}_o\cos\theta+\dot{y}_o\sin\theta))\right|$$

$$+\left|\frac{x_\xi}{J}(v-x\dot{\theta} -(-\dot{x}_o\sin\theta+\dot{y}_o\cos\theta))\right| + \left|\frac{-\tau}{2J^2}\right| + \left|\frac{-\sigma}{2J^2}\right|)$$

$$+\frac{2}{ReJ^2}(\alpha'+\gamma')\}$$ (64)

The static pressure throughout the flow field was calculated using the Poisson pressure equation (Refs 38 and 39). Second order accurate central differences were used to approximate the second derivatives of pressure in the transformed Laplacian term. The first derivative of pressure in the Laplacian was approximated by second order accurate upwind differences based on the sign of σ and τ. The remaining terms were differenced in the same manner as the momentum equations. The requirement that the velocity divergence at the nth time step be zero was incorporated into the difference equation by setting D'^n to zero. The numerical non-zero quantity D'^{n-1} was retained as a correction factor. Equation (55) was written in finite difference form.

$$P_{ij}^n = \{-\frac{D'^{,n-1}}{\Delta t} + (\frac{y_\eta u_\xi}{J})^2 + 2(\frac{y_\eta v_\xi}{J})(\frac{x_\xi u_\eta}{J})+(\frac{x_\xi v_\eta}{J})^2$$

$$+\frac{\alpha'}{J^2}(p_{i+1}+p_{i-1})+\frac{\gamma'}{J^2}(p_{j+1}+p_{j-1})-(4p_{i\pm1}-p_{i\pm2})\left|\frac{-\tau}{2J^2}\right|+(4p_{j\pm1}-p_{j\pm2})\left|\frac{-\sigma}{2J^2}\right|+3\left(\left|\frac{-\tau}{2J^2}\right|+\left|\frac{-\sigma}{2J^2}\right|\right)-$$

$$\frac{2}{J^2}(\alpha'+\gamma') \tag{65}$$

Equations (63) through (65) formed a set of difference equations for the flow variables u, v, and p at location (i,j) in terms of the transformation derivatives and the values of the variables at neighboring points. The linearization and differencing methods decoupled the equations with respect to the higher order terms for the unknowns at location (i,j).

The large system of finite difference equations was solved using a successive-over-relaxation (SOR) iteration technique given by

$$u_{ij}^{(s+1)} = \omega_{uv}\, u_{ij}^{*} + (1-\omega_{uv})\, u_{ij}^{(s)} \tag{66}$$

$$v_{ij}^{(s+1)} = \omega_{uv}\, v_{ij}^{*} + (1-\omega_{uv})\, v_{ij}^{(s)} \tag{67}$$

$$p_{ij}^{(s+1)} = \omega_{p}\, p_{ij}^{*} + (1-\omega_{p})\, p_{ij}^{(s)} \tag{68}$$

where s is the iterate number and * designates the current value obtained from the difference equation (Ref 40). The acceleration parameters were always 1.0 for the first iteration.

The pressure on the plate was calculated separately using the Chorin iteration technique which avoided the difficulty of formulating one sided differences at the plate for the Laplacian of pressure. Second order accurate upwind differences were used for the transformation and velocity first derivatives in equation (56). The

acceleration parameter, ϕ, which is related to SOR iteration of the Poisson pressure equation was given by Hodge (Ref 15) as

$$\phi = 2\omega_{pb} / (\Delta t \left(\frac{\alpha'}{J^2} + \frac{\gamma'}{J^2}\right)) \tag{69}$$

The iteration procedure followed a prescribed order at each point. Only the surface pressure was computed on body points. At field points, the u velocity component was computed first, then the v velocity component, and finally the field pressure p.

The SOR sweep directions were developed to minimize favoring any one direction. Hodge (Ref 41) found the flow fields on the upper and lower surfaces were slightly different on a symmetrical airfoil at zero angle of attack. This was caused by always sweeping in the same direction. The sweep method used in this study is described in Appendix B.

C. Initial and Boundary Conditions

The initial conditions for the Navier-Stokes equations solver were modified depending on the application of the solver. Simple initial conditions were used when calculating the aerodynamics of a plate at a fixed angle of attack (Ref 42). More refined initial conditions were required when the plate was allowed to rotate or free fall.

Zero velocity was used as the initial condition for a plate at a fixed angle of attack. An impulsive start was modeled by instantaneously imposing the freestream velocity on the plate. It was

not necessary to start with an inviscid solution because the relatively low Reynolds number did not present any numerical stability problems. The numerical results did not represent the physical phenomenon during the impulsive start because continuity was initially not satisfied throughout the flow field. As the calculation evolved, continuity was eventually satisfied throughout the flow field and the numerical solution represented the physical phenomenon.

When the Navier-Stokes equations solver was used to calculate the flow field around a plate undergoing forced rotation, the solution for a plate at a fixed angle of attack was used as an initial condition. The plate was then forced to rotate. As long as the plate was at a small angle of attack and was not shedding vortices, the start up accurately modeled the physical phenomenon.

The flow field around a plate moving at a fixed angle of attack was used as an initial condition for a plate about to undergo fixed or free fall autorotation. This represented the case of a plate translating at a constant velocity without rotation. The aerodynamic forces produced by the plate were used as forcing functions in the flight mechanics equations. The flight mechanics equations were solved to initiate autorotation which accurately modeled a physical start up.

The Navier-Stokes boundary conditions used in this research effort were the reverse of those used the more classical body fixed formulation. When using a body fixed formulation, the boundary conditions were usually freestream velocity and pressure on the outer

boundary and no flow on the inner boundary or plate. For the inertial formulation used in this study, the different boundary conditions were equivalent in their respective reference systems.

The motion of the plate was imposed on the inner boundary or plate. The translation and rotation of the plate were modeled by changing the boundary conditions on the inner boundary. The velocity imposed at each grid point on the plate was calculated using the following equations:

$$u_b = V_{cg} (\cos \Theta \cos \gamma + \sin \Theta \sin \gamma) - \dot{\Theta} y \tag{70}$$

$$v_b = V_{cg} (\sin \Theta \cos \gamma - \cos \Theta \sin \gamma) + \dot{\Theta} x \tag{71}$$

The translational velocity, angular velocity, glide path angle, and rotational angle were all known from the previous solution of the flight mechanics equations. Examples of various inner boundary conditions for one side of the plate are shown in Figure 7. Figure 7a shows the inner boundary conditions imposed on a plate moving down and to the right at a $\pi/4$ radians angle in the computational domain. This represents any combination of flight path angle and rotation angle which produces an angle of attack of $\pi/4$ radians where the angle of attack is defined as:

$$\alpha = \Theta - \gamma \tag{72}$$

Figure 7b shows the inner boundary conditions for a plate rotating without translation. The magnitude of the velocity in this case is purely a function of the angular rotation of the plate. The translation from Figure 7a was combined with the rotation in Figure 7b to produce the boundary conditions shown in Figure 7c.

The velocity boundary conditions on the outer boundary were zero velocity in either the x or y directions. The pressure on the outer boundary was set equal to the ambient pressure or a nondimensional pressure of zero. These boundary conditions closely corresponded to the physical conditions in an inertial reference system. The outer boundary conditions were not changed and remained constant throughout the calculations. Neglecting the momentum deficit had a small effect on the flow field near the plate as outlined in Appendix A.

D. Determination of Aerodynamic Coefficients

The flow field around the plate was calculated by the Navier-Stokes equations solver. The viscous and pressure forces imposed upon the plate by this flow field were summed to give the aerodynamic forces generated by the plate.

The aerodynamic coefficients were calculated at each time step, whereas for a steady state solution they are only calculated for the final state (Ref 43). Because the coefficients were calculated so often in this study, the method of calculation was customized to this particular geometry to reduce the computing requirements.

The total pressure force acting on the plate was calculated by summing the pressure acting on all the descrete segments of the plate. The translational and rotational velocities of the plate were specified as boundary conditions. The pressure distribution on the plate was calculated using equation (65). The pressure differences around the plate were summed to give the normal and axial forces. The

corresponding moment was calculated by multiplying the pressure differences by their respective distances from the center of gravity.

The viscous forces acting on the plate were calculated using the following equation for shear stress:

$$\tau' = \mu u_n \tag{73}$$

where u_n is the derivative of the velocity normal to the surface of the plate (Ref 44). The normal velocity derivative was approximated by a first order difference. The viscous normal and axial forces were calculated by summing the shear stresses around the plate and the moment produced by the viscous forces was calculated by multiplying the shear stress by its corresponding distance from the center of gravity.

The viscous and pressure forces were combined according to

$$L = (F_{yv} + F_{yp}) \cos \alpha - (F_{xv} + F_{xp}) \sin \alpha \tag{74}$$

$$D = (F_{yv} + F_{yp}) \sin \alpha + (F_{xv} + F_{yp}) \cos \alpha \tag{75}$$

$$M = \Sigma \Delta p (\Delta x)\, x_i + \Sigma \Delta \tau (\Delta x)\, y_i \tag{76}$$

giving the overall aerodynamic forces produced by the plate. The aerodynamic forces were produced primarily by the pressure differences around the plate.

SECTION IV

FLIGHT MECHANICS SOLVER

A three degree of freedom flight mechanics equations solver was developed to predict the flight path of a free falling, autorotating, flat plate. The three flight mechanics equations were rewritten as four coupled first order ordinary differential equations. The equations were solved using an open Adams formula to obtain the velocity of the center of gravity of the plate, the flight path angle, the rate of rotation, and the rotational angle.

The general unsteady motion of a body in three dimensional space is described by a vector force and moment equation. This produces six scalar ordinary differential equations. Much of the complexity of these equations results from the inclusion of the rotation of the earth and its curvature in the mathematical model. Assuming the earth is flat, the absence of gyroscopic effects and planar motion reduces the system of equations to three coupled differential equations which model the motion of a free falling, autorotating plate in a plane (Ref 45).

Two alternative reference systems are available for the dynamical force equations: the wind axes and the body axes. Both are used in practice with no overriding advantages to either system (Ref 46). The equations used in this research effort were cast in the wind axes reference system.

Experimental data and previous analyses indicated the motion of the

autorotating plate could be modeled accurately using the following three degrees of freedom:

1) Horizontal translation, x

2) Vertical translation, y

3) Rotation about the center of gravity, θ

The reference system for these three degrees of freedom is shown in Figure 8 (Ref 47). The positive x direction was to the right while the positive y direction was up. The angle of rotation, like all angles in this problem, is positive in a counter-clockwise direction. This conforms to a standard right hand rule reference system.

The equations of motion modeling these three degrees of freedom are:

$$-m\dot{V} = D + W \sin \gamma \tag{77}$$

$$mV\dot{\gamma} = L - W \cos \gamma \tag{78}$$

$$I_y \ddot{\theta} = M \tag{79}$$

This was an initial value problem involving a system of three nonlinear ordinary differential equations (two first order and one second order). Several methods exist for solving systems of first order equations, therefore, the second order equation was reduced to two first order equations.

$$I_y \dot{q} = M \tag{80}$$

$$\dot{\theta} = q \tag{81}$$

Equation (79) was reformulated using equations (80) and (81) to give equations (82). Equations (77) and (78) were rearranged to give

equations (83) and (84).

$$\dot{q} = \frac{M}{I_y} \tag{82}$$

$$\dot{V} = \frac{-(D+W \sin \gamma)}{m} \tag{83}$$

$$\dot{\gamma} = \frac{(L-W \cos \gamma)}{mV} \tag{84}$$

Several implicit, or closed, and several explicit, or open, methods are available for solving systems of equations (Ref 48). The closed methods offer improved accuracy over the open methods, however, they require multiple solutions of the Navier-Stokes equations at each time step. During the formulation of this problem, it was estimated the Navier-Stokes equation solver would consume at least 90% of the computing time while the flight mechanics equations solver would consume less than 10%. Based on this assumption, an open initial value problem solver was selected as the most computationally efficient method. A predictor-corrector scheme was ruled out because it required two solutions of the Navier-Stokes equations at each time step, thus almost doubling the computing time.

The simplest explicit method is Euler's method. This method requires one initial condition for each variable and one evaluation of the function at each time step to advance to the next time step. The following set of equations represents Euler's method:

$$V^{n+1} = V^n + \Delta t \dot{V} \tag{85}$$

$$\gamma^{n+1} = \gamma^n + \Delta t \dot{\gamma} \tag{86}$$

$$q^{n+1} = q^n + \Delta t \dot{q} \tag{87}$$

$$\theta^{n+1} = \theta^n + \Delta t \dot{\theta} \tag{88}$$

Euler's method is first order accurate in time which is consistent with the time differencing used in the Navier-Stokes equations solver.

Few additional computer resources are required to increase the accuracy of the method by using higher order Adams-Bashforth formulae (Ref 48). These methods are described in Appendix D. Equations (81) through (84) were nondimensionalized using the same operators that were used in the Navier-Stokes equations solver. The equations are cast in the Adams-Bashforth formulae

$$V^{n+1} = V^n + \Delta t \frac{cg}{WV_\infty} \sum_{i=1}^{n} ACOEF_i \ (D_i + W \sin \gamma_i) \tag{89}$$

$$\gamma^{n+1} = \gamma^n + \Delta t \frac{cg}{WV_\infty} \sum_{i=1}^{n} ACOEF_i \left(\frac{L_i - W \cos \gamma_i}{V_i}\right) \tag{90}$$

$$q^{n+1} = q^n + \Delta t \frac{12g}{WV_\infty} \sum_{i=1}^{n} ACOEF_i \ M_i \tag{91}$$

$$\theta^{n+1} = \theta^n + \Delta t \sum_{i=1}^{n} ACOEF_i \ q_i \tag{92}$$

where n represents the order of the solution technique. A list of the coefficients used in the summation are included in Appendix D. If the order of the equations is set to one, equations (85) through (88) reduce to equations (89) through (92). Increasing the order of the flight mechanics equations solver had an insignificant effect on the overall storage requirements and computational times. An Euler solution required storing 20 pieces of information. Each increase in the order of the solver required saving an additional 10 pieces of information.

Therefore, a sixth order method required saving 70 pieces of information as opposed to 20 for a first order solver. This was insignificant compared to the thousands of storage locations required for the Navier-Stokes equations solver. A comparison between different order Adams-Bashforth formulae was made and is discussed in Section VI.

The initial conditions necessary to start the higher order methods are not known. A common technique is to start with Euler's method and increase the order of the method at each time step until the desired order is obtained. This in essence generates the initial conditions necessary to start the higher order techniques. In this study, the past initial conditions necessary to start the higher order methods were obtained by linear extrapolation backward in time from the one set of initial conditions which were specified.

Everything on the right hand side of equations (89) through (92) is known. The velocity, glide path angle, rotational angle, and rotational velocity were all known from previous solutions of the flight mechanics equations. The aerodynamic forces (lift, drag and moment) are known from the present and previous time step solutions of the Navier-Stokes equations. The aerodynamic forces and plate characteristics were all referenced to a plate with a span of 1.0.

SECTION V

COUPLED SYSTEMS

The Navier-Stokes equations solver and the flight mechanics equations solver were solved simultaneously. Initial conditions were specified for both sets of equations. The aerodynamic forces produced by the plate were calculated by the Navier-Stokes equations solver and used as forcing functions in the flight mechanics equations solver. The flight mechanics equations were solved to obtain the translation and rotation of the plate for the next time step. The updated translation and rotation were used as new boundary conditions in the Navier-Stokes equations solver. The iterative procedure was repeated thousands of times, therefore, a solution dependent, variable time step was introduced into the computational procedure to improve the computational efficiency.

Zero velocity in the computational domain was used as the initial condition in the Navier-Stokes equations solver. The plate was impulsively accelerated to some prespecified velocity at a fixed angle of attack. A relatively large time step was used to converge to the steady state solution with the minimum expenditure of computer time. Therefore the flow field which evolved during start up did not accurately represent physics. The solution at a fixed angle of attack included periodic shedding of vortices when the angle of attack was more than a few degrees. The intent at this point was not to accurately model the impulsive start up, but rather to obtain a fully developed flow field which could be used to start the rotating calculations. The

aerodynamic forces were calculated from the pressure and velocity field around the plate.

The initial conditions for the flight mechanics equations were specified at the beginning of the calculation. The initial conditions for previous time steps necessary to start the higher order solvers were linearly extrapolated backwards in time. The aerodynamic forces produced by the plate were entered into the flight mechanics as boundary conditions in equations (89) through (92). The same time step was used in the flight mechanics equations solver as was used in the Navier-Stokes equations solver. The flight mechanics equations were solved for the next time step. This solution produced a new velocity, glide path angle, rotation angle, and rotational velocity.

These conditions were used in equations (71) and (72) to obtain new inner boundary conditions for the Navier-Stokes equations solver. The outer boundary conditions of no flow and ambient pressure remained unchanged. A new flow field and the corresponding aerodynamic coefficients were calculated. At this point the solution procedure was started. The motion of the free falling plate was calculated by repeating the process just outlined.

The time steps required to obtain an accurate Navier-Stokes solution and an accurate flight mechanics solution were not the same. The Navier-Stokes equations solver was an implicit scheme. A stability analysis of an implicit technique used to solve a model linear partial differential equation with the same character as the Navier-Stokes

equations showed the numerical method to be unconditionally stable (Ref 36). However, when working with the complete system of Navier-Stokes equations, Hegna (Ref 37) found the existence of an upper limit on the time step. The flight mechanics equations were stable for any time step. Therefore, the time step was selected to meet the limitations of the Navier-Stokes equations solver.

The Navier-Stokes equations solver was found to tolerate only a certain unquantifiable level of change in the boundary conditions from time step to time step. The solver still met the error criteria specified for convergence within an acceptable number of iterations. This occured because the Navier-Stokes equations were not solved simulataneously. The updated velocity boundary conditions on the plate introduced large changes in u and/or v near the body. These changes in velocity caused large changes in pressure on the plate through the velocity divergence term in equation (46). The large pressure changes in turn influenced v at the points adjacent to the plate because of the p_y coupling. This interaction between equations made convergence difficult for large changes in the boundary conditions on the plate. Numerical experimentation was used to establish the tolerable level of change.

The maximum allowable change in the boundary conditions was used as the basis for a solution dependent time step. The maximum change in the boundary condition was asssumed to be a result of the rate of rotation of the plate. A heuristic method was developed around the following equation:

$C_c = \Delta t \, \Delta\omega$ (5.1)

The constant for a variable time step, C_c, was established through numerical experimentation to a value which allowed the SOR procedure to meet the specified convergence criteria. This allowed approximately the same amount of rotation during each time step regardless of the rate of rotation. When the plate was rotating rapidly, a relatively small time step was used resulting in a certain amount of change in the boundary conditions between calculations. When the plate was rotating slowly, a relatively large time step was used resulting in approximately the same amount of change in the boundary conditions as the rapidly rotating case. Without the solution dependent time step, a very small time step would have been required to accurately calculate the most rapid rotation thereby resulting in inefficiency at slower rotation rates.

The higher order Adam-Bashforth formulae used to solve the flight mechanics equations were derived for constant time steps. The first order formula or Euler's method was the only scheme which was used with the variable time step. Higher order methods with variable time steps exist, however, their derivation is rather complex.

SECTION VI

DISCUSSION OF RESULTS

Several major stepping stones were investigated on the way to coupling the Navier-Stokes equations with the flight mechanics equations. A building block approach was used to validate the overall approach and the computer code. Four different cases were investigated in this study.

(A) The Navier-Stokes equations solver was used to calculate the flow field around a plate at several static angles of attack.

(B) The effect of forcing the plate to rotate was also investigated using the Navier-Stokes equations solver.

(C) The Navier-Stokes equations were coupled with a one degree of freedom equation of motion and solved to model the pinned autorotation of a plate.

(D) Finally the flight path of a free falling, autorotating, flat plate was predicted by a numerical method which coupled the two dimensional incompressible Navier-Stokes equations with the three degrees of freedom equations of motion.

The finite difference grid which modeled the flow field was constructed to obtain approximately the same resolution in the x and y directions. The minimum and maximum grid spacing determined the total number of grid points required to cover the flow field. Numerical experimentation was used to select a grid with a maximum number of points compatible with calculations on the CYBER 750. The minimum grid spacing in the y direction, which defined the thickness of the plate,

was 6.25% chord or 0.0156 feet on a plate with a 0.25 feet chord. The minimum grid spacing and the requirement for an outer spacing of approximately one chord dictated a grid with 54 points in the y direction. An exponential stretching coefficient of 2.988 produced a maximum grid spacing of 1.110 chords on the outer boundary in the y direction. The physical domain extended 10.03125 chords in the y direction, or 2.508 feet for a plate with a 0.25 feet chord.

The same minimum grid spacing was used in the x direction. Sixteen grid points were evenly spaced along the chord of the plate at 6.25% chord intervals. The grid was stretched from the end of the plate to the outer boundary using an exponential coefficient of 3.157. This required 65 points to produce an outer grid spacing of 1.287. The physical domain extended 10.5 chords in the x direction or 2.625 feet for a plate with a 0.25 feet chord. Hence the complete grid was comprised of 3510 points.

The finite difference grid was generated by piecing together analytical functions. This presented the opportunity to use analytical transformation derivatives as well as the more commonly used numerical derivatives. The flow field around a plate at $\pi/2$ radians angle of attack was calculated using analytical and numerical derivatives. The analytical transformation derivatives produced a drag coefficient five drag counts (C_D=0.0005) higher than the numerical derivatives. Analytical derivatives were used throughout the study because they were thought to be more accurate.

The Reynolds number of a plate with a 0.25 feet chord moving at a freestream velocity of 3.0 feet per second on a standard day at sea level is approximately 5000. The Navier-Stokes equations were not mass averaged because of the relatively small Reynolds number (Ref 49). No turbulence modeling was included in the equations.

Implicit methods were shown by linear stability analysis to be unconditionally stable (Ref 50). Despite this, Hegna (Ref 51) found convergence of the SOR solver required a nondimensional time step less than 0.001 for flow around an airfoil at a Reynolds number of approximately 170,000. The relatively low Reynolds number flow in this study produced a system of equations which could be solved using a larger time step. Through numerical experimentation, a time step of 0.01 was found to converge and was used for all calculations at fixed angles of attack.

There was a tradeoff in the SOR procedure between the size of the time step and the number of iterations performed at each time step. Increasing the time step and increasing the number of iterations at each time step can have the same effect as decreasing the time step and decreasing the number of iterations. In this study a maximum of four SOR iterations were used at each time step. An even number of iterations was always used in an attempt to avoid using one sweep direction more than another.

The same SOR acceleration parameters were used throughout the study. The parameters had values of 1.0 for the velocity components,

0.9 for the surface pressure, and 1.1 for the field pressure. These parameters were determined by previous researchers and their influence on convergence was not investigated in this study (Refs 16 and 37).

The convergence criterion for the SOR iterations required the maximum change in the relative magnitudes of u,v, and p for all locations be less than 1%. This criterion occasionally was not satisfied, however, previous researchers tolerated maximum changes as large as 5% (Ref 37). The convergence criterion was maintained at a relatively low level throughout this study because of the strong time dependent nature of the problem.

Several methods of SOR sweeping were investigated. The method described in Appendix B was found to be the best combination of efficiency and accuracy. This method, while not favoring any direction, maintained good numerical efficiency because it did not require an excessive amount of logic to execute.

The movement of the plate was calculated using first order and sixth order flight mechanics equations solvers. There was virtually no difference in the solutions because the small time step required to solve the Navier-Stokes equations minimized the error in the first order flight mechanics equations to an acceptable level.

The numerical technique required approximately 0.645 seconds of central processing time on the CYBER 750 computer to advance a solution one time step. This equated to approximately 2.582 seconds of computing

time per SOR iteration. The computing time for each SOR iteration included approximately 0.001 seconds to solve the flight mechanics equations. This means 98.5 percent of the computing requirements support the solution of the Navier-Stokes equations.

The numerical procedure was executed on the CRAY-1 computer to reduce the overall computing time. The computer code was not modified to incorporate the vectorized programming techniques available on the CRAY-1. The computing time on the CRAY-1 was slightly more than a fifth of the computing time required on the CYBER 750 to perform identical calculations.

A. Static Angle of Attack

The static lift curve for a flat plate, shown in Figure 9, was calculated using the Navier-Stokes equations solver. A flow field was considered to achieve steady state by previous researchers when the aerodynamic coefficients changed less than 1% in one unit of nondimensional time (Ref 52). The maximum steady state lift coefficient was approximately 0.44 at 0.15 radians angle of attack. The flow separated from the upper surface of the plate at a relatively small angle of attack. Above 0.15 radians angle of attack the flow field was unsteady and a band of lift coefficients were plotted on the static lift curve.

The instantaneous streamlines around a plate at 0.4 radians angle of attack can be seen in Figure 10. The streamlines were calculated by integrating:

$$u = \frac{\partial \psi}{\partial y} \tag{94}$$

$$v = -\frac{\partial \psi}{\partial x} \tag{95}$$

using a first order method. A vortex can be seen behind the plate in Figure 10 (Ref 53). At t=5.2 a vortex is just leaving the plate. It is swept downstream until finally, at t=6.0, another vortex is forming above the plate. The Strouhal number for this case was approximately fc/U_∞=0.34. The Strouhal number, however, is reduced to 0.13 when the frontal area of the plate was used as the reference length. The unsteady lift coefficient produced by a plate at 0.4 radians angle of attack is illustrated in Figure 11.

The flow field produced by a plate at $\pi/2$ radians angle of attack was calculated. The symmetric vortex formation behind the plate can be seen in the Figure 12. Experiment indicates that a vortex street should have been formed behind the plate (Refs 54 and 55), however, it was not predicted by the numerical calculation. An instability of the magnitude necessary to initiate asymmetric shedding was not present in the numerical method. No attempt was made to initiate the asymmetry because it was beyond the scope of the present study. The drag coefficient produced by the plate at $\pi/2$ angle of attack was 1.494. This compares well with the experimental data of 1.4 obtained for a flat plate with asymmetric shedding and 1.6 obtained for a flat plate with a splitter plate behind it (Ref 56).

B. Forced Rotation

From this point to the end of this section, the flow fields

presented combine translation and rotation. Steady motions can usually be presented in a body fixed reference system in which the flow becomes steady. In unsteady flows no preferred reference frame exists, therefore, the reference frame is selected on the basis of other criteria as discussed in Appendix C. A reference frame fixed to the plate in translation in which the plate rotates will be used throughout this section. This frame was selected because of its analogy to instantaneous streamlines of a plate rotating in a wind tunnel.

A solution dependent time step was developed to improve the computational efficiency of the rotating calculations. The constant in equation (92), which was used to determine the maximum allowable change, was derived from numerical experimentation. The constant was selected to reduce the number of calculations required for a solution while maintaining the specified error criterion and using a maximum of four SOR iterations. A maximum allowable change constant of C_c=0.005 was used for most calculations. In addition, the time step was never larger than 0.01.

The flow field around a plate undergoing forced rotation was calculated at three nondimensional rotational velocities. The plate was initially fixed in a uniform freestream flow at zero angle of attack. It was subjected to a constant angular acceleration until it reached the desired rotational velocity. First, the plate was forced to rotate counterclockwise at a nondimensional rotational velocity ($\omega c/U_\infty$) of one. At this rate of rotation the translational velocity everywhere on the plate was greater than the rotational velocity. This meant vortices

formed at the endpoints of the plate were always shed downstream of the plate. The instantaneous streamlines for this case are shown in Figure 13.

The rate of rotation was increased to an angular velocity of two. The rotational velocity of the end of the plate was equal to the translational velocity of the center of gravity of the plate. This meant that when the plate was at an angle of attack of $\pi/2$ or $3\pi/2$ there was no relative flow around the retreating end of the plate and thus no vortex was shed. This can be seen in Figure 14.

Finally, the rotational rate was increased to an angular velocity of four. At this rate of rotation, the linear velocity of the ends of the plate induced by the rotation was twice that of the center of gravity of the plate. This meant a vortex was shed upstream of the retreating end of the plate as shown by the instantaneous streamlines in Figure 15.

The aerodynamic coefficients produced by a plate undergoing forced rotation at three different rates are shown in Figures 16, 17, and 18. In these plots, angle of attack and rotation angle are synonymous. The maximum lift coefficients were approximately 3.2, 5.8, and 9.5 for nondimensional rotational rates of 1.0, 2.0, and 4.0, respectively. These values are considerably larger than the maximum lift coefficient of approximately 1.2 produced by a flat plate at a static angle of attack.

Rotating the plate caused a shift in the phase relationship among the aerodynamic coefficients. The maximum drag coefficient was found to lag the maximum lift coefficient by 1.1, 1.0, and 0.75 radians angle of attack for nondimensional angular velocities of 1.0, 2.0, and 4.0 respectively. At a rotational rate of one, the maximum moment coefficient slightly lagged the maximum lift coefficient. At a rotational rate of two the phase lag increased to approximately 0.3 radians. The maximum moment lagged the maximum lift by approximately 0.5 radians at a rotational velocity of four. Visual integration of the area under the moment curve over a revolution indicated the slowest rate of rotation produced an average moment which would accelerate the rate of rotation. The plate rotating at an angular velocity of two generated an integrated moment which was almost neutral while the most rapidly rotating case produced an overall retarding moment. This analysis of the moment suggested the plate would autorotate at a mean rotational velocity of approximately two.

C. Pinned Autorotation

A calculation was performed for a plate undergoing pinned autorotation. This was analogous to a plate being held at its center of gravity by frictionless bearings in a wind tunnel. Pinned autorotation was numerically modeled by eliminating equations (88) and (89) in the flight mechanics equations. The only permissible degree of freedom was rotation which meant only equations (94) and (95) were solved to determine the motion of the plate.

The flow field around a plate moving at sea level in a freestream

velocity of 3.0 ft/sec at a fixed angle of attack of 0.1 radians was calculated and used as an initial condition for rotation. The plate with the physical characteristics displayed in Table I was "released" and allowed to autorotate by solving equations (94) and (95).

Table I. Physical Characteristics of the Plate

Chord	3 inches
Span	8 inches
Aspect Ratio	2.67
Weight	7.02×10^{-3} lbs
Moment of Inertia	1.13×10^{-6} lb_f sec^2 ft

The plate began rotating and established autorotation at a mean nondimensional rate of rotation of 1.58. This rate of rotation was within the range suggested by analyzing the moment in the forced rotation studies. The aerodynamic coefficients produced by the plate undergoing pinned autorotation are shown in Figure 19. In this plot, angle of attack and rotation angle are synonymous. The magnitude of the coefficients are comparable to those produced by the plate undergoing forced rotation at a nondimensional rotational velocity of 2.0. The maximum drag coefficient lags the maximum lift coefficient by approximately 0.70 radians. The maximum moment coefficient is in phase with the maximum lift coefficient. The numerically integrated area under the moment curve was zero for a complete revolution after

equilibrium autorotation was established.

The rate of rotation varied considerably during pinned autorotation because of the relatively small mass of the plate used in this study. E.H. Smith (Ref 14) found that the rate of rotation of a relatively dense plate undergoing pinned autorotation in a wind tunnel was almost constant. Lugt assumed a constant rate of rotation in his numerical research (Ref 57). The relatively small mass of the plate in this study produced the variations in the rate of rotation shown in Figure 20.

D. Free Fall Autorotation

Finally the plate with the physical characteristics presented in Table I was allowed to undergo free fall autorotation. The initial conditions for the plate were moving down and to the right with a velocity of 3.0 ft/sec at a glide path angle of $-\pi/4$ radians. The plate was fixed at a rotation angle of $-\pi/4+0.1$ radians which resulted in an angle of attack of 0.1 radians. The plate was "released" and allowed to free fall by solving the complete set of flight mechanics equations, equations (86) through (89) . The plate established autorotation within two revolutions as depicted in Figure 21. The trace of the numerically predicted flight path began at the point where the card was "released" and allowed to free fall. Experimental data of a plate with identical physical characteristics obtained using high speed photography (Ref 58) is shown in Figure 22. The experimental flight path was photographed after autorotation was fully established and thus did not include data for the launch phase.

The calculation of the free falling, autorotating, flat plate correctly predicted the complex relationship between the plate's rotational velocity and the linear velocity of its center of gravity. The experimental data presented in Figure 22 illustrates how the plate appears to pivot about its endpoints. The magnitude of the nondimensional linear velocity of the center of gravity and the nondimensional rate of rotation were changing periodically as illustrated in Figures 23 and 24 respectively. The angle of attack in these figures was obtained using equation (72). The relationship between the phasing and magnitude of the angular velocity and linear velocity must be precise to present the appearance that the plate rotates alternately about its endpoints. This complex phenomenon was accurately predicted by the numerical calculations indicating the procedure correctly modeled the complex flow field and properly related the flow field to the three degrees of freedom.

The plate in the numerical simulation was released at 3.0 ft/sec and developed into autorotation with a mean velocity of approximately 3.01 ft/sec. The mean velocity of the experimental plate was approximately 3.75 ft/sec. The plate in the numerical simulation autorotated at a mean rotational velocity of 19.56 rad/sec while the experimental plate was found to rotate at approximately 23.4 rad/sec.

The predicted flight path of the plate did not compare well with the experimental flight path. The calculations predicted a mean flight path angle of approximately -0.20 radians compared to -0.81 radians in the experimental data. This discrepancy in flight path angle may have

been caused by three dimensional effects. The experimental plate may have produced a complex three dimensional vortex which degraded the lift to drag ratio. The calculations simulated a plate with an infinite aspect ratio and did not model the three dimensional effects. The numerical plate should therefore have a higher lift to drag ratio than the experimental plate which would tend towards a more shallow flight path angle.

The calculated aerodynamic coefficients produced by the plate during free fall autorotation are shown in Figure 25. The maximum drag lags the maximum lift by approximately 0.71 radians. The moment is in phase with the lift. In contrast to the plate undergoing forced rotation, the moment is not in phase with the lift. The moment being in phase with the lift seems to be a necessary condition for autorotation. The moment averaged over each cycle is zero which is required in fully established autorotation. The experimentally determined coefficients for a plate with the same physical characteristics (Ref 58) are shown in Figure 26.

The aerodynamic coefficients encountered in the free falling autorotation calculations were considerably larger than the coefficients obtained at static angles of attack. A comparison between the static drag polar for a flat plate and the drag polar for a free falling, autorotating, flat plate are shown in Figure 27. The large differences between the static and dynamic aerodynamic coefficients are the primary reason that past attempts to calculate autorotation using quasi-steady numerical techniques have failed. The unsteady, nonlinear aerodynamic

forces are an essential ingredient in autorotation.

For the first time since initial attempts were made to explain the free falling, autorotating, flat plate in 1854, the complete flow field around the plate is known. The instantaneous streamlines and corresponding lines of constant vorticity at several angles of attack are shown in Figure 28 and 29, respectively. Each plot has been rotated so the freestream velocity is always coming from the right. It is difficult to see the vortices being shed from the plate in Figure 28. However, the vorticity contours shown in Figure 29 illustrate the asymmetry caused by the rotation. A.M.O. Smith realized in 1953 that this asymmetry is essential for autorotation.

The flight paths of the plate released with different initial conditions were also found to compare qualitatively with experiment. The plate was released similarly to the previous case, however, the initial velocity was increased to 6.0 ft/sec. The initial flight path was slightly different as shown in Figure 30 but the fully developed autorotation was identical to the previous case.

In another launch mode the plate was initially moving to the right with a velocity of 6.0 ft/sec at a glide path angle of -0.1 radians and a fixed angle of attack of 0.1 radians. The plate was "released" and reversed direction as shown in Figure 31. The plate did not have sufficient inertia to rotate past the portion of the flight where it experienced a retarding moment. The plate stopped rotating, reversed direction, and established autorotation, falling in the opposite

direction. After autorotation was established, the flight characteristics of the plate were identical to the previous free fall autorotation cases only the plate was moving in the opposite direction. A similar flight path was demonstrated experimentally by the author, however, it was not documented with high speed photography. Numerical experimentation with the different launch modes indicates the plate will establish the same autorotation mode independently of the launch mode.

SECTION VII

CONCLUSIONS AND RECOMMENDATIONS

The goal of this research was to develop a method of coupling an unsteady, nonlinear aerodynamic prediction technique with the flight mechanics equations and to show the method was a valid approach to use in predicting the flight path of a free falling, autorotating, flat plate. A numerical technique which combined a two dimensional Navier-Stokes aerodynamic prediction program with a three degrees of freedom trajectory program was developed and used to predict the flight path of a free falling, autorotating, flat plate. The overall approach was validated by comparing the numerically predicted flight path with the experimental flight path.

An numerical method which coupled a Navier-Stokes equations solver and a flight mechanics equations solver was developed. The two dimensional incompressible Navier-Stokes equations were solved using an implicit, finite difference, numerical solution technique. The physical domain, which was modeled by a patched, exponentially stretched, Cartesian grid, was transformed into an evenly spaced computational domain. The Navier-Stokes equations were formulated in a coordinate system attached to the plate and the corresponding velocities were formulated in an inertial reference system. The translation and rotation of the plate were modeled by imposing them as a boundary conditions on the body. The resulting system of equations was solved using a successive-over-relaxation iteration technique. The aerodynamic coefficients were calculated by summing the viscous and pressure forces

around the plate.

The three degrees of freedom flight mechanics equations were reduced to four simultaneous first order ordinary differential equations. The aerodynamic coefficients were entered as forcing functions into the flight mechanics equations. The system of equations was solved using an open Adams method. The calculated translation and rotation of the plate were used as new boundary conditions in the Navier-Stokes equations solver. The procedure was repeated thousands of times to generate the flight path of the plate.

The Navier-Stokes equations solver was used to predict the flow field around a flat plate at several fixed angles of attack. The flow field was unsteady above approximately 0.15 radians angle of attack which corresponded to a lift coefficient of approximately 0.44. The maximum static lift coefficient for a flat plate was found to be approximately 1.2.

The flow fields around a flat plate undergoing forced rotation at three different rates of rotation were calculated. The maximum lift coefficients were approximately 3.2, 5.8 and 9.5 for nondimensional rotational rates of 1.0, 2.0, and 4.0 respectively. The maximum drag coefficient and the maximum moment coefficient lagged the maximum lift coefficient.

A flat plate undergoing pinned autorotation was modeled by allowing one degree of freedom (rotation). The plate was released at a small

angle of attack and established autorotation at a mean nondimensional angular velocity of 1.58. The magnitude of the aerodynamic coefficients were comparable to these produced by the plate undergoing forced rotation at an angular velocity of 2.0. The maximum drag coefficient again lagged the maximum lift coefficient, however, the maximum moment coefficient was in phase with the maximum lift coefficient.

Finally the complete set of equations was used to calculate the flight path of a free falling, autorotating, flat plate. The flight path predicted by the numerical method compared well with the experimental flight path. The maximum lift coefficient produced during fully developed autorotation was approximately 6.2 which was several times larger than the maximum lift coefficient obtained at a fixed angle of attack. This explains why previous attempts were unsuccessful in using quasi-steady aerodynamic techniques to predict autorotation. The maximum moment was in phase with the maximum lift which seems to indicate the moment must be in phase with the lift to support autorotation.

Developing and demonstrating a procedure to solve a problem which incorporates the essential elements of a spinning aircraft is a path finder. This path finder will assist in the future analyses of the complete aircraft spin problem. In addition, this research effort has advanced the state of the art in several other areas:

1) Identifying the "mixed" reference system for future application to spin computations was the most important contribution of this study. Previous aerodynamic calculations for rotating bodies were performed in

coordinate and velocity reference systems attached to the body. This approach was found to have undesirable characteristics as faster rotation rates were introduced. More accurate results were obtained when the coordinate system was attached to the rotating plate and the corresponding velocities were formulated in an inertial reference system.

2) Lugt solved the two dimensional Navier-Stokes equations for a thin ellipsoid rotating at a constant, predetermined rate of rotation. However, it was not until this research effort that the rate of rotation was allowed to vary during the calculation. The rate of rotation was calculated from the aerodynamic moment which resulted in true pinned autorotation.

3) First principle aerodynamic calculations have not been used when solving the three degrees of freedom equations of motion. A method was developed to couple a two dimensional Navier-Stokes equations solver with a three degrees of freedom equations of motion solver. To the author's knowledge, this was the first time an unsteady, nonlinear aerodynamic prediction technique was used in solving the three degrees of freedom equations of motion. The overall approach was verified by comparing the numerical results with experimental data.

4) The time steps used in finite difference solutions of the Navier-Stokes equations are usually constant throughout a calculation or are changed manually by the programmer. This study was the first time the time step in a Navier-Stokes equations solver was varied during a calculation based on the results of the movement of a body. This significantly reduced the computing time necessary to obtain a solution.

It is recommended that the pursuit of a numerical solution of a complete spinning aircraft be continued even though the final goal is not feasible on today's computers. Three near term research efforts are recommended to continue building the technology base necessary to eventually calculate the flight path of a spinning aircraft:

1) The cause of the discrepancy between the numerically predicted and experimental flight paths should be determined. The numerical procedure should be modified to improve the correlation between the two flight paths.

2) The six degrees of freedom autorotation of a three dimensional object should be calculated using linear aerodynamics. The spinning maple seed offers a good physical example of such a problem. The flow field around the maple seed is probably attached, therefore lending itself to analysis by linear aerodynamics. This would allow the researcher to couple the two systems of equations without expending the large amount of computer resources to support a Navier-Stokes aerodynamic solution.

3) Finally, a three dimensional Navier-Stokes equations solver should be coupled to a six degrees of freedom equations of motion solver. The computational method should be used to calculate the autorotation of a relatively simple aerodynamic shape such as a pure delta wing. This problem can probably be solved on today's computers.

BIBLIOGRAPHY

1. Westbrook, C.B. (Chairman) Symposium Stall/Post-Stall/Spin, WPAFB, 1971.

2. Burns, B.R.A. "Advanced Fighter Design," Air International. pp 123-129. September 1983.

3. Neilhouse, A.I. et al. "Status of Spin Research for Recent Airplane Designs." NASA TR R-57, 1960.

4. Bairstow, L. Applied Aerodynamics. New York: Longmans, Green and Co., 1939. 212.

5. Spangler, S.B. and Dillenius, M.F.E. "Investigation of Aerodynamic Loads at Spin Entry." ONR-CR212-225-2, May 1976.

6. Hankey, W.L. "Introduction to Computational Aerodynamics." AFWAL-TR-82-3031. April 1983.

7. Lugt, H.J. "Autorotation of Plates." DTNSRDC-78/058, August 1978.

8. Maxwell, J.C. "On a Particular Case of the Descent of a Heavy Body in a Resisting Medium." Scientific Papers, Cambridge University Press, p 115, 1890.

9. Riabouchinsky, D.P. "Thirty Years of Theoretical and Experimental Research in Fluid Mechanics," Journal of the Royal Aeronautical Society, 39 (1935), 282.

10. Dupleich, P. "Rotation in Free Fall of Rectangular Wings of Elongated Shape." NACA TM 1201, April 1949.

11. Smith, A.M.O. "On the Motion of Tumbling Body," The Journal of Aeronautical Sciences, Vol 20, No 2, pp 73-84, February 1953.

12. Bustamante, A.C. and Stone, G.W. "The Autorotation Characteristics of Various Shapes in Subsonic and Hypersonic Flows." SC-RR-69-159, August 1969.

13. Iversen, J.D. "Autorotating Flat-Plate Wings: The Effect of the Moment of Inertia, Geometry and Reynolds Number," Journal of Fluid Mechanics, Vol 92, pp 327-348, 1979.

14. Smith, E.H. "Autorotating Wings: An Experimental Investigation," Journal of Fluid Mechanics, Vol 50, pp 513-534, 1971.

15. Kry, P.R. and List, R. "Angular Motion of Freely Falling Spheroidal Hailstone Models," The Physics of Fluids, Vol 17, No 6, pp 1093-1102, June 1974.

16. Hodge, J.K. Numerical Solution of Incompressible Laminar Flow About Arbitrary Bodies in Body-Fitted Curvilinear Coordinates. PhD

Dissertation. Mississippi State University, December 1975.

17. Shang, J.S. "Oscillatory Compressible Flow Around a Cylinder." AIAA-82-0098, 1982.

18. Hodge, J.K. and Stone, A.L. "Numerical Solution for Airfoils Near Stall in Optimized Boundary-Fitted Curvilinear Coordinates," AIAA Journal, 17 (1979), 458.

19. Takemitsu, N. and Matunobu, Y. "Unsteady Stagnation-Point Flow Impinging on an Oscillating Flat Plate," Journal of the Physical Society of Japan, Vol 47, No 4, October 1979.

20. Hasen, G.A. "Navier-Stokes Solution for an Axisymmetric Nozzle in a Supersonic External Stream," AFWAL-TR-81-3161. March 1982.

21. Brent, R.P. "An Algorithm with Guaranteed Convergence for Finding a Zero of a Function," The Computer Journal, 14(4), 1971. pp 422-425.

22. Harlow, F.H. and Welch, J.E. "Numerical Calculation of Time-Dependent Viscous Incompressible Flow of Fluid with Free Surface," The Physics of Fluids, Vol 8, No 12, December 1965.

23. Hirt, C. and Harlow, F. "A General Corrective Procedure for the Numerical Solution of Initial Value Problems," Journal of Computational Physics, 2 (1967), 114.

24. Steger, J.L. and Bailey, A.E. "Calculation of Transonic Aileron Buzz," AIAA Journal, Vol 18, No 3, March 1980, pp. 249-255.

25. Sankar, N. and Wu, J.C. "Viscous Flow Around Oscillating Airfoils - A Numerical Study," AIAA Paper 78-1225, 1978.

26. Hegna, H.A. "Numerical Prediction of Dynamic Forces on Arbitrarily Pitched Airfoils in Turbulent Flow." AIAA-82-0092, January 1982.

27. Thompson, J.F. "Numerical Solution of the Incompressible, Two-Dimensional, Time-Dependent Navier-Stokes Equations for a Body Oscillating in Pitch in a Moving Fluid." Mississippi State University, Research Report No. 86, October 1968.

28. Raucher, M. Introduction to Aeronautical Dynamics. New York. Wiley and Sons, Inc., 1953.

29. Schlichting, H. Boundary Layer Theory. New York: McGraw-Hill. 1968.

30. Kuethe, A.M. and Schetzer, J.D. Foundations of Aerodynamics. London: Wiley and Sons, Inc., 1959.

31. Chorin, A. "Numerical Solution of the Navier-Stokes Equations," Math. Comp., 22(1968), 745.

32. Ghia, K., Hankey, W. and Hodge, J. "Study of Incompressible

Navier-Stokes Equations in Primitive Variables Using Implicit Numerical Technique," AIAA Paper 77-0648, 1977.

33. Buzbee, B.L. et al "On Direct Methods for Solving Poisson's Equations," SIAM Journal of Numerical Analysis, 7 (1970), 627.

34. Steger,J. "Implicit Finite Difference Simulation of Flow About Arbitrary Two-Dimensional Geometries," AIAA Journal, 16 (1978), 679.

35. Beam, R. and Warming, R. "An Implicit Finite Difference Algorithm for Hyperbolic Systems in Conservative-Law-Form," Journal of Computational Physics, 22 (1976), 87.

36. Roache, P. Computational Fluid Mechanics. New Mexico: Hermosa Publishers. 1976.

37. Hegna, H.A. "The Numerical Solution of the Navier-Stokes Equations for Incompressible Turbulent Flow Over Airfoils." AFWAL-TR-81-3053, October 1981.

38. Hokenson, G. "Numerical Experiments with the Two-and-Three-Dimensional Unsteady Navier-Stokes Equations." Naval Postgraduate School-57Hw73041A, April 1973.

39. Chien, J. "Vorticity-Stream Function Formulation of Compressible and Incompressible Turbulent Internal Flows." AEDC-Tr-79-13, 1979.

40. Reddy, R. and Thompsom, J. "Numerical Solution of Incompressible Navier-Stokes Equations in the Integro-Differential Formulation Using Boundary-Fitted Coordinate Systems," AIAA Paper 77-659, 1977.

41. Hodge, J.K. Professor Air Force Institute of Technology (personal communications). 1982-1983.

42. Sankar, N.L. and Tassa, Y. "Reynolds Number and Compressibility Effects on Dynamic Stall on a NACA 0012 Airfoil." AIAA-80-0010, January 1980.

43. Mehta, U. and Lavan, Z. "Starting Vortex, Separation Bubbles, and Stall: A Numerical Study of Laminar Unsteady Flow Around an Airfoil," Journal of Fluid Mechanics, 67 (1975). 227.

44. Hughes, W.F. and Brighton, J.A. Theory and Problems of Fluid Dynamics. New York: Shaums Publishing Company. 1967.

45. Etkins, B. Dynamics of Flight. New York: Wiley and Sons. 1959.

46. Perkins, C.D. and Hage, R.E. Airplane Performance Stability and Control. New York: Wiley and Sons, Inc., 1949.

47. Soong, T.C. "The Dynamics of Discus Throw," Journal of Applied Mechanics. pp 531-536, December 1976.

48. Hornbeck, R.W. Numerical Methods. Quantum Publishers. 1975.

49. Napolitano, M. "Simulation of Viscous Steady Flow Past an Arbitrary Two-Dimensional [illegible]." AFWAL-TR-80-3038. February 1980.

50. Briley, W. and McDonald, H. "Solution of the Multidimensional Compressible Navier-Stokes Equations by a Generalized Implicit Method," Journal of Computational Physics, 24 (1977), 372.

51. Hegna, H.A. "Numerical Solution of Incompressible Turbulent Flow Over Airfoils." PhD Dissertation, Air Force Institute of Technology. 1980.

52. Thompson, J.F. "Computer Experimentation with an Implicit Numerical Solution of the Navier-Stokes Equations for an Oscillating Body." AIAA Paper No. 69-185. 1969.

53. Lugt, H.J. "The Dilemma of Defining a Vortex. Naval Ship Research and Development Center, CMD-11-74, March 1974.

54. Belotserkovskiy, S.M. and Nisht, M.I. "Attached and Separated Flow of an Ideal Fluid Around Thin Wings." Moscow. 1978.

55. Sarpkaya, T. "An Analytical and Experimental Study of the In-Line and Transverse Oscillations of a Circular Cylinder in Uniform Flow." Naval Postgraduate School Rep. NPS-59SL75051-B, May 1975.

56. Hoerner, S.F. Fluid-Dynamic Drag. Published by the Author. 1958.

57. Lugt, H.J. "Autorotatin of an Elliptic Cylinder About an Axis Perpendicular to the Flow,", Journal of Fluid Mechanics, Vol 99, pp 817-840, 1980.

58. Gallaway, C.R., Graham, J.E., and Hankey, W.L. "Flight Analysis of a Free-Falling Autorotating Plate." AFWAL-TM-83-177. 1983.

59. Shames, I.H. Mechanics of Fluids. New York: McGraw-Hill, pp 109-113 and pp 279-280, 1962.

60. Constant, W.F. Theoretical Physics, Mechanics of Particles, Rigid and Elastic Bodies, Fluids, and Heat Flow. Reading-Mass: Addison-Wesley Publishing Company, pp 69-73.

61. Lugt, H.J. and Ohring, S. "Rotating Elliptic Cylinder in a Viscous Fluid at Rest or in a Parallel Stream," Journal of Fluid Mechanics. 79, 1977.

62. Lugt, H.J. "Recent Advances in the Numerical Treatment of the Navier-Stokes Equations," AGARD Lecture Series No 86 on Computational Fluid Dynamics. 1977.

63. Milne-Thompson, L.M. Theoretical Hydrodynamics. New York: The MacMillan Co., 1968.

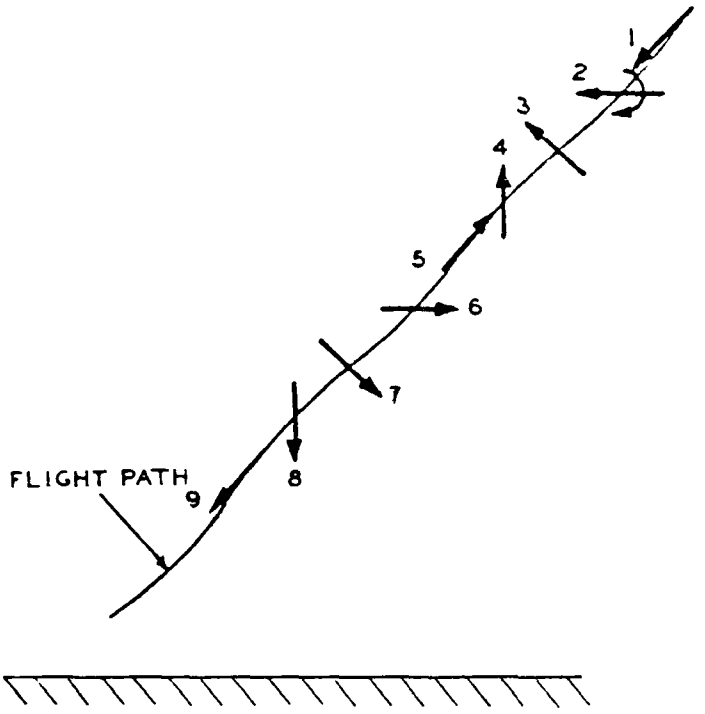

a)

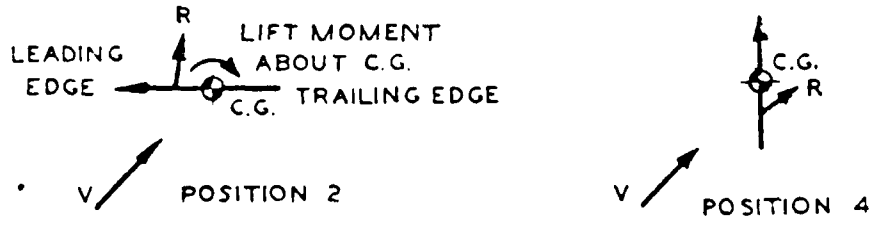

b)

Figure 1 Path of Free Falling Autorotating Flat Plate

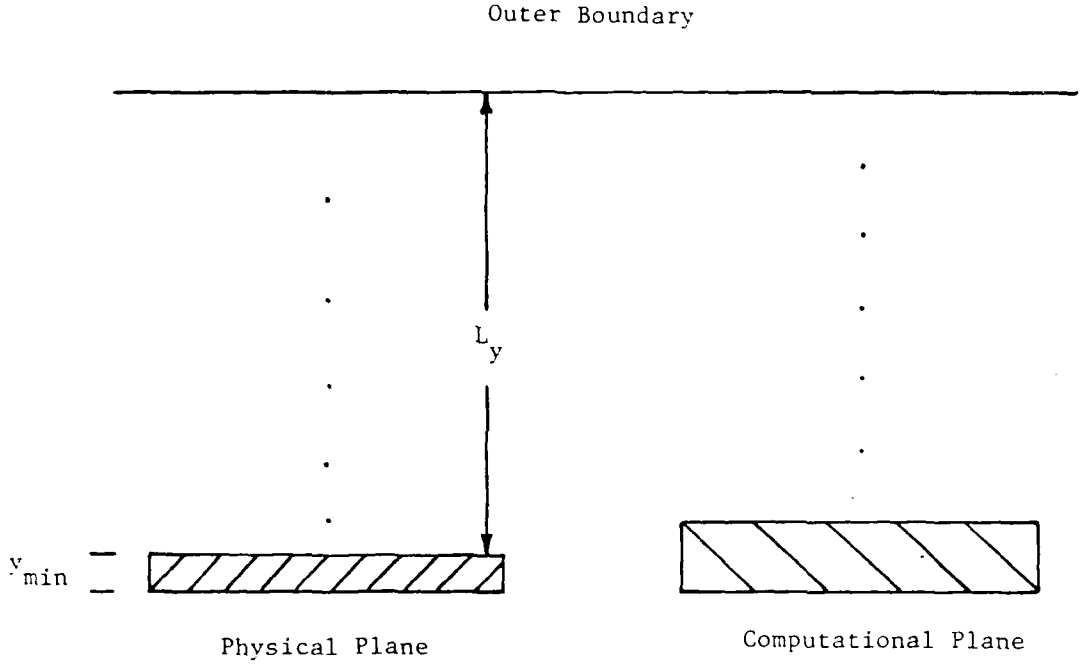

Figure 2 Physical and Computational Planes

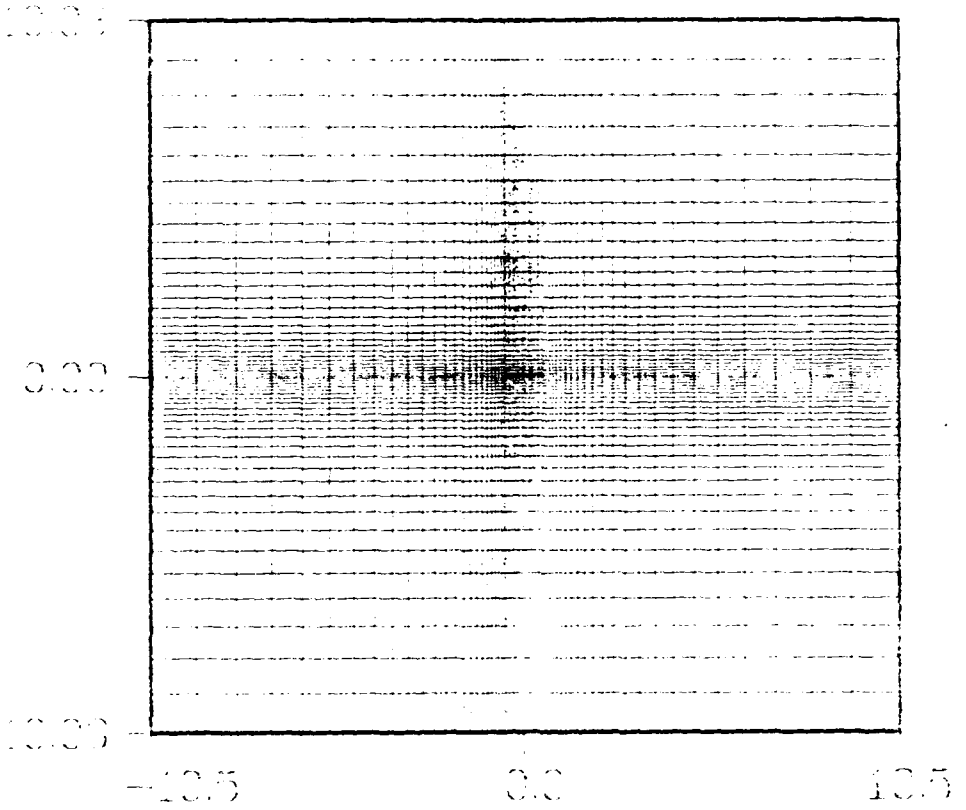

Figure 3 Physical Domain

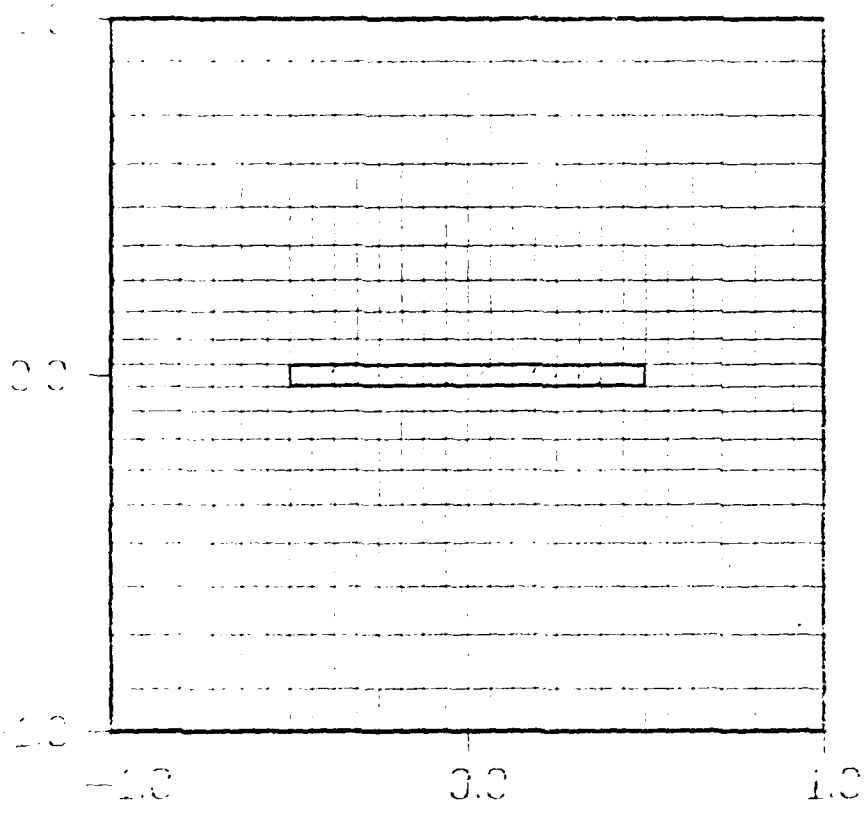

Figure 4 Close-Up of Physical Domain

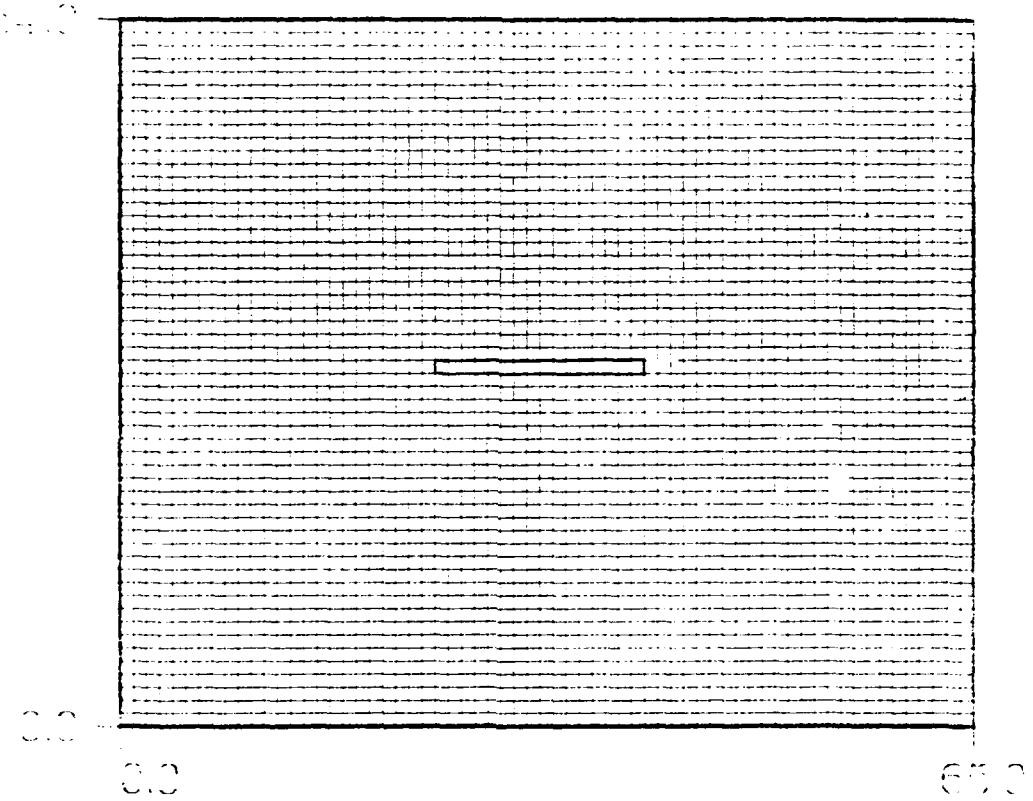

Figure 5 Computational Domain

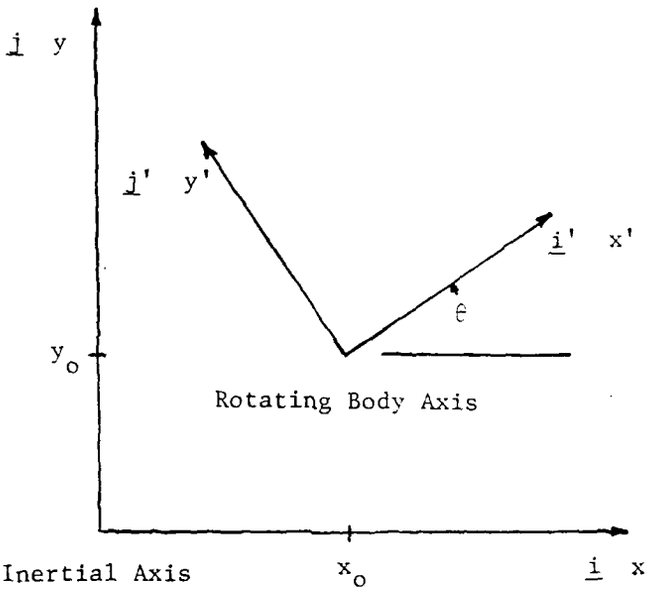

Figure 6 Flow Field Coordinate System

a) Translation

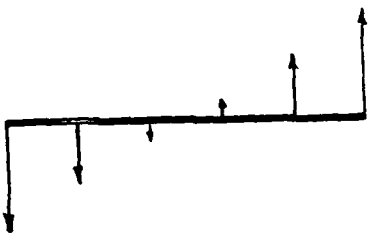

b) Rotation

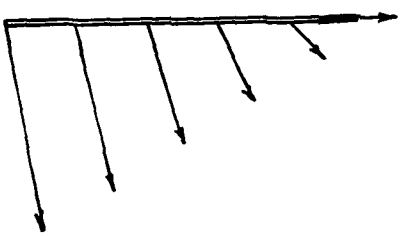

c) Translation and Rotation

Figure 7 Examples of Boundary Conditions

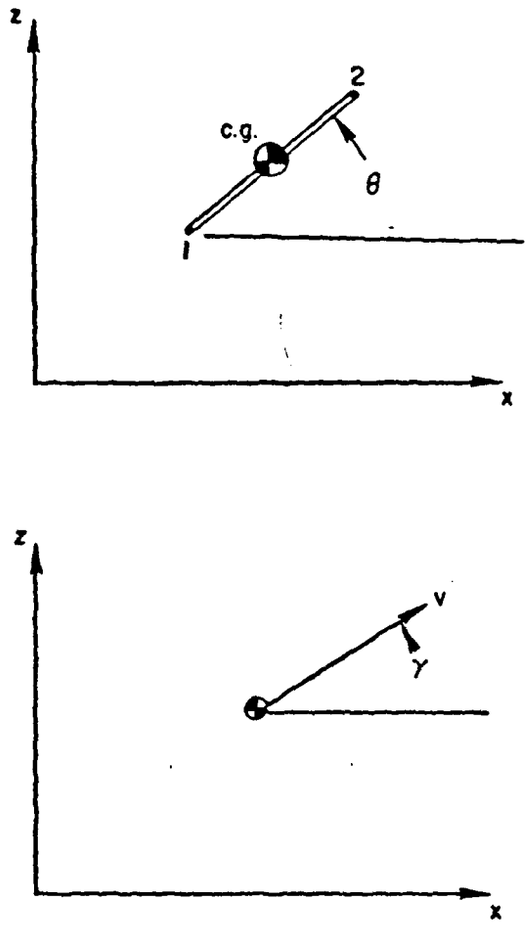

Figure 8 Flight Mechanics Reference System

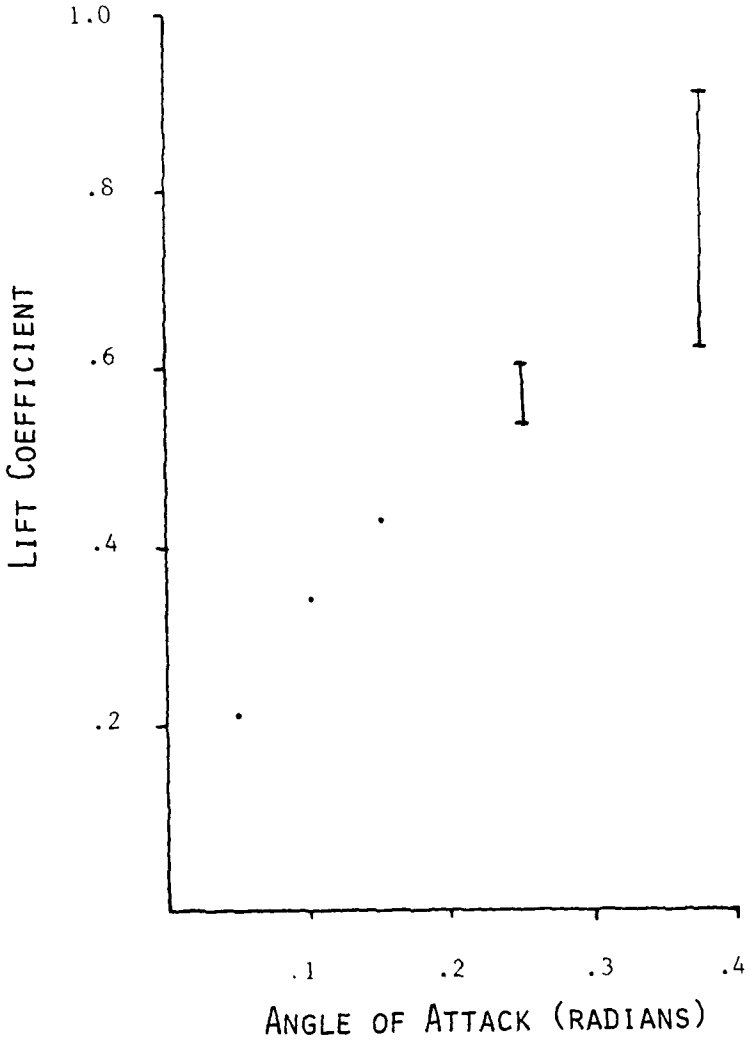

Figure 9 Static Lift Curve of a Flat Plate at Re≈5000

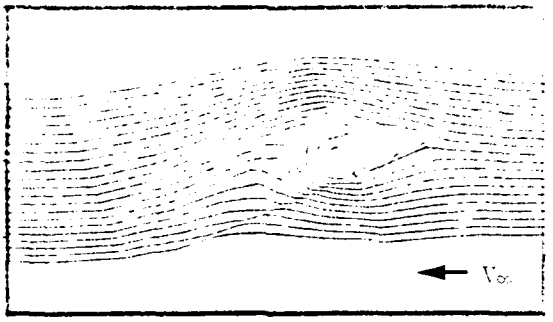

t=5.2

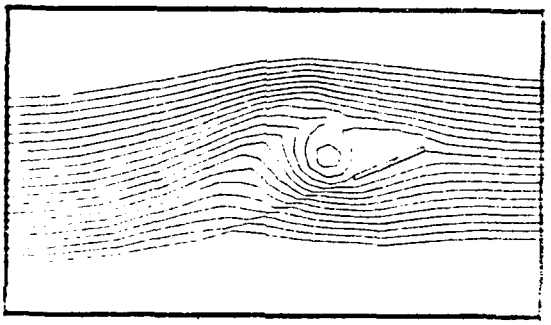

t=5.4

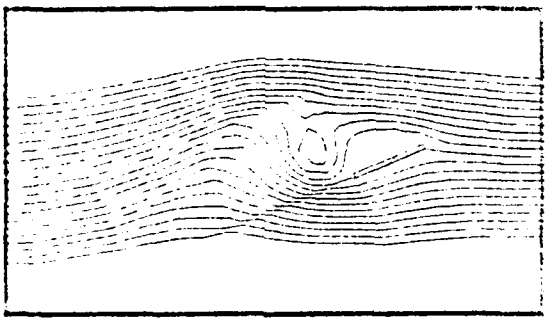

t=5.6

Figure 10 Unsteady Shedding Vortex Behind Flat Plate at α=0.4 radians and Re≅5000

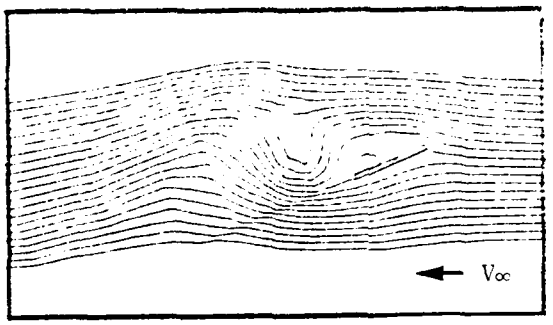

t=5.8

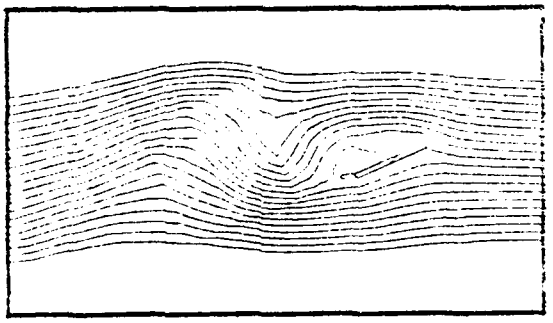

t=6.0

Figure 10 (cont.)

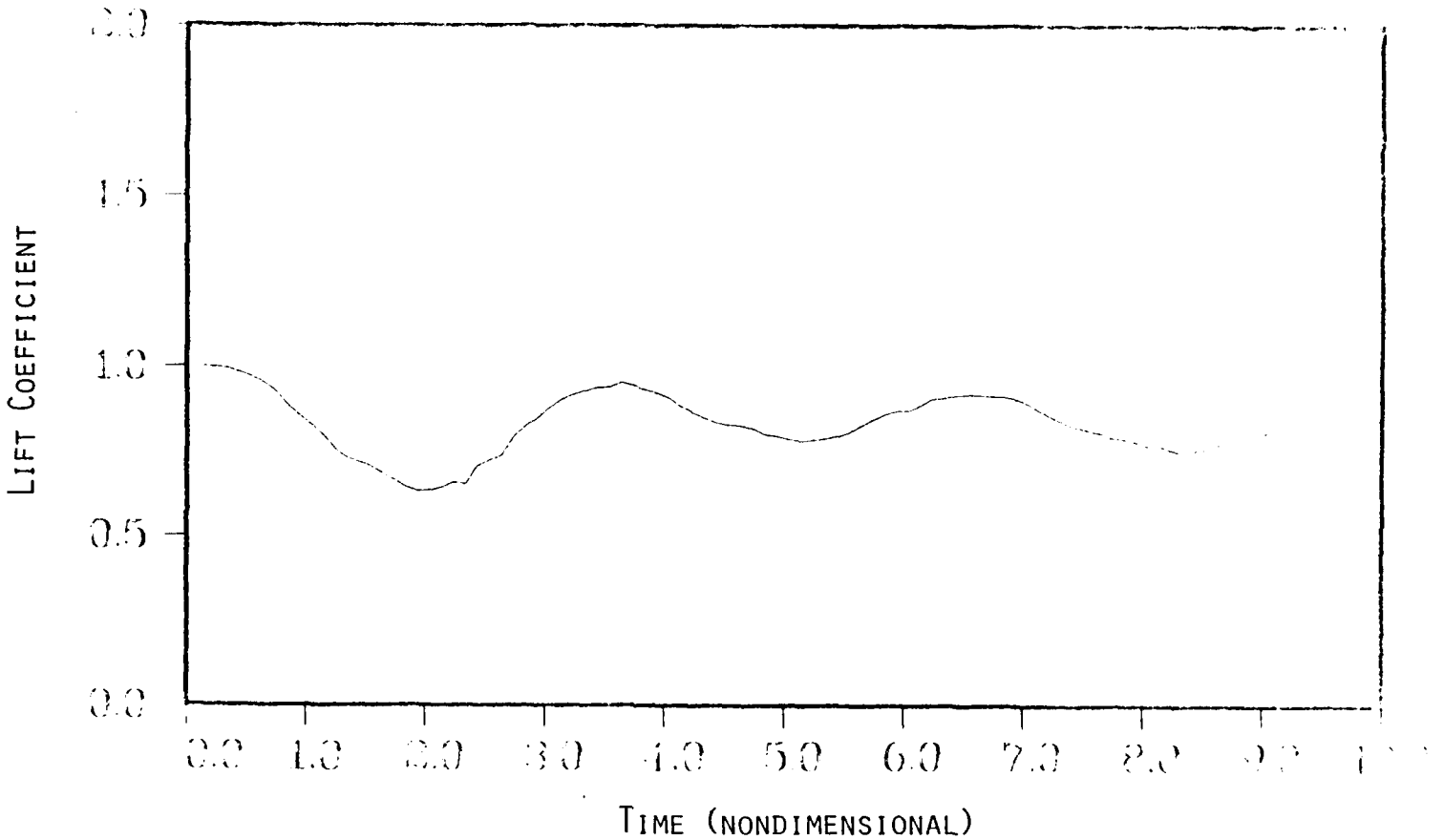

Figure 11 Lift Histogram of Flat Plate at α=0.4

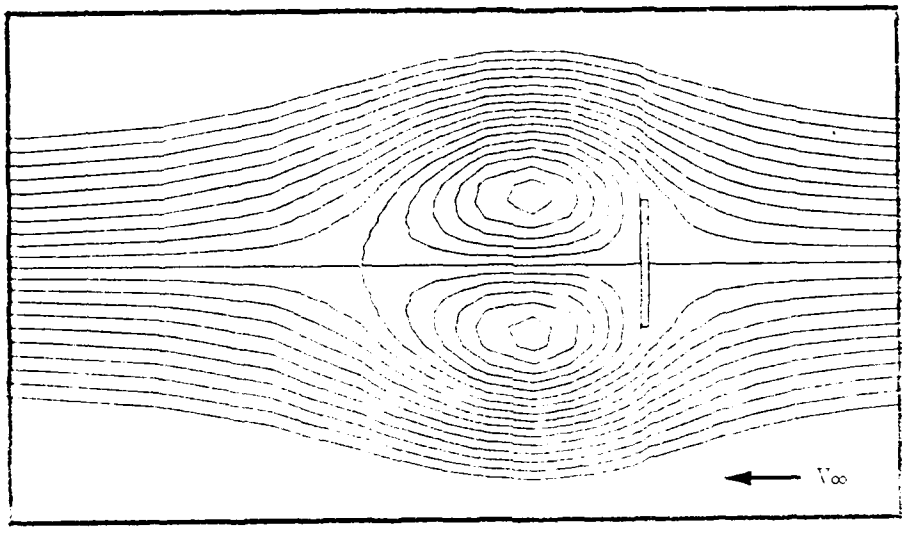

Figure 12 Steady Flow field Streamlines Around a Plate at $\alpha=\pi/2$, $Re\cong5000$

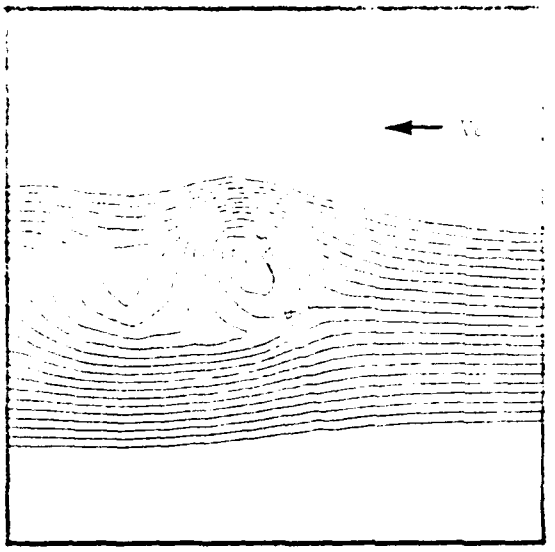

α =1.32

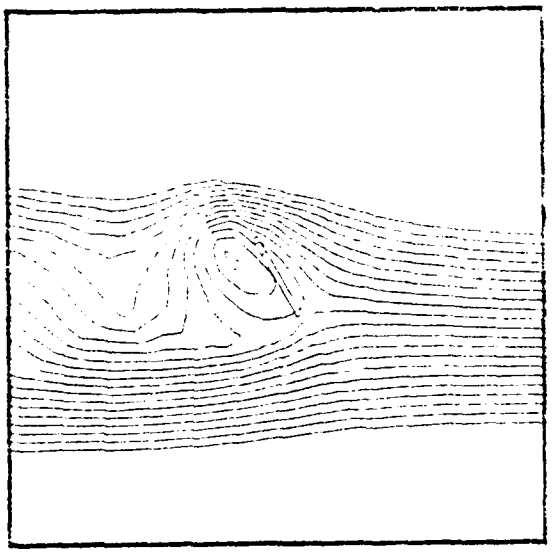

α =1.38

Figure 13 Streamlines Around a Flat Plate Undergoing Forced Rotation at $\dot{\theta}$=1

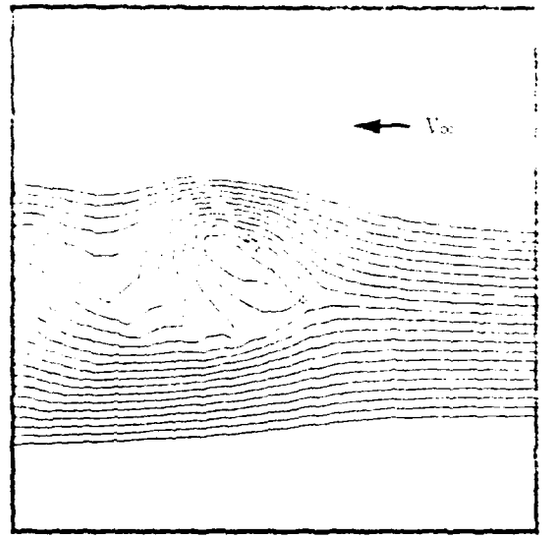

α =1.44

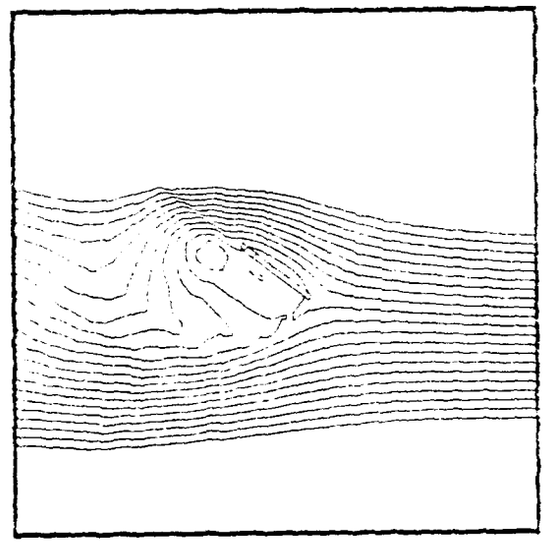

α =1.51

Figure 13 (cont.)

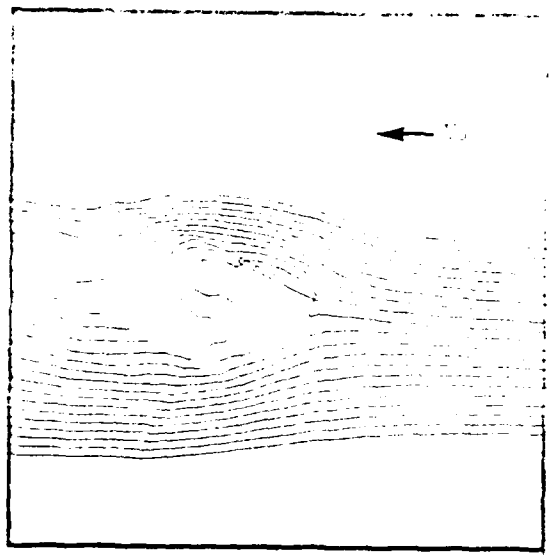

α =1.58

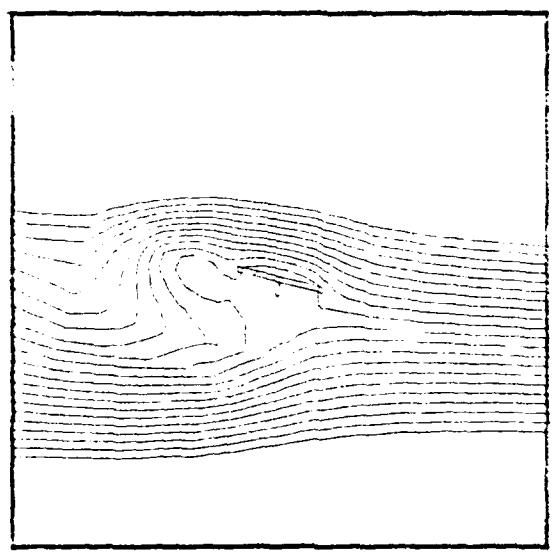

α =1.64

Figure 13 (cont.)

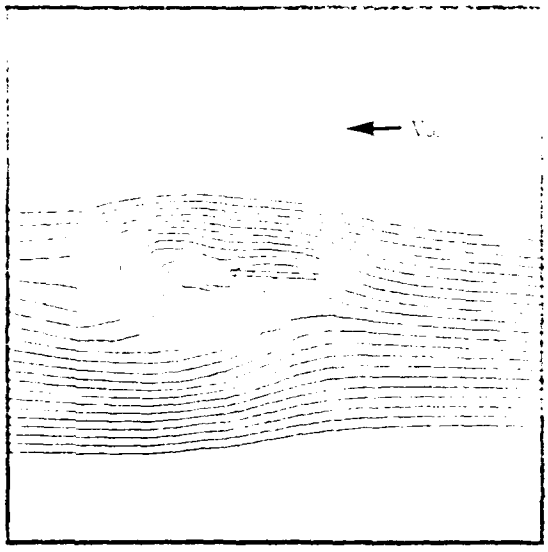

$\alpha = 1.70$

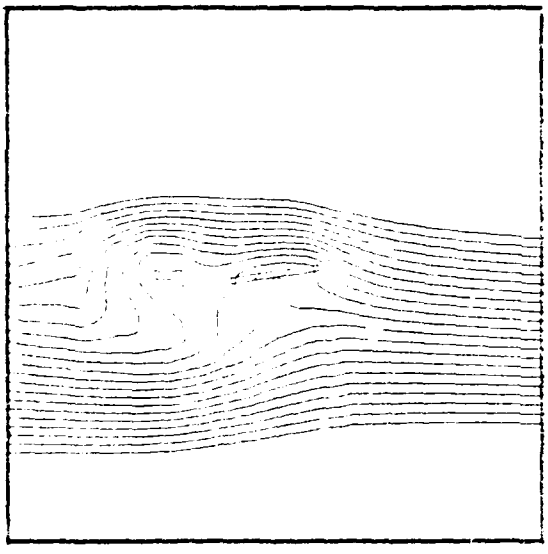

$\alpha = 1.77$

Figure 13 (cont.)

AD-A138 900 NUMERICAL AERODYNAMIC ANALYSIS OF A FREE FALLING AUTOROTATING PLATE(U) AIR FORCE INST OF TECH WRIGHT-PATTERSON AFB OH SCHOOL OF ENGINEERING

UNCLASSIFIED C R GALLAWAY OCT 83 AFIT/DS/AA/83-2 F/G 1/2 NL

2/2

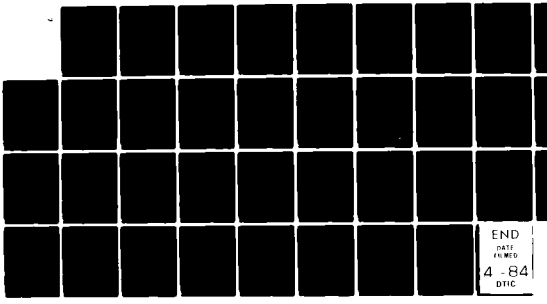

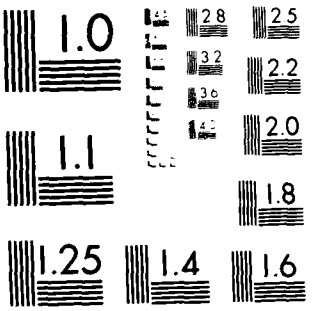

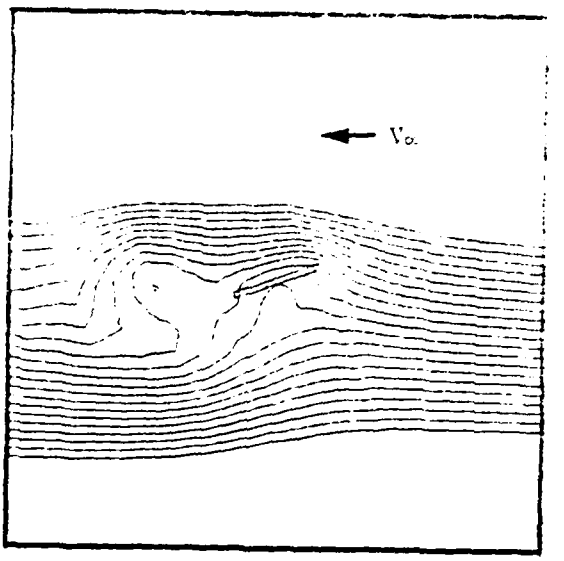

$\alpha = 1.84$

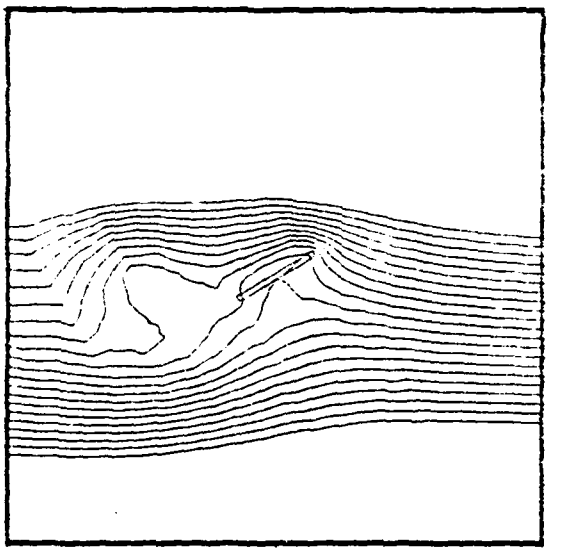

$\alpha = 1.91$

Figure 13 (cont.)

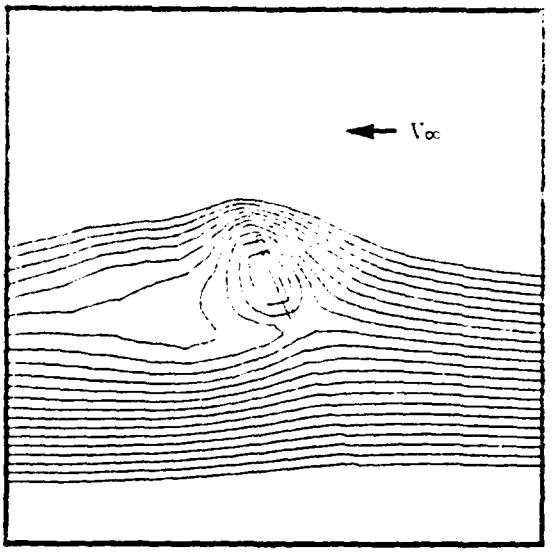

α =1.99

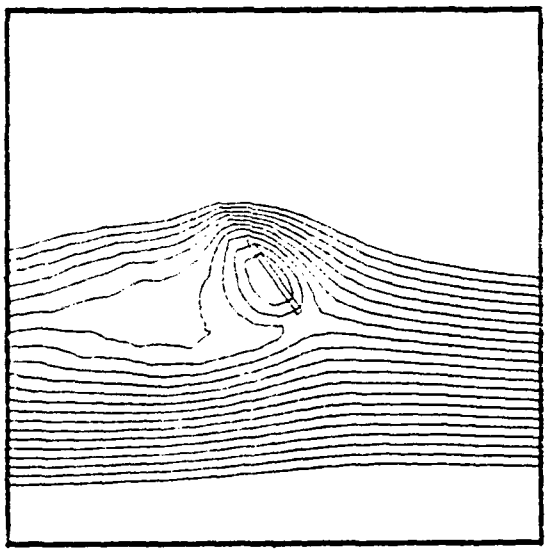

α =2.19

Figure 14 Streamlines Around a Flat Plate Undergoing Forced Rotation at $\dot{\theta}$=2

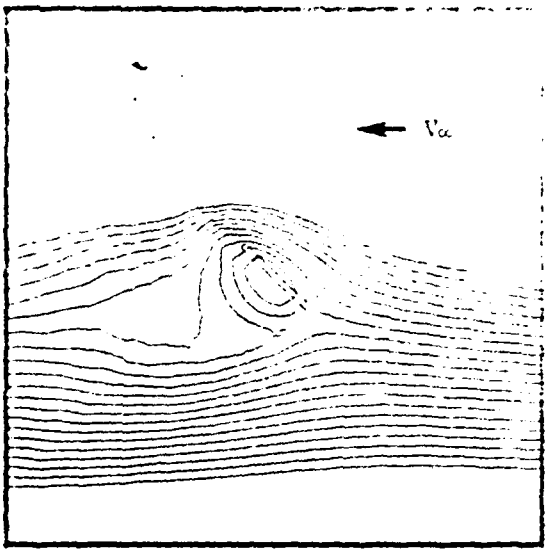

α =2.39

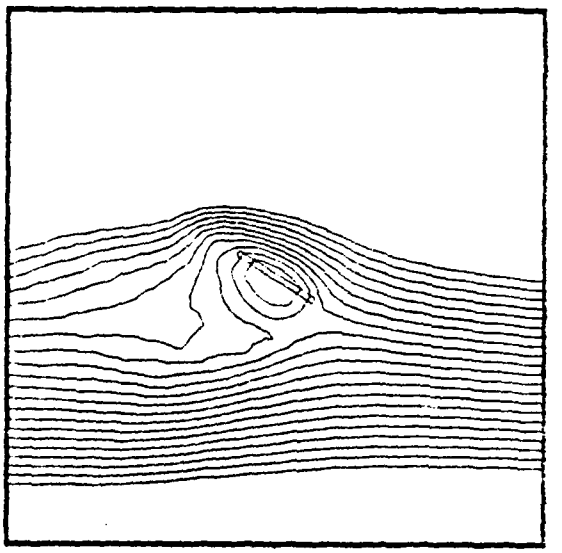

α =2.59

Figure 14 (cont.)

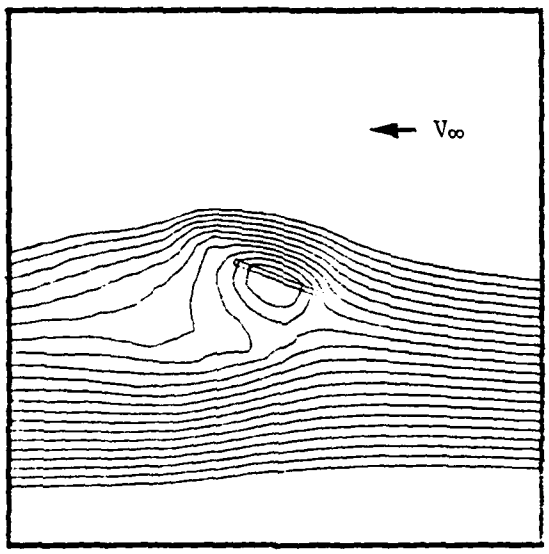

$\alpha = 2.79$

Figure 14 (cont.)

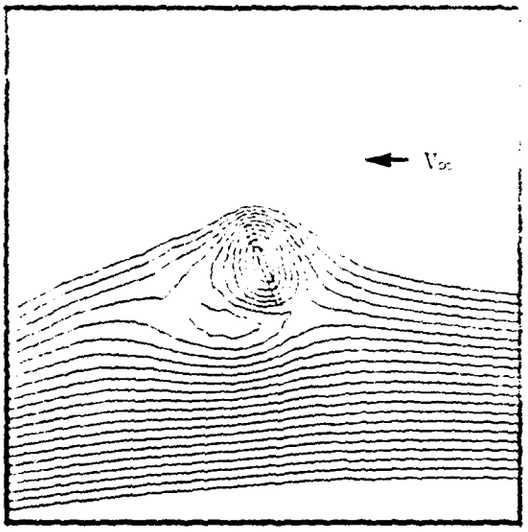

$\alpha = 1.99$

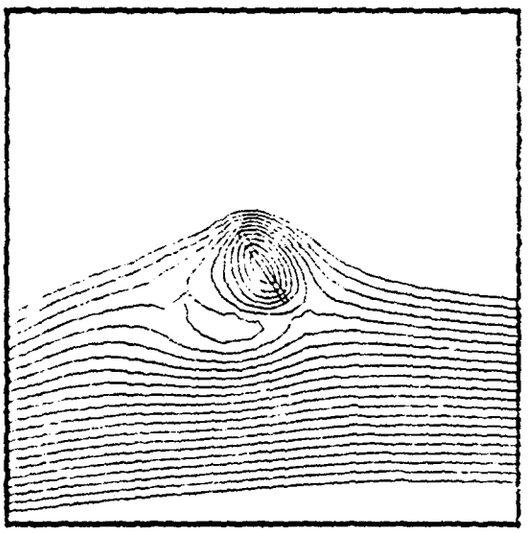

$\alpha = 2.19$

Figure 15 Streamlines Around a Flat Plate Undergoing Forced Rotation at $\dot{\theta}=4$

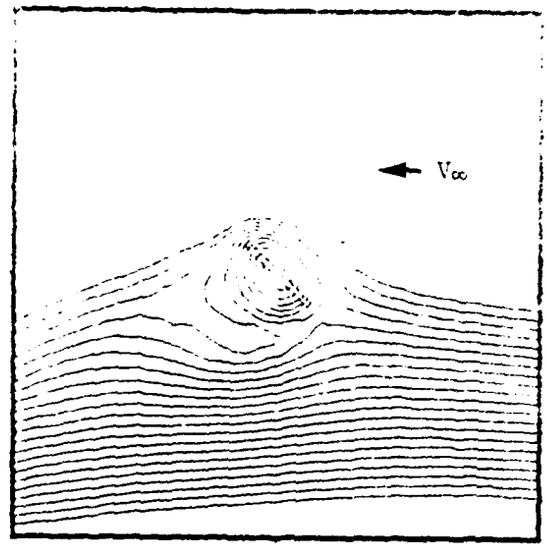

α =2.39

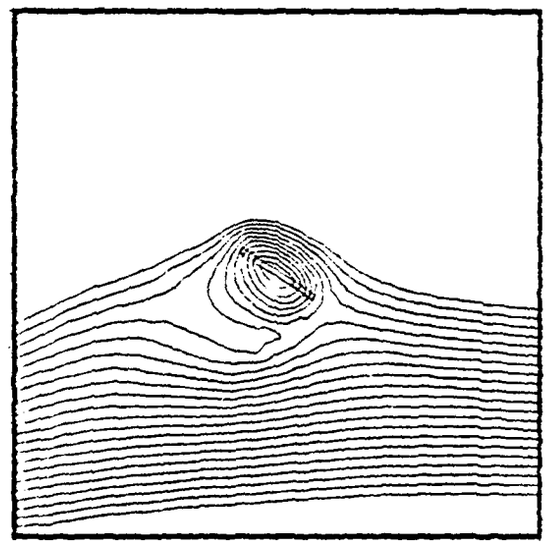

α =2.59

Figure 15 (cont.)

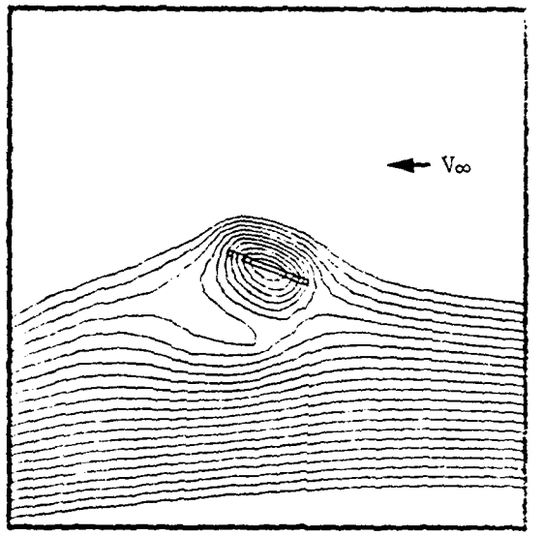

α =2.79

Figure 15 (cont.)

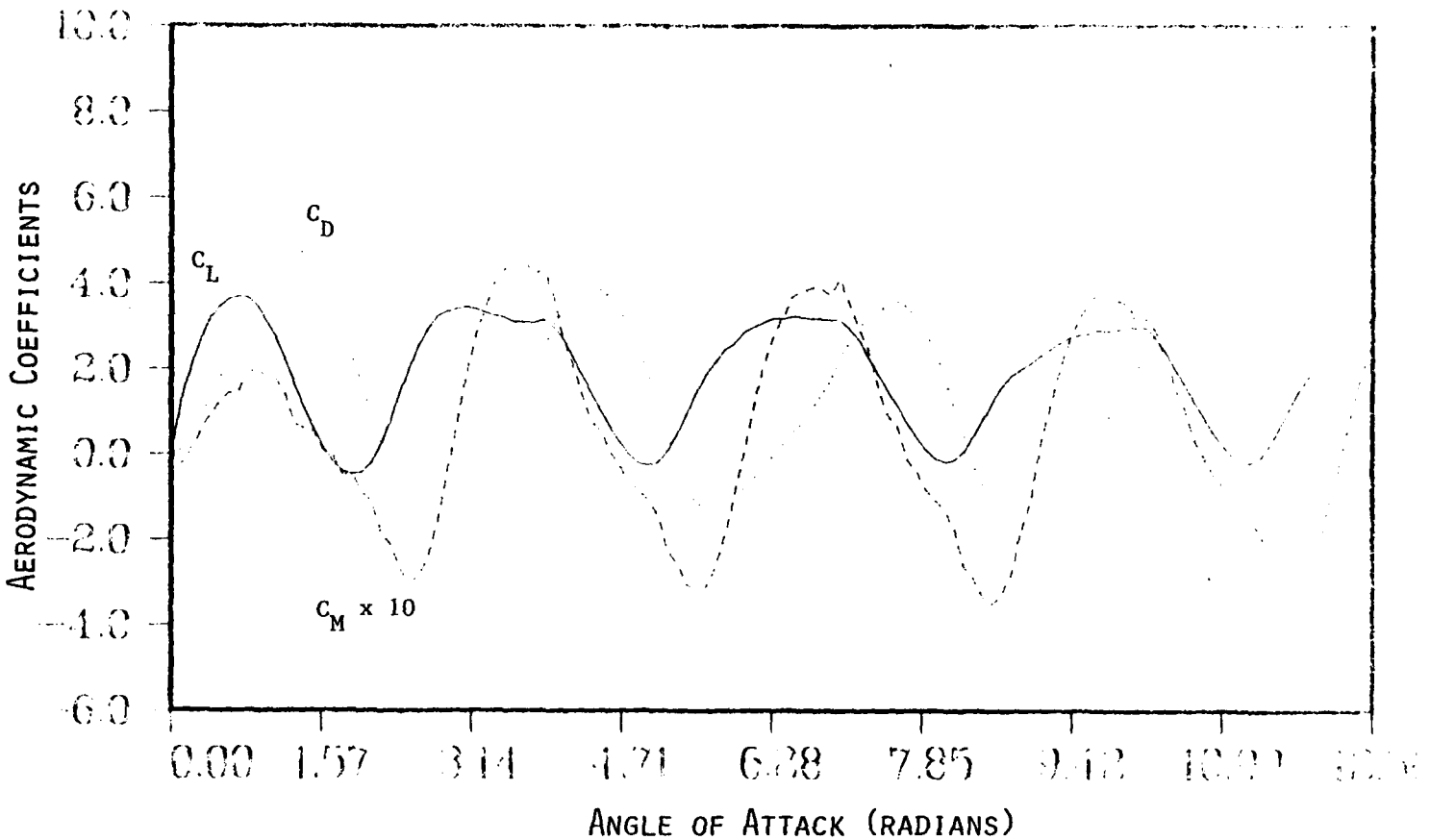

Figure 16 Aerodynamic Coefficients Produced by a Flat Plate Undergoing Forced Rotation at $\dot{\theta}$=1

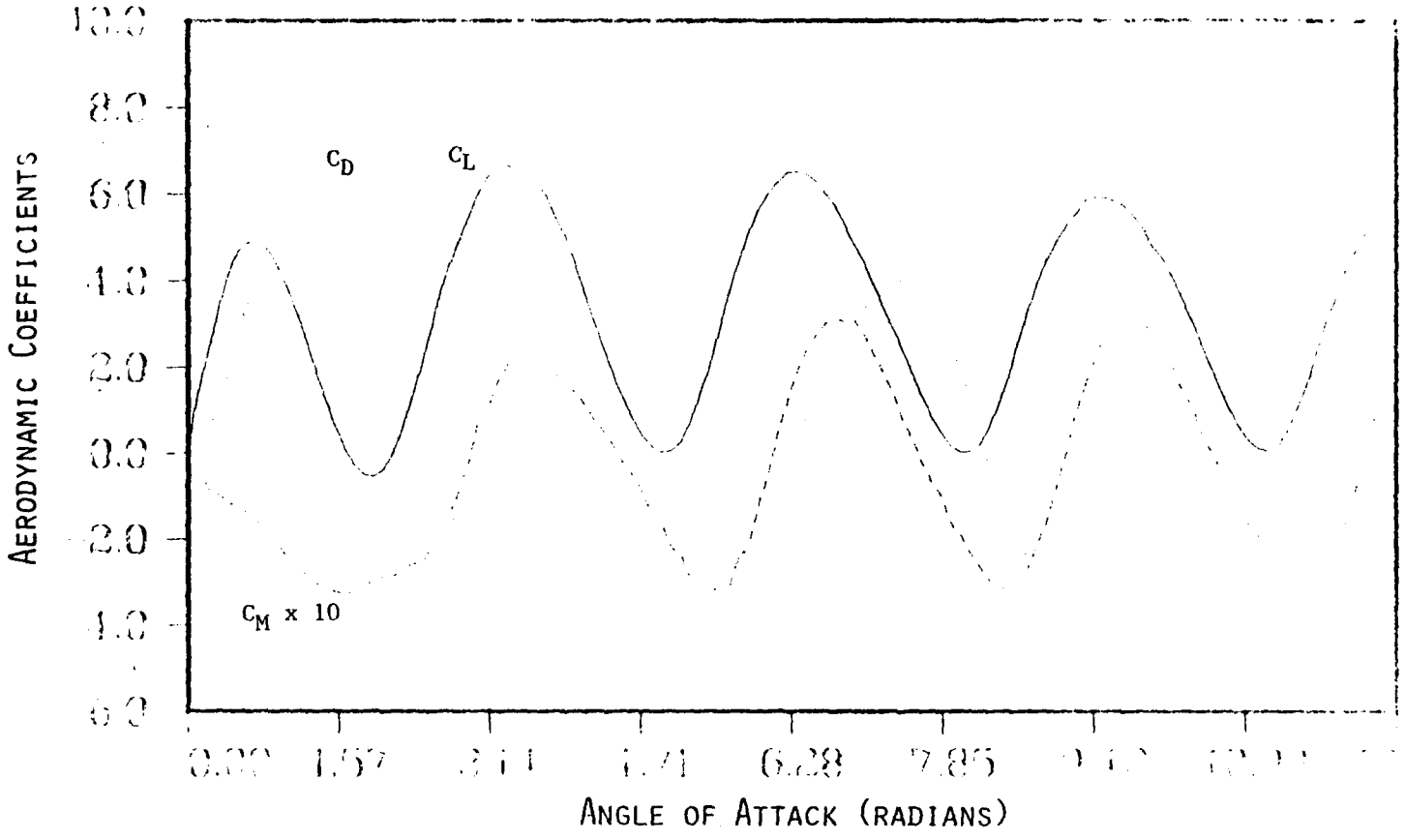

Figure 17 Aerodynamic Coefficients Produced by a Flat Plate Undergoing Forced Rotation at $\dot{\theta}=2$

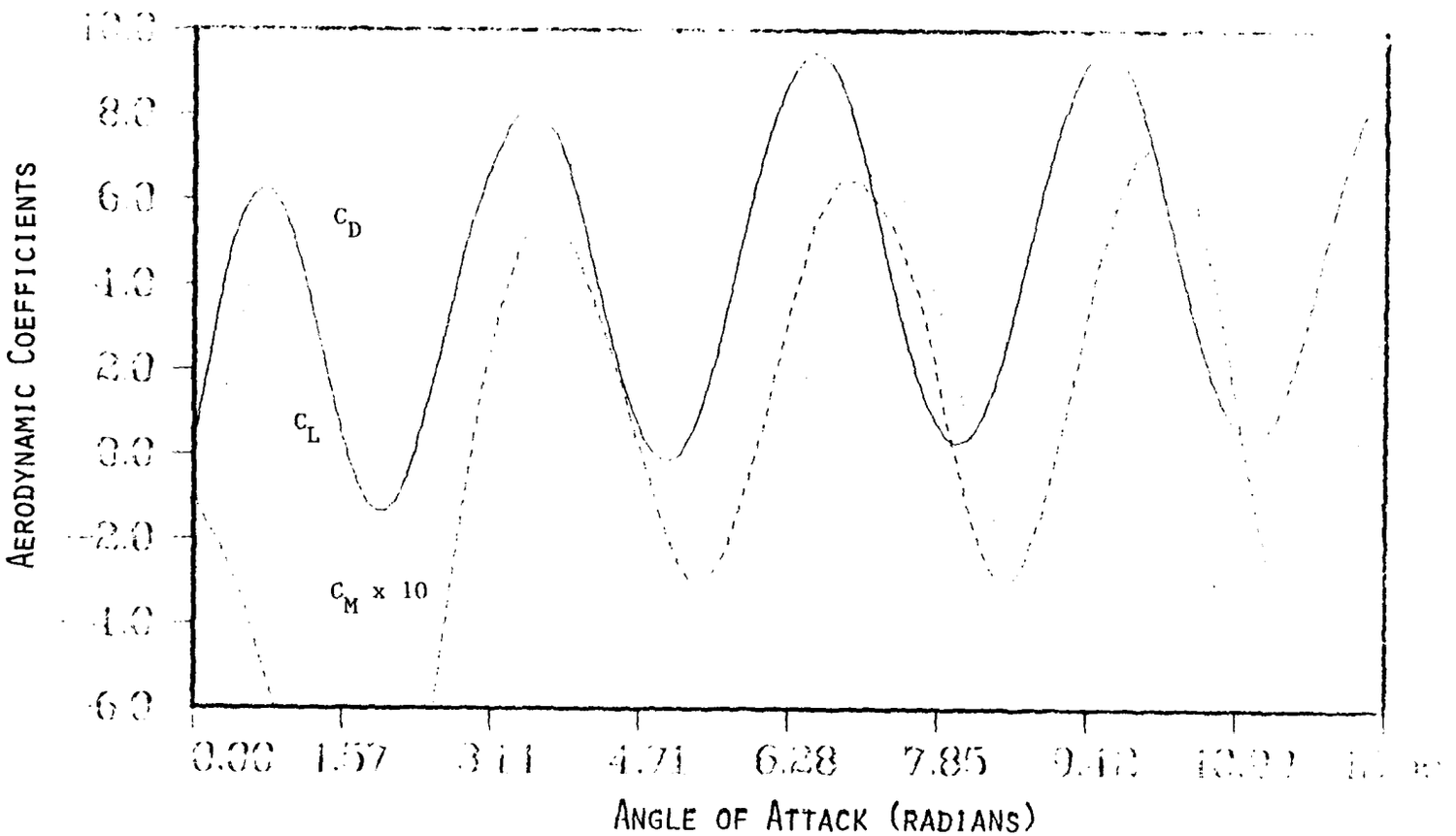

Figure 18 Aerodynamic Coefficients Produced by a Flat Plate Undergoing Forced Rotation at $\dot{\theta}$=4

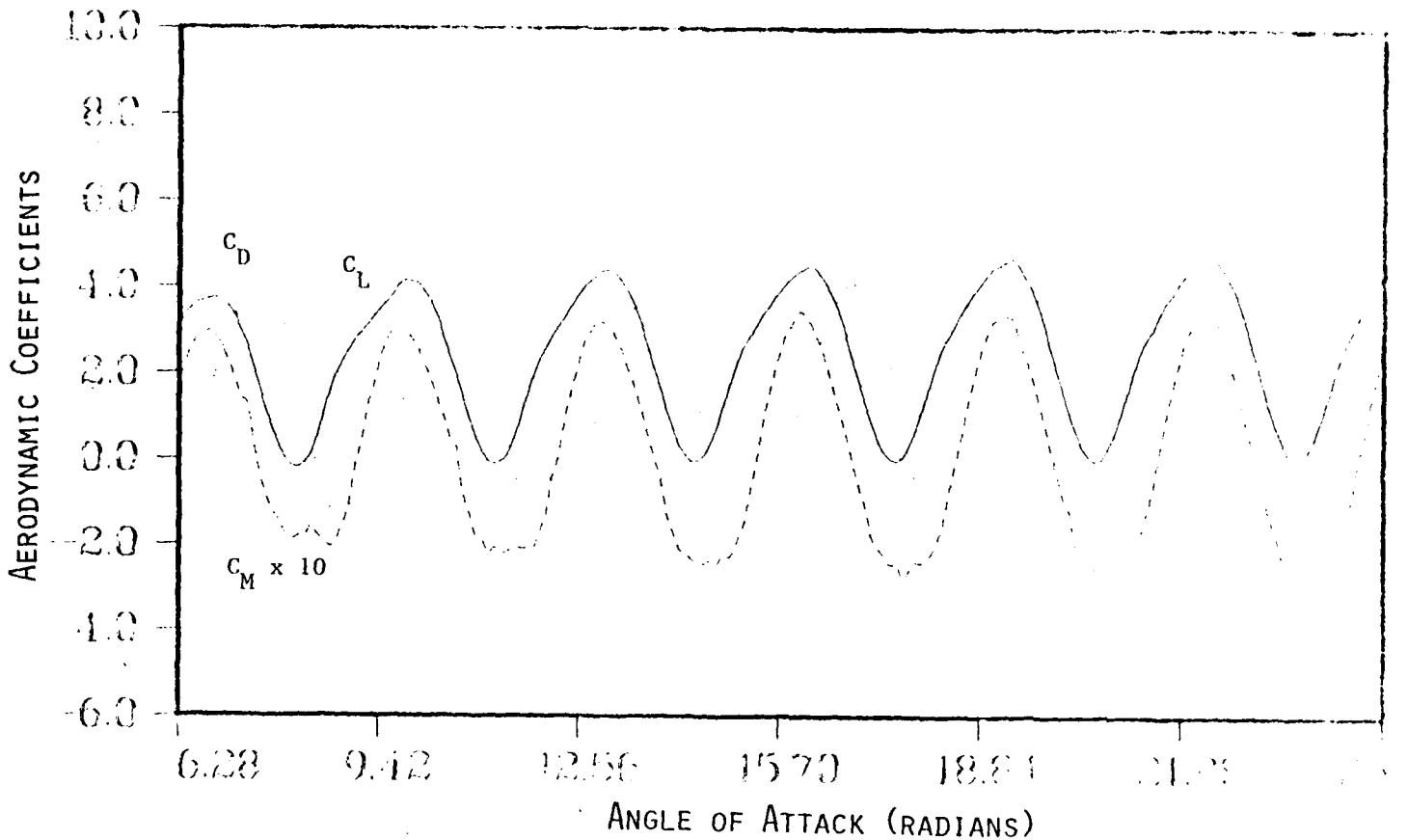

Figure 19 Aerodynamic Coefficients Produced by a Flat Plate Undergoing Pinned Autorotation

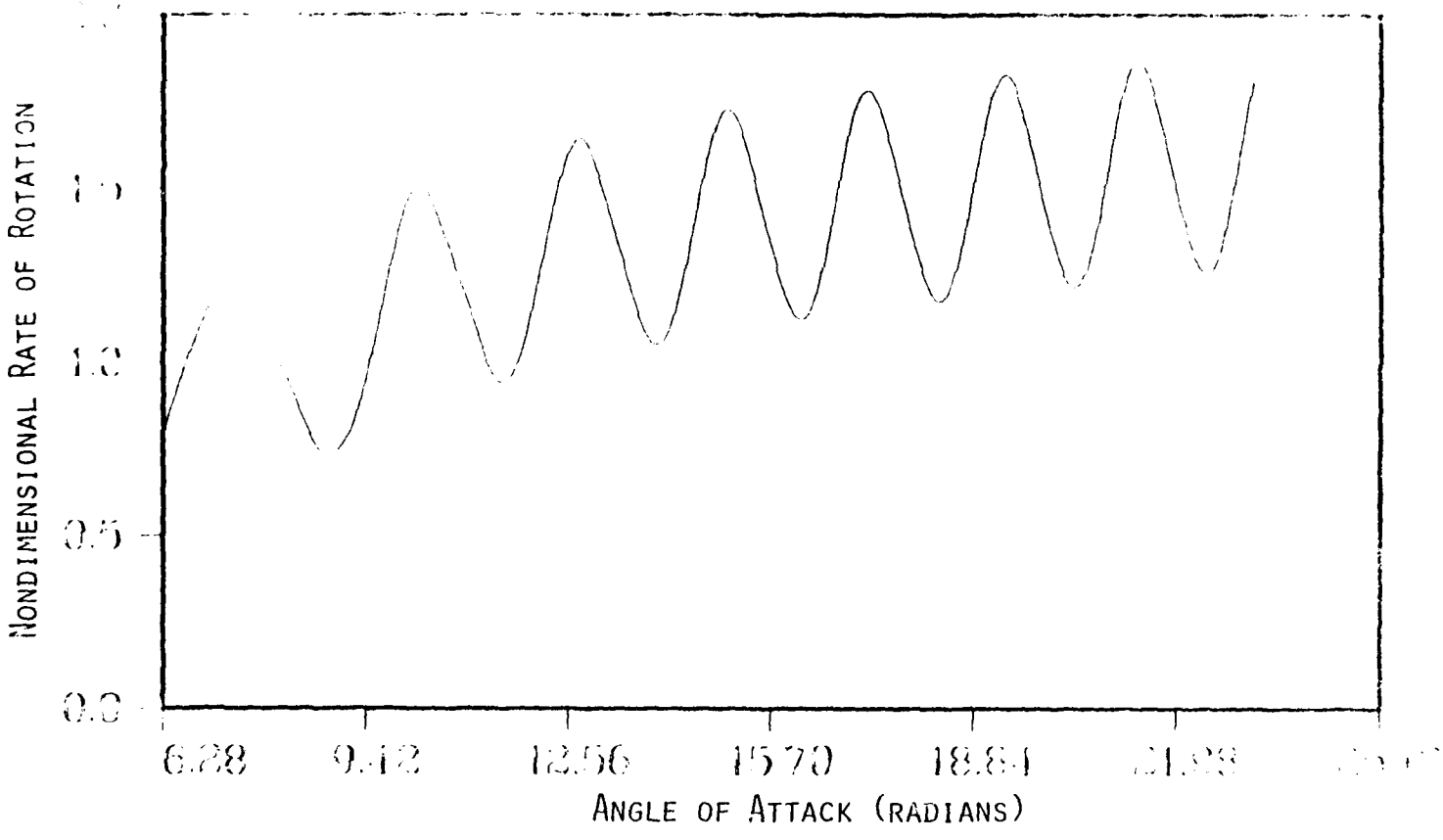

Figure 20 Rotation Rate of Flat Plate Undergoing Pinned Autorotation

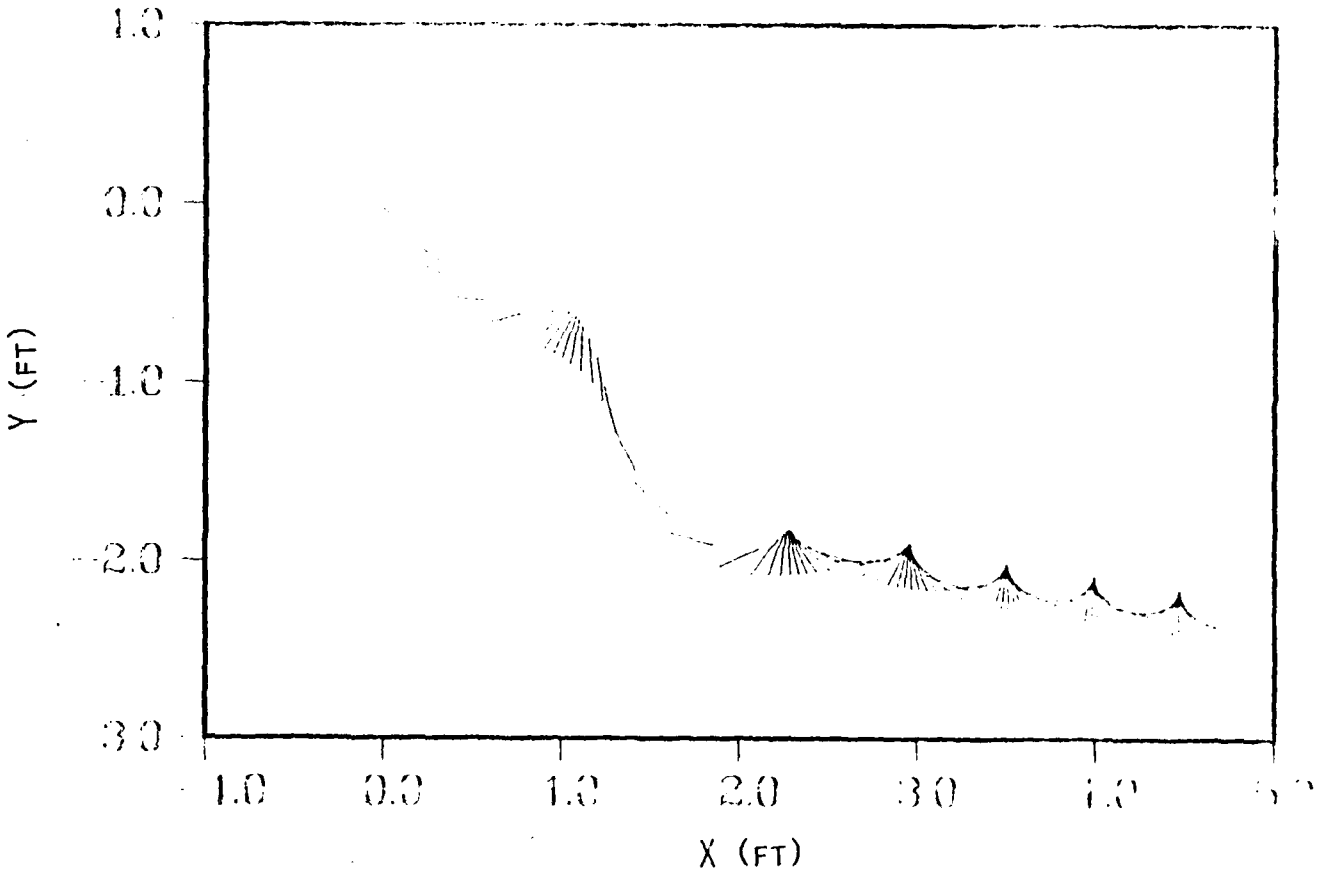

Figure 21 Calculated Plate Position During Free Fall Autorotation, $\gamma_o=-\pi/4$, $V_o=3.0$, $\theta_o=0.1$

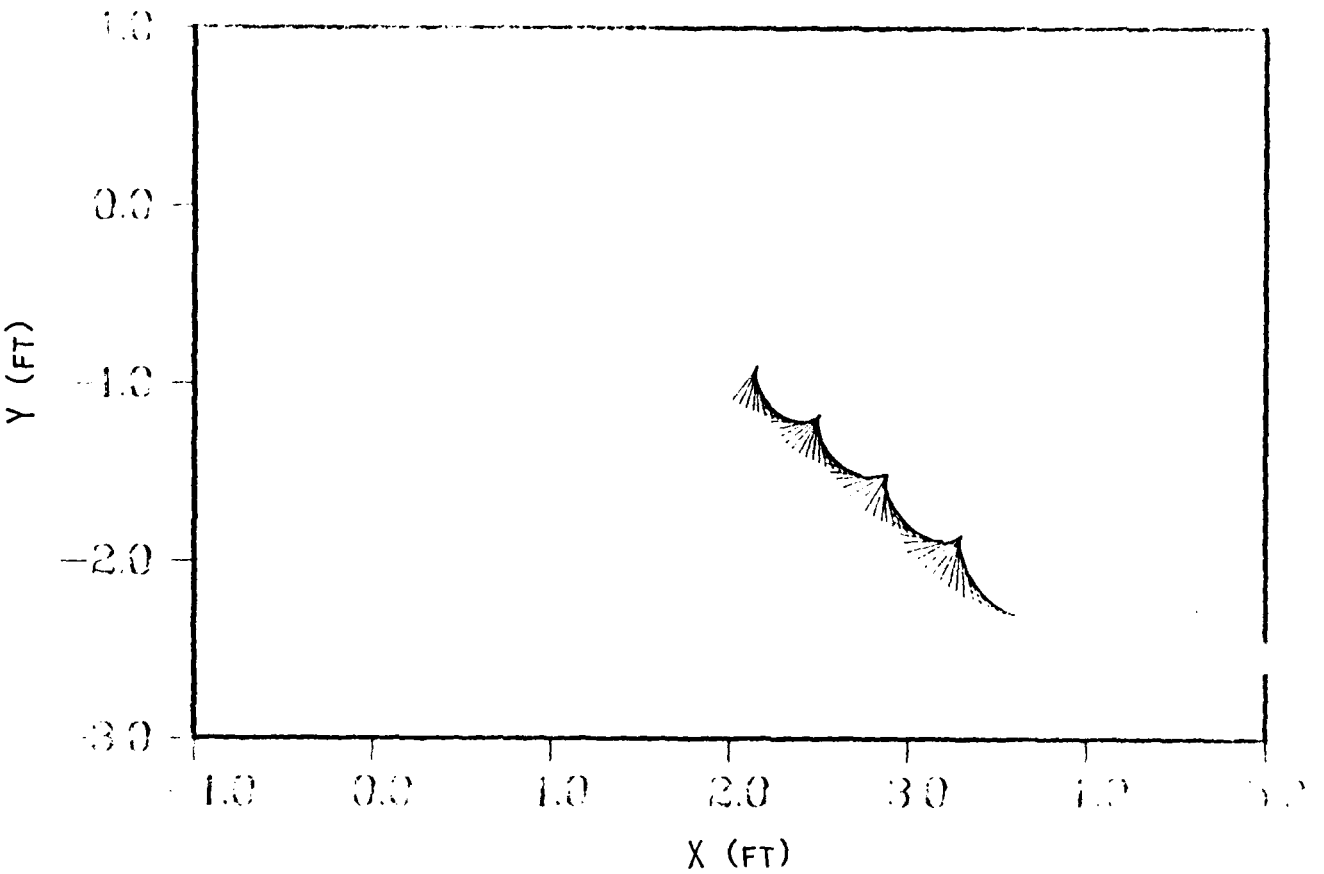

Figure 22 Experimental Plate Position During Free Fall Autorotation

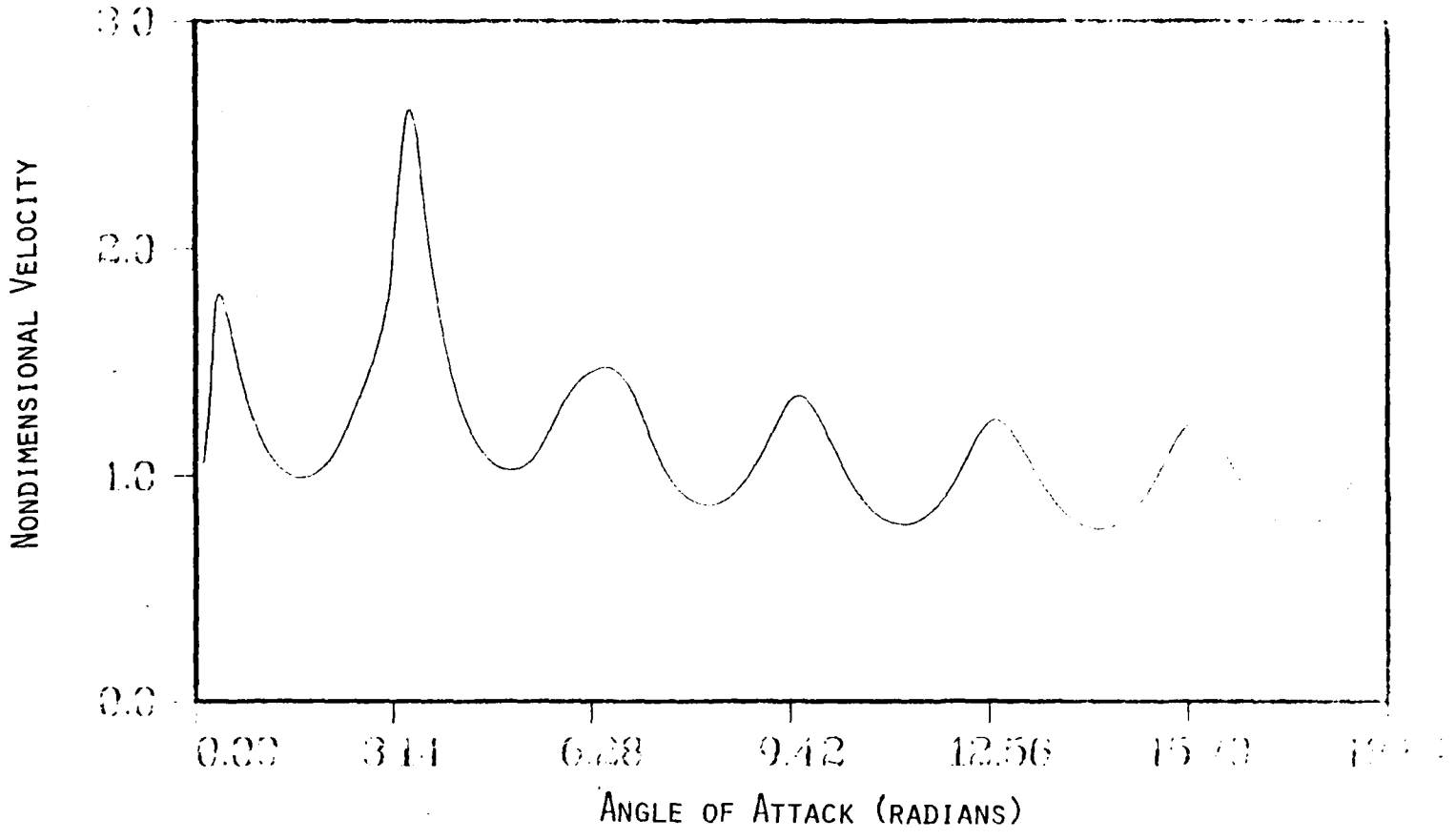

Figure 23 Nondimensional Velocity of the Center of Gravity of a Flat Plate in Free Fall Autorotation

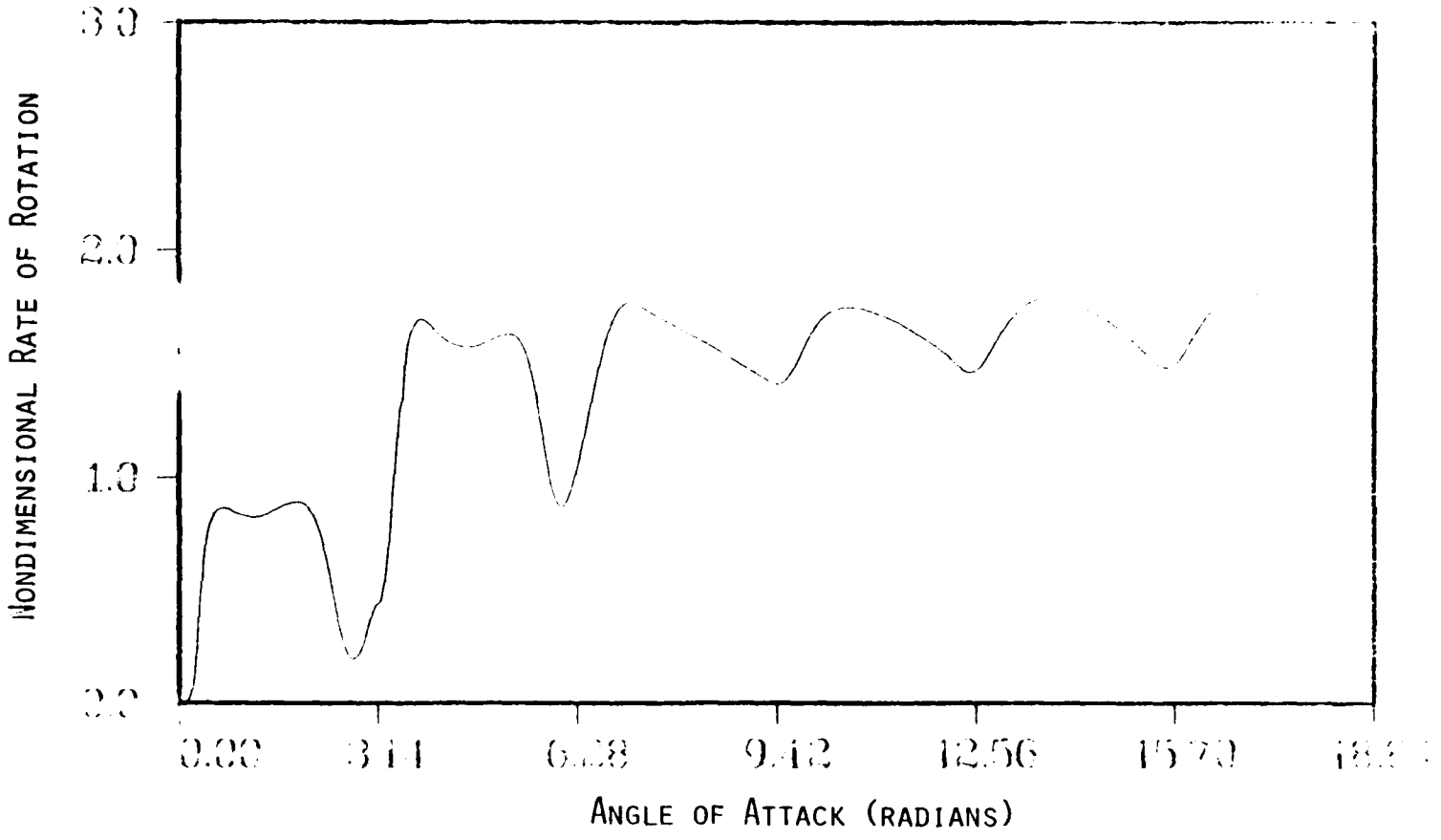

Figure 24 Nondimensional Rate of Rotation of a Flat Plate in Free Fall Autorotation

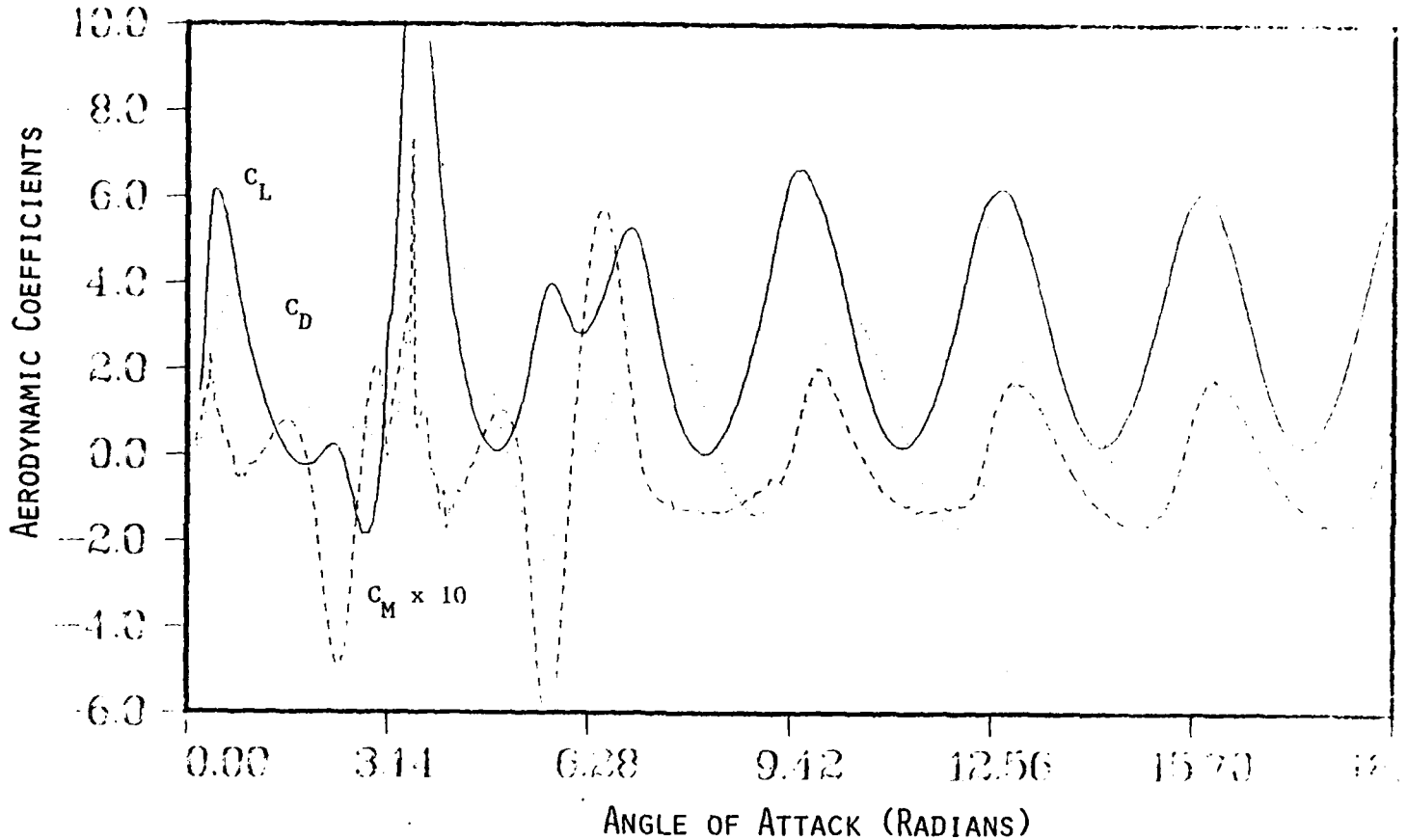

Figure 25 Calculated Aerodynamic Coefficients for a Flat Plate in Free Fall Autorotation

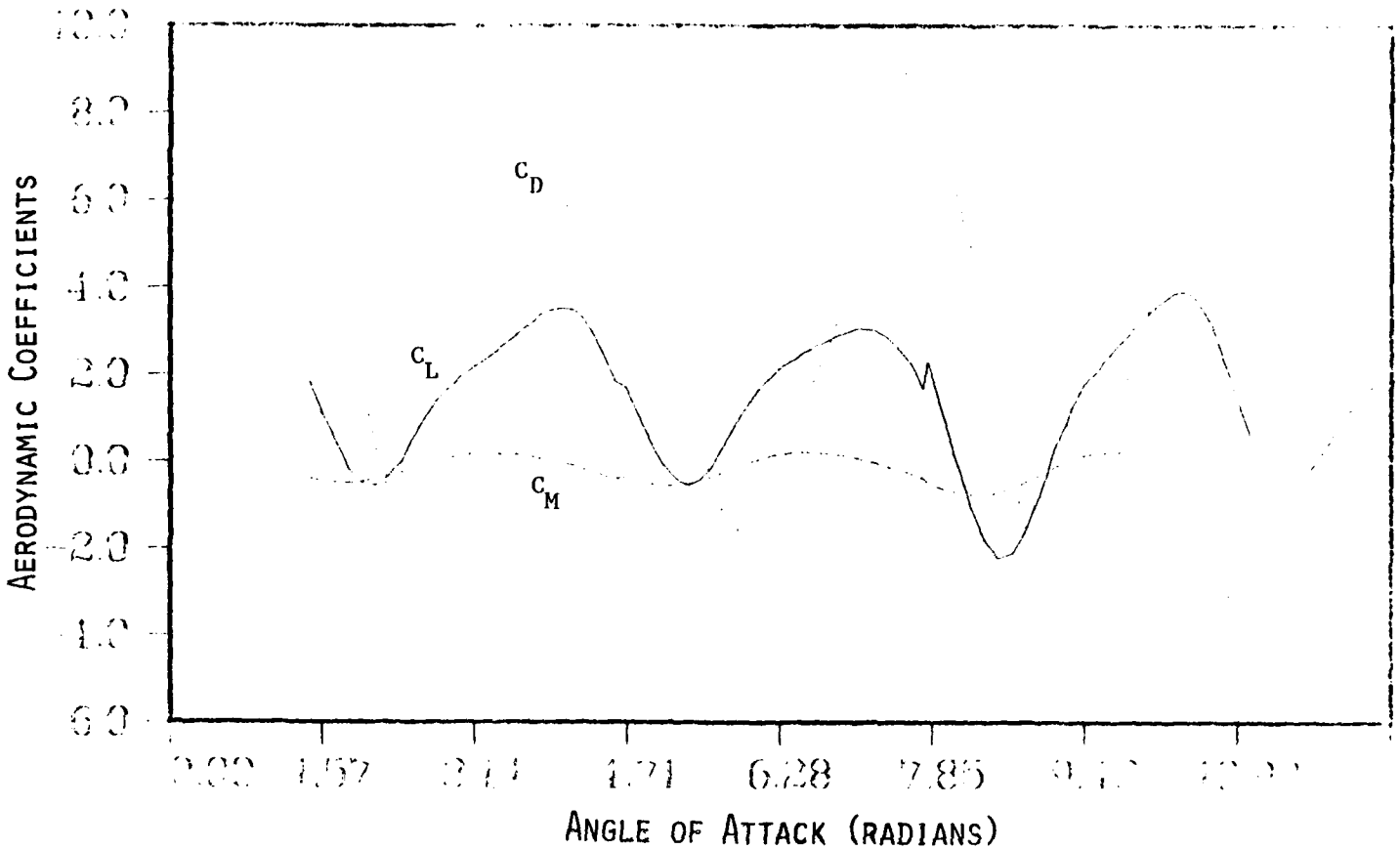

Figure 26 Experimental Aerodynamic Coefficients for a Flat Plate in Free Fall Autorotation

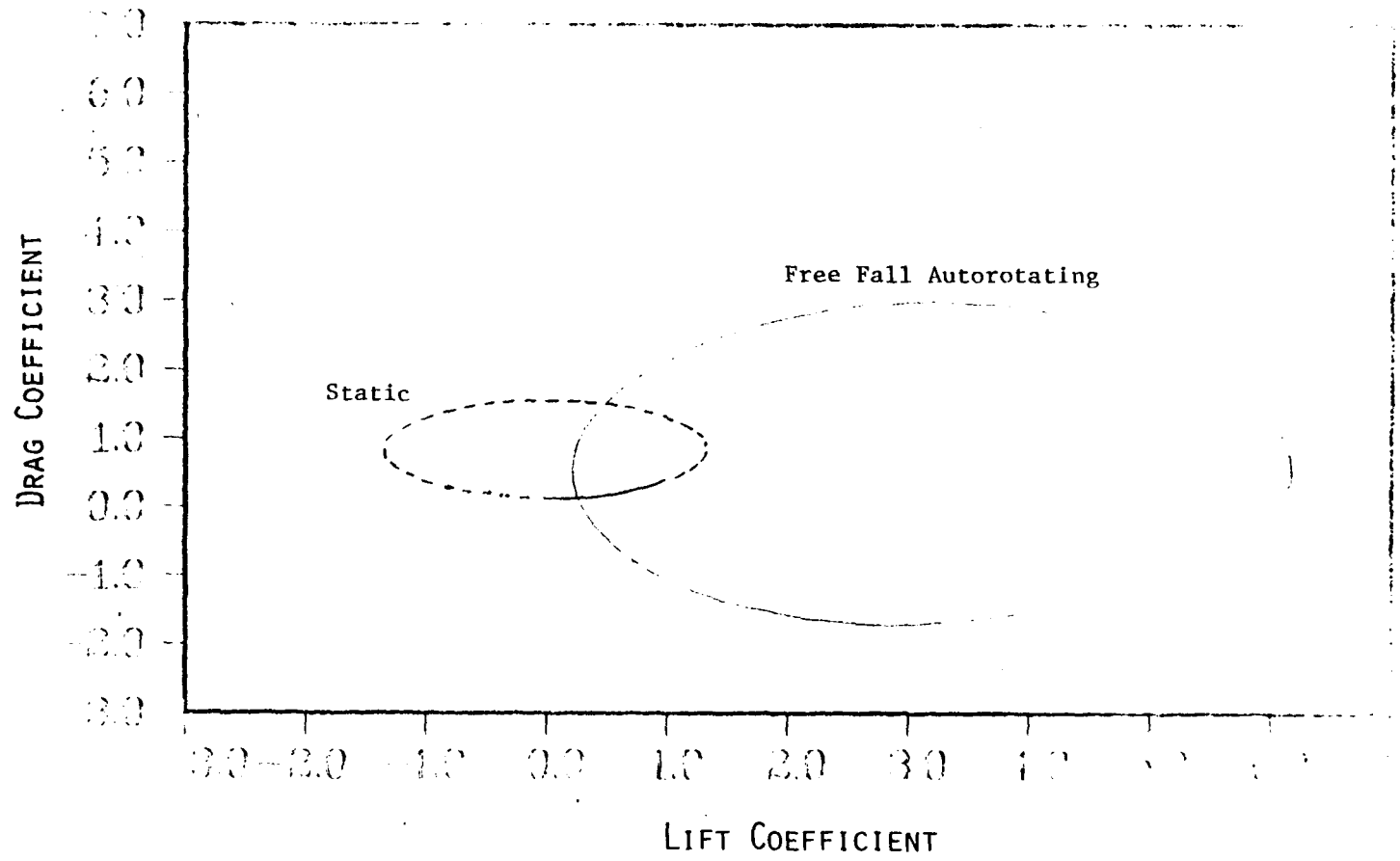

Figure 27 Comparison of Static and Dynamic Drag Polars

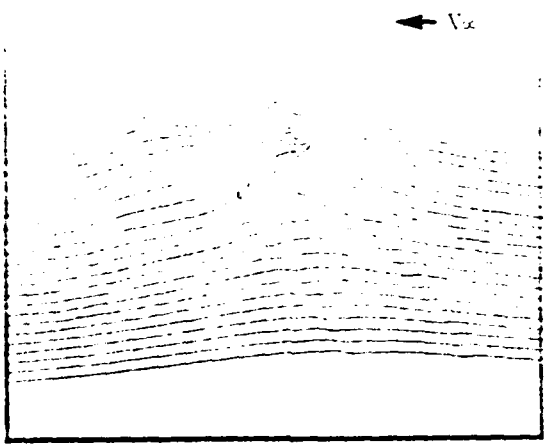

$\alpha = 5\pi + 0.63$

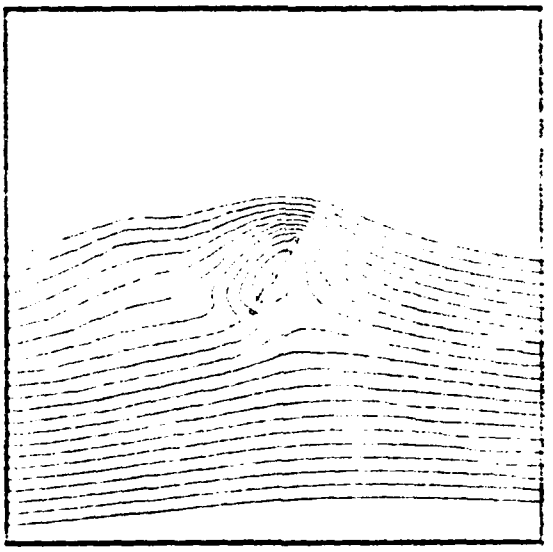

$\alpha = 5\pi + 1.03$

Figure 28 Instantaneous Streamlines Around a Flat Plate Undergoing Free Fall Autorotation

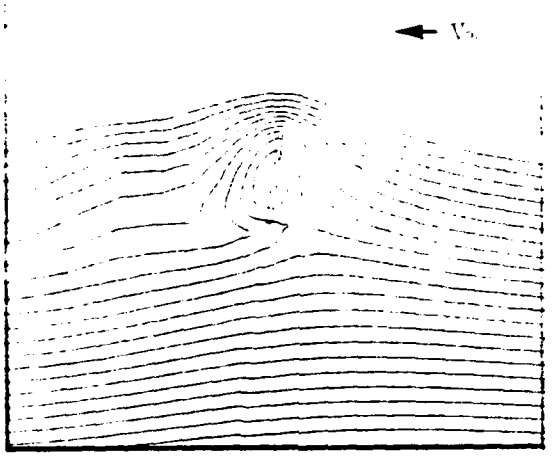

$\alpha = 5\pi + 1.43$

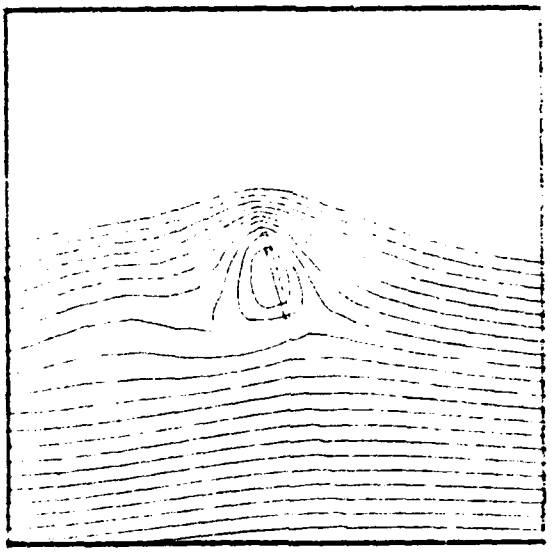

$\alpha = 5\pi + 1.83$

Figure 28 (cont.)

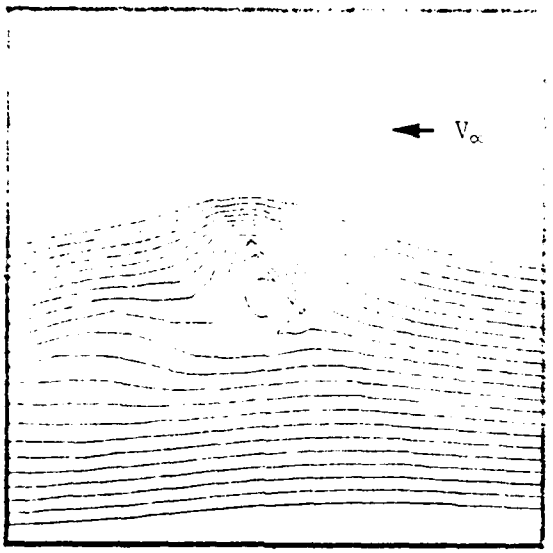

$\alpha = 5\pi + 2.23$

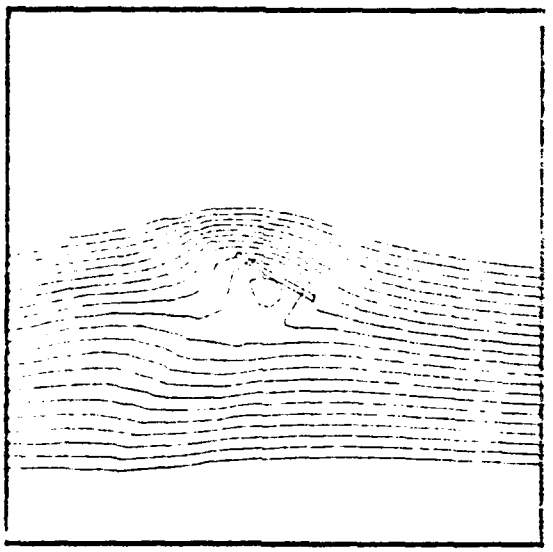

$\alpha = 5\pi + 2.63$

Figure 28 (cont.)

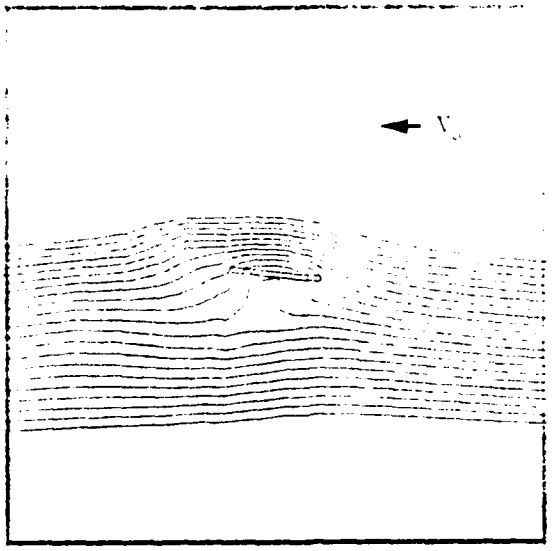

$\alpha = 5\pi + 3.03$

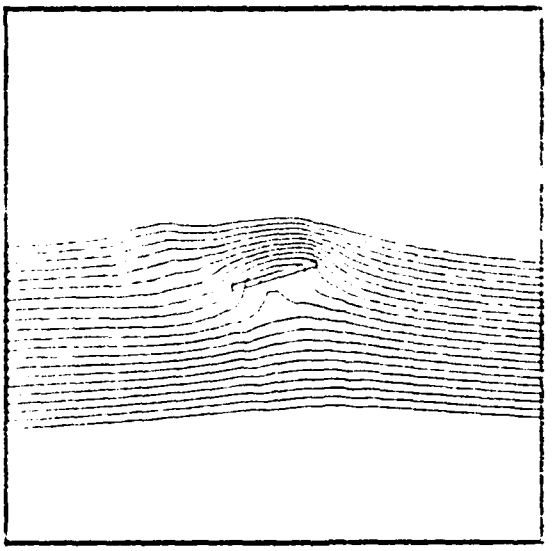

$\alpha = 6\pi + 0.29$

Figure 28 (cont.)

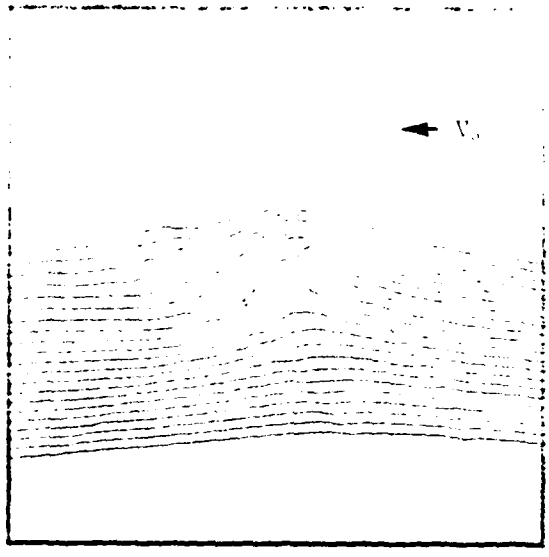

$\alpha = 6\pi + 0.69$

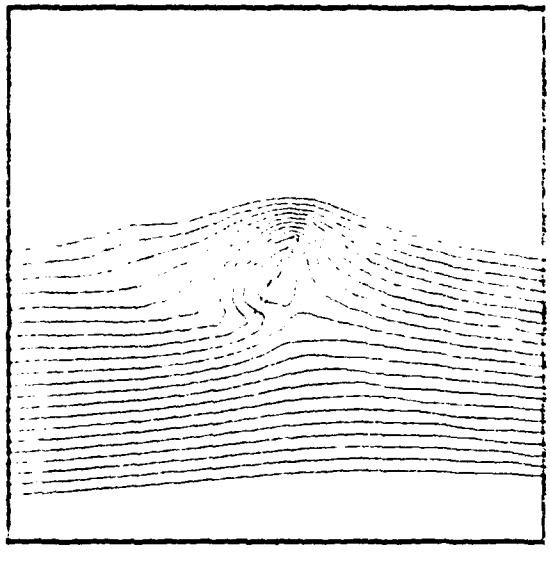

$\alpha = 6\pi + 1.09$

Figure 28 (cont.)

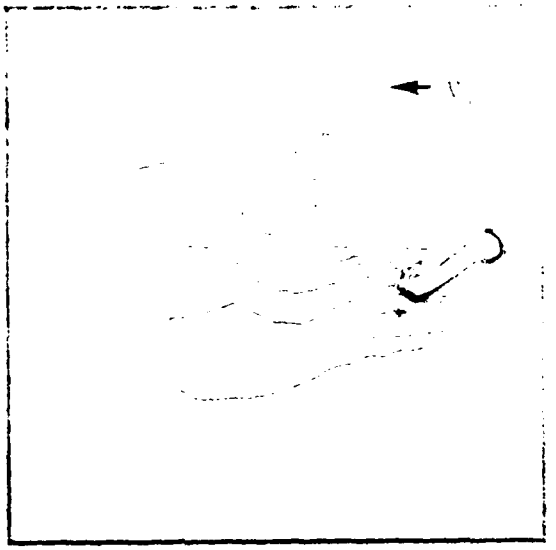

$\alpha = 5\pi + 0.63$

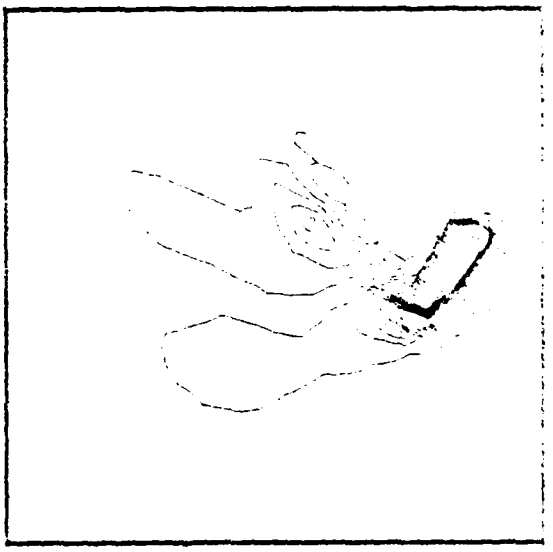

$\alpha = 5\pi + 1.03$

Figure 29 Vorticity Contours for a Flat Plate Undergoing Free Fall Autorotation

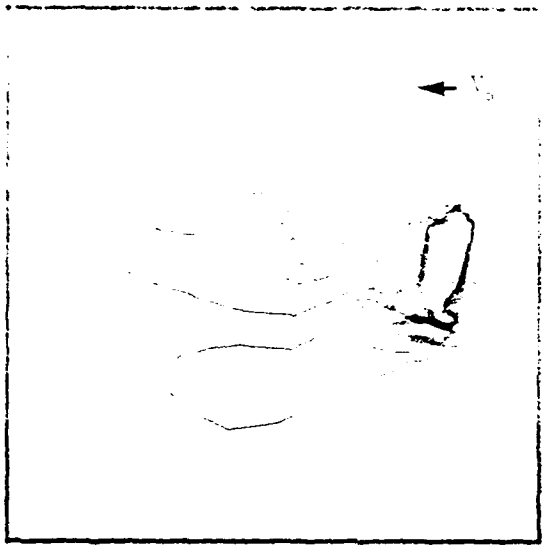

$\alpha = 5\pi + 1.43$

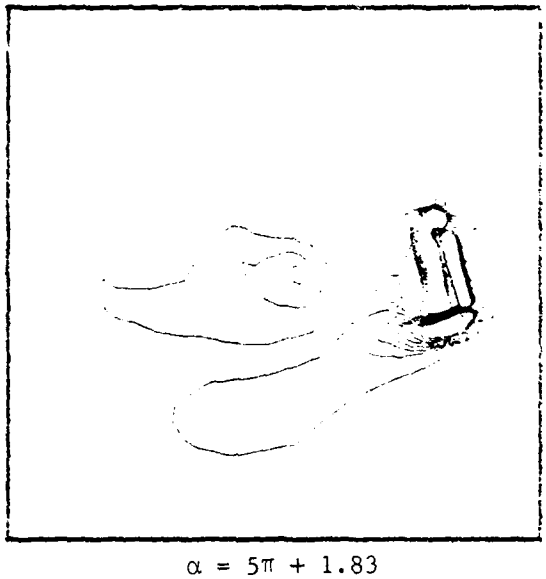

$\alpha = 5\pi + 1.83$

Figure 29 (cont.)

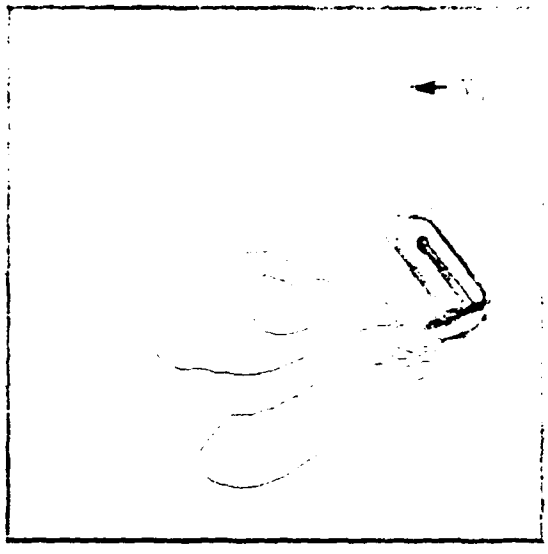

$\alpha = 5\pi + 2.23$

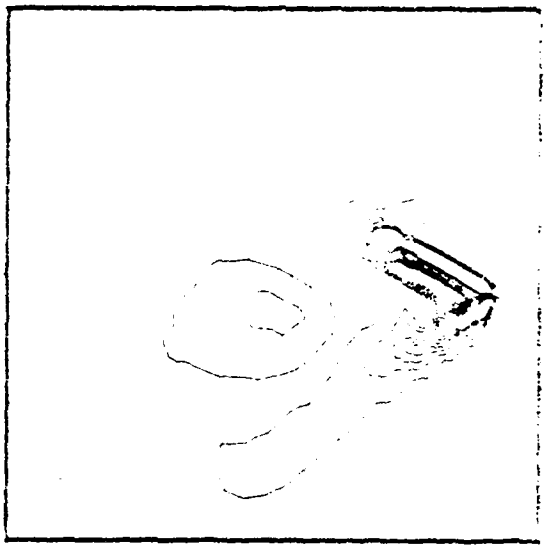

$\alpha = 5\pi + 2.63$

Figure 29 (cont.)

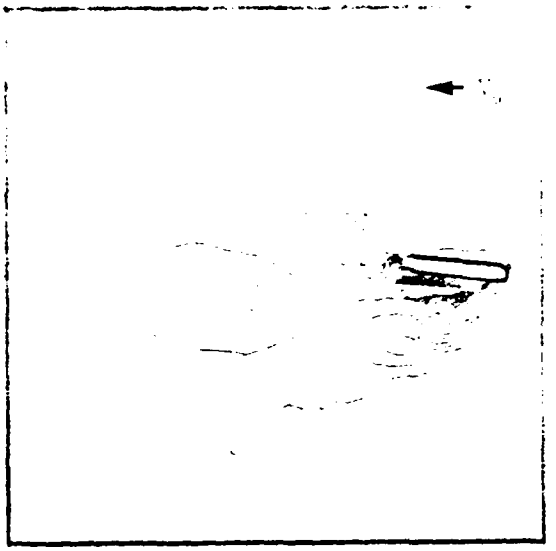

$\alpha = 5\pi + 3.03$

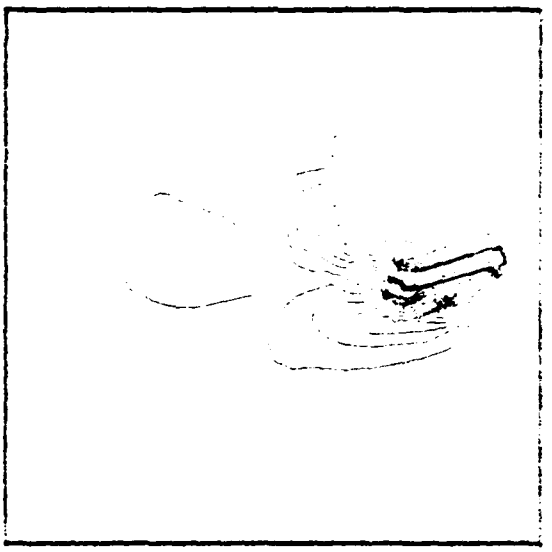

$\alpha = 6\pi + 0.29$

Figure 29 (cont.)

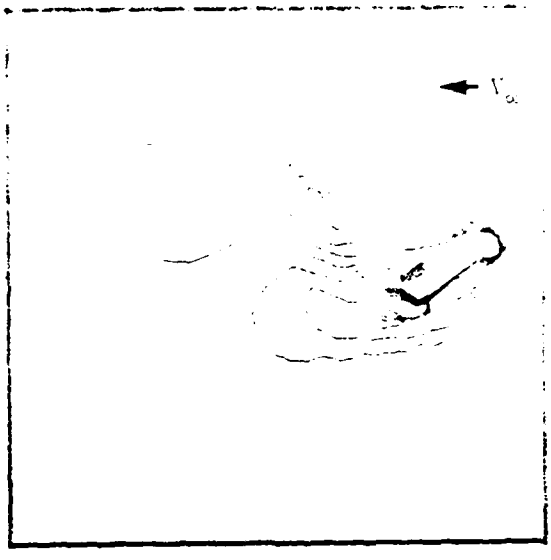

$\alpha = 6\pi + 0.69$

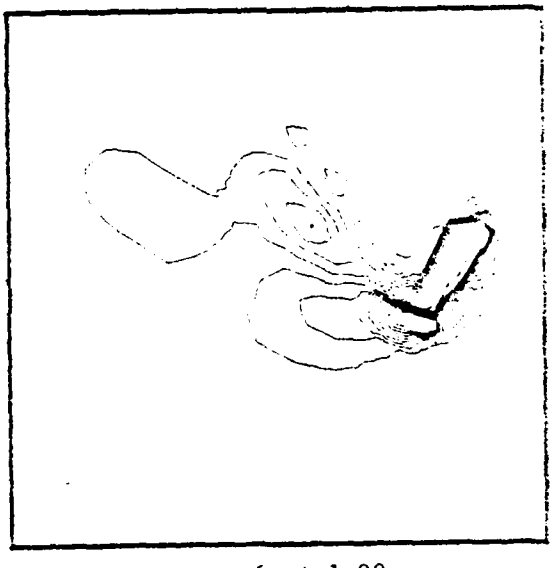

$\alpha = 6\pi + 1.09$

Figure 29 (cont.)

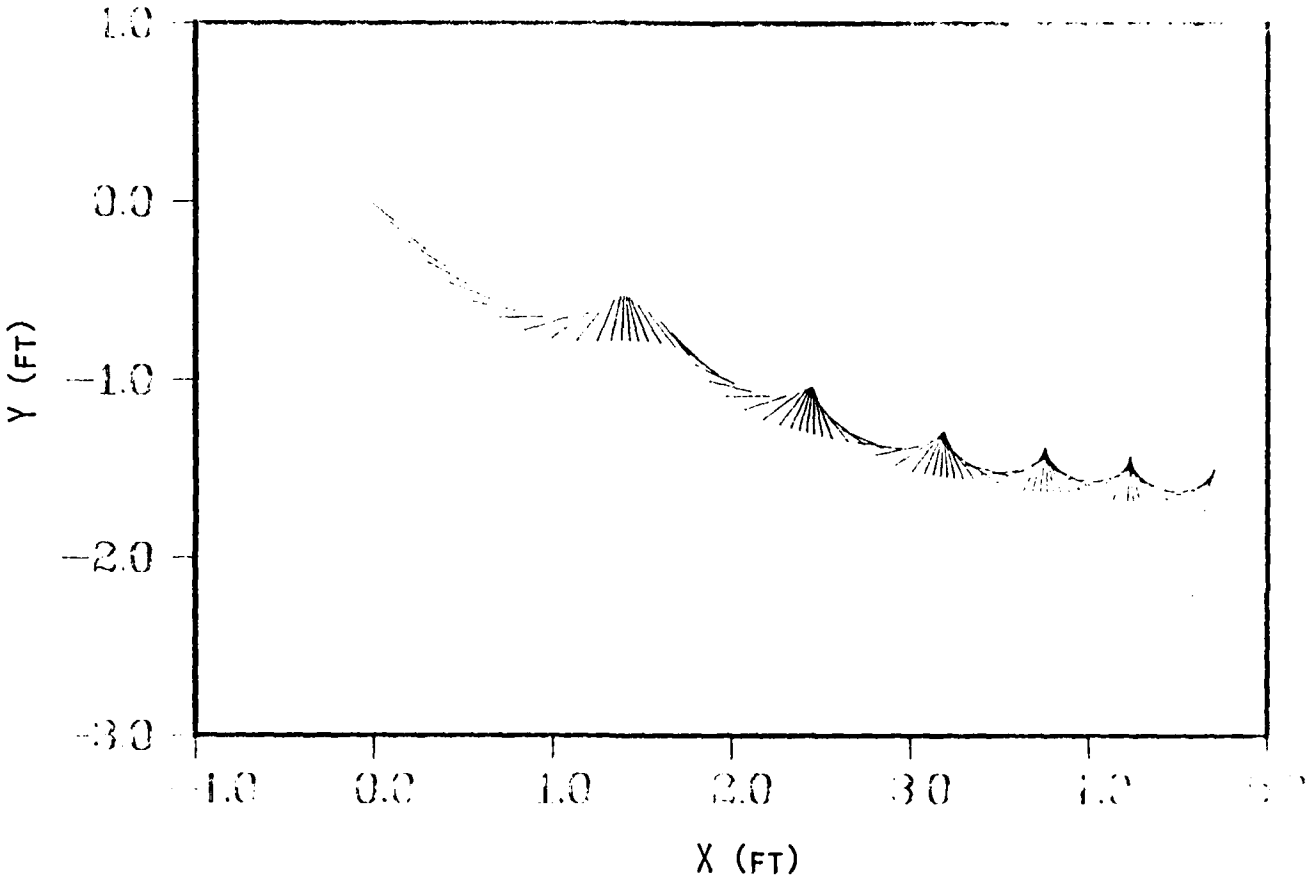

Figure 30 Calculated Flat Plate Position During Free Fall Autorotation, γ_o=-π/4, V_o=6.0, θ =0.1

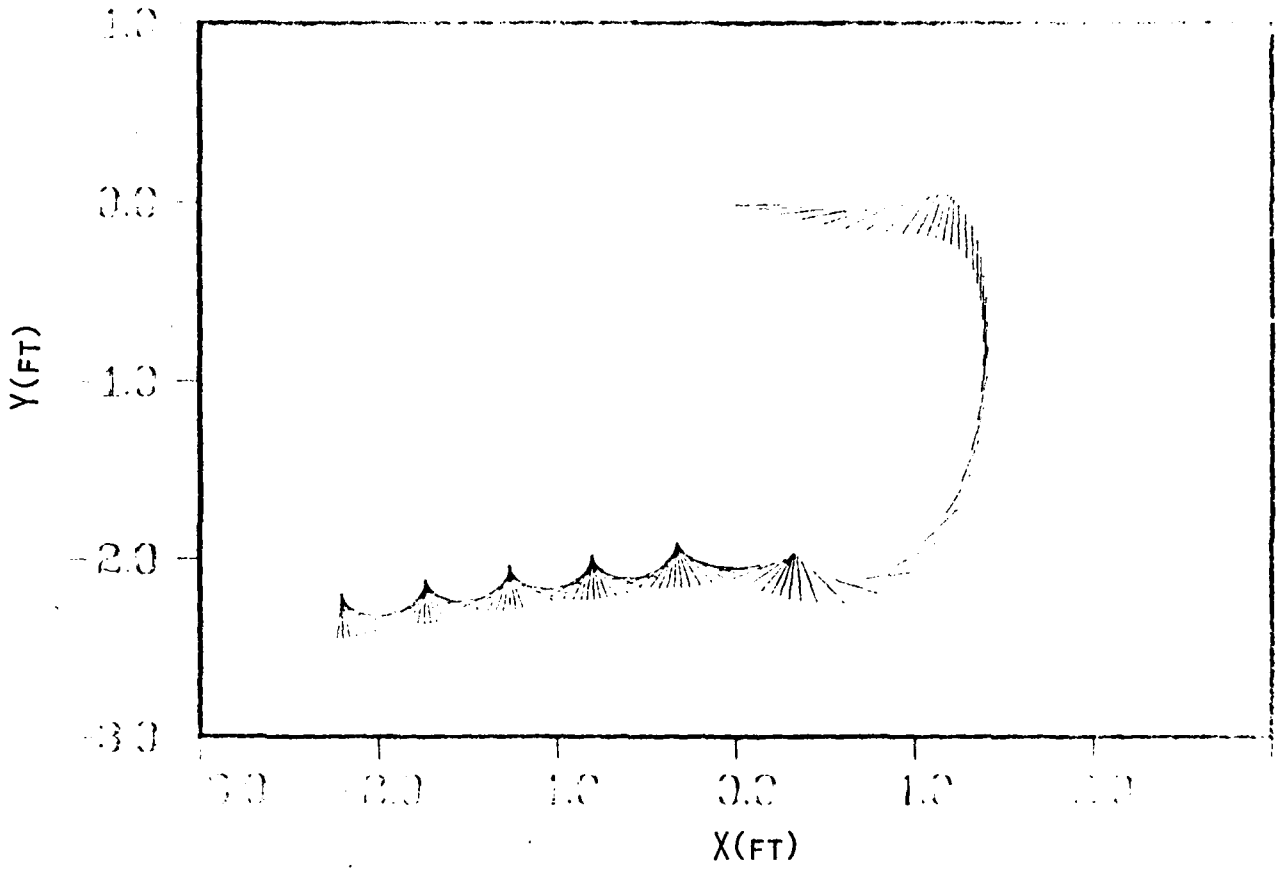

Figure 31 Calculated Flat Plate Position During Free Fall Autorotation, γ_0=0, V_0=3.0, θ=0.1

APPENDIX A

BODY FIXED ROTATING SYSTEM

The Navier-Stokes equations, (14) through (16), were modified slightly when expressed in a body fixed coordinate system undergoing arbitrary pitching. Arbitrary translation was not included at this point (Refs 59 and 60). The body fixed Navier-Stokes equations are:

$$u_t + uu_x + vu_y = -p_x + \frac{1}{Re}(u_{xx} + u_{yy}) + \dot{\theta}^2 x + 2\dot{\theta}v + \ddot{\theta}y \qquad (A1)$$

$$v_t + uv_x + vv_y = -p_y + \frac{1}{Re}(v_{xx} + v_{yy}) + \dot{\theta}^2 y - 2\dot{\theta}u - \ddot{\theta}x \qquad (A2)$$

$$u_x + v_y = 0 \qquad (A3)$$

The far field boundary conditions for velocity and pressure were given by the freestream flow field in the inertial reference frame. These conditions are equations (A4) through (A6) when written in the body fixed coordinate system.

$$u = u_\infty \cos(\alpha_o - \theta) + \dot{\theta}y \qquad (A4)$$

$$v = u_\infty \cos(\alpha_o - \theta) - \dot{\theta}x \qquad (A5)$$

$$p = p_\infty \qquad (A6)$$

The no change boundary condition, which allows a wake to pass through the boundary, was imposed on the downstream boundary velocity component. Numerical experimentation showed that imposing freestream boundary conditions on the downstream boundary, instead of the no change condition, had little effect on the aerodynamic characteristics of the plate. The downstream outer boundary conditions on pressure retained the freestream value. In the fixed system, these conditions are given

by

$$u_\eta = \dot{\theta} y_\eta \tag{A7}$$

$$v_\eta = -\dot{\theta} x_\eta \tag{A8}$$

$$p = p_\infty \tag{A9}$$

where the derivatives are normal to the outer boundary.

The flow field around a plate undergoing forced rotation was calculated using a numerical technique similar to the one developed by Hegna (Ref 25). The solutions were acceptable for slow rotational rates. The results of the calculations became increasingly worse as the rotational rates approached a reduced frequency, $\omega c/U_\infty = k$, of approximately one. The solution remained numerically manageable with the evolution of time even though the pressures near the outer boundary approached values one to two orders of magnitude too large.

A calculation of a rapidly rotating flow field without a body produced similar pressures near the outer boundary. This indicated the problems were probably caused by the outer region and/or the boundary conditions. The same calculation was performed with the outer boundary moved farther away from the plate; nearly the same results were obtained.

Hodge (Ref 41) found the junction between the upstream Dirichlet and downstream Neumann boundary conditions was a source of a small error. This error was amplified in the calculation with rotation. The small changes in the velocity components necessary to satisfy the boundary conditions and continuity at the intersection of the upstream

and downstream boundary conditions became unacceptably large. The small changes produced a pressure wave which propagated into the flow field at each time step. In the steady calculations, the flow field was allowed to stabilize. Eventually the intersection of the boundary conditions was a source of only a small error. However, in the rotating cases the source of error was continuous and increased as the rate of rotation increased. Averaging and smoothing, which considerably complicated implementing the outer boundary conditions, were tried as methods to alleviate the problem but to no avail.

The velocities near the outer boundaries became very large as the rotation rates became large (Ref 61). One approach to alleviating numerical problems in many numerical investigations is to move the outer boundary farther away from the body (Ref 17). In this formulation, moving the outer boundary increased the velocities in the outer region, thereby compounding the problems. The grid spacing was coarse in the radial direction. The grid spacing was equally coarse in the tangential direction or as fine as the minimum grid spacing used during the problem. The exponential grid and rotating formulation combined large and small velocity components over large aspect ratio finite difference grid cells. This combination occurs at the location of the largest velocities. The mismatch in grid spacing and velocities did not offer numerical compatibility, however, it did not directly attribute to numerical difficulties.

Hegna (Ref 25) was successful in using this approach to calculate the flow field around slowly rotating airfoils at relatively large

Reynolds numbers. Very small time steps were used to obtain numerical stability at large Reynolds numbers for flow fields without rotation. This also helped stabilize the rotating problem. Using a time step similar in magnitude to the one used by Hegna was not a practical alternative for this research project. The computational time necessary to do several rotations of the plate would have been prohibitive.

Finally, a Von Neumann stability analysis performed at certain locations within the flow field showed the rotational terms could destabilize equations (A1) and (A2). A Fourier representation of each variable was substituted into the momentum equations. The flow field was assumed to be rotating at a constant velocity. The rotational terms were treated as source terms in the Navier-Stokes equations solver. In the stability analysis, however, the rotational terms were formulated as functions of u and v by assuming that u and v were of the same order of magnitude. The viscous terms were assumed to be small in the flow field away from the plate. The stability of one SOR iteration was found to be a function of the rate of rotation. Above some rotational velocity the rotational terms will destabilize the equations.

The rotating reference approach was abandoned because of the difficulties outlined in this appendix. A "mixed" system was adopted as described in Section III.B. A Von Neumann stability analysis showed the "mixed" system had better stability characteristics than the rotating formulation. A plate could rotate three times faster in the "mixed" system and maintain the same stability characteristics as the rotating formulation.

APPENDIX B

SOR SWEEP METHOD

Calculating the flight path of a free falling flat plate was truely time dependent which required more attention than normal to be paid to the successive over relaxation (SOR) sweep direction. The sweeping direction was important because it effectively produced a numerical propagation speed. This speed was not constant throughout the flow field because of uneven physical step sizes. Alternating the sweeping direction allowed the numerical propogation speed to be similar in all directions. An even number of iterations were used at each time step to avoid favoring one direction. An "infinite" numerical propagation speed more closely approximated the infinite speed of sound of incompressible flow.

The concept of numerical propagation speed is illustrated in Figure B1. A disturbance was imposed at point 5 in the flow field shown in Figure B1a. One iteration of a calculation used a left to right sweep which only allowed the influence of the disturbance to be felt at point 4 as illustrated in Figure B1b. A second iteration allowed the disturbance to be felt at point 3 and so forth. Four iterations were required to propagate the disturbance from point 5 over to point 1 using a left to right sweep. Figure B1c illustrates that a calculation performed with a right to left sweep allowed the disturbance to propogate throughout the complete flow field in one iteration.

The most ideal SOR sweep mode would have been alternating the sweep

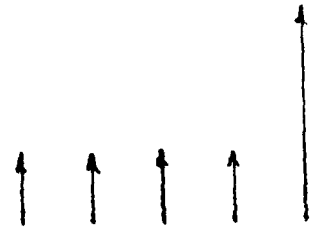

a) Initial Conditions

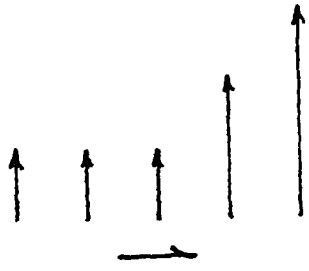

b) Sweeping to the Right

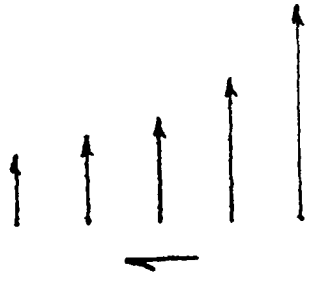

c) Sweeping to the Left

Figure B1 Concept of Numerical Propagation Speed

outward from the plate in all directions and inward from the outer boundary in all directions. This mode however, would have been difficult and inefficient to implement in a computer program. A more efficient sweep mode was used. During the first iteration, the sweep started at the middle of the computational domain, then swept up and down from the plate to the outer boundaries. The starting points were moved to the left and right one grid space and swept up and down from the plate to the outer boundaries. This process was repeated until the complete domain was covered. The second iteration began at the corners of the outer boundary. The calculations were then swept to the center of the computational grid then moved back to the outer boundaries. The starting points were moved in one grid space and the process repeated until the complete domain was covered.

APPENDIX C

REFERENCE SYSTEMS FOR DATA PRESENTATION

Selecting a reference frame in which to present unsteady motion is difficult. Steady motions can usually be presented in a body fixed reference system in which the flow becomes steady. In this steady state system, streamlines, pathlines and streaklines coincide. Unfortunately, in unsteady flows, no preferred reference frame exists, therefore, the reference frame was selected on the basis of other criteria. Streamlines, pathlines and streaklines generally do not coincide in unsteady flow fields (Ref 62).

The simplest case of a rotating body in two dimensions is that of a flat plate rotating with constant angular velocity in a fluid at rest at infinity. Figure C1a shows the approximate instantaneous streamlines of a potential flow around a rotating plate (Ref 63). This flow is unsteady, but by superimposing the rotation of the plate, the flow became steady as shown in Figure C1b.

The flow becomes more complicated when the plate rotates with constant rotation, Ω , in a uniform freestream, V_∞ , because no steady state exists. Four different frames are distinguishable (Ref 62). When U^* and Ω^* are the translational velocity and rotation of the plate relative to the reference frame, these four different frames are:

1) $U^*=0$, $\Omega^*=0$; the frame is fixed to the plate.

2) $U^*=V_\infty$, $\Omega^*=0$; the frame does not rotate relative to the plate; but translates relative to the plate.

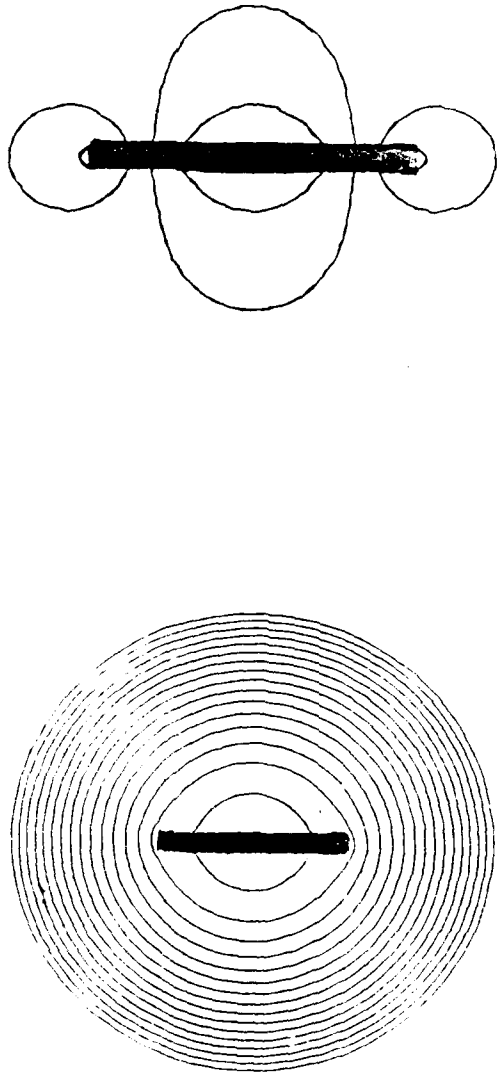

Figure C1 Potential Streamlines Around a Rotating Flat Plate

3) $U^*=0$, $\Omega^*=\Omega$; the frame is fixed to the plate with regard to translation; but rotates relative to the plate.

4) $U^*=V_\infty$, $\Omega^*=\Omega$; the frames is in translational and rotational motion relative to the plate.

The streamlines around a free falling, autorotating, flat plate at $\alpha=18.34$ radians angle of attack for the four different cases are illustrated in Figure C2. Since the streamlines are not invariant, all patterns differ from each other. Frame 1 is advantageous since the body contour was a streamline and the flow field near the plate could be examined. Frame 3 is appealing because of its analogy to instantaneous streamline photos of a rotating plate in a wind tunnel. Frames 2 and 4 are of less interest in this study.

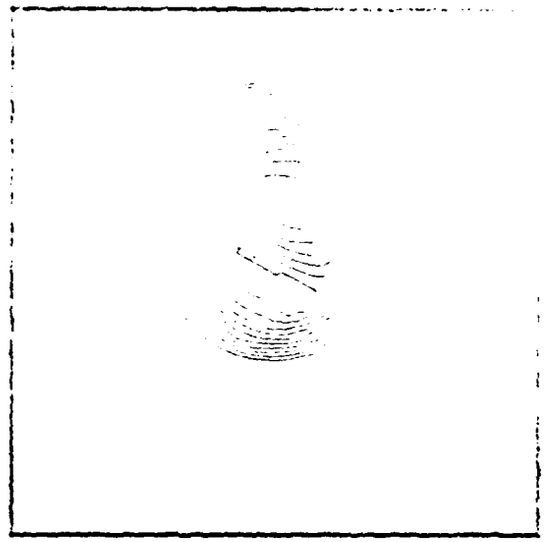

a) Frame 1

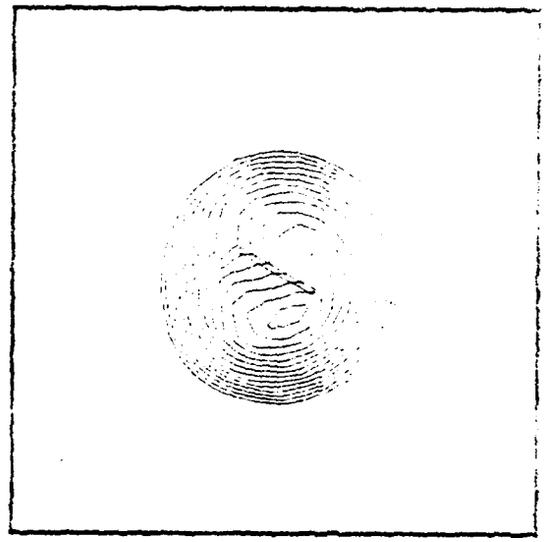

b) Frame 2

Figure C2 Comparison of Four Reference Frames

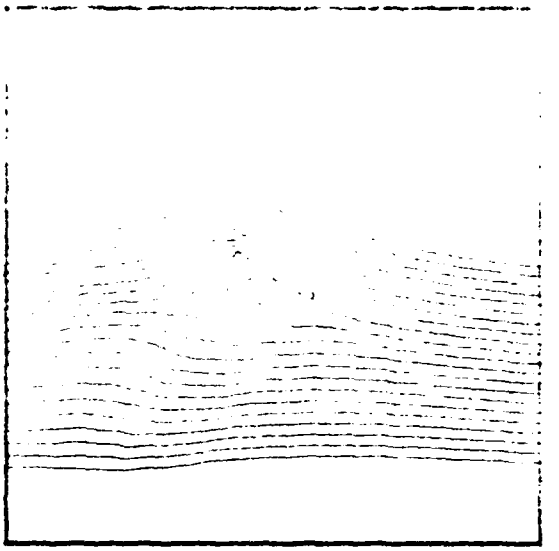

c) Frame 3

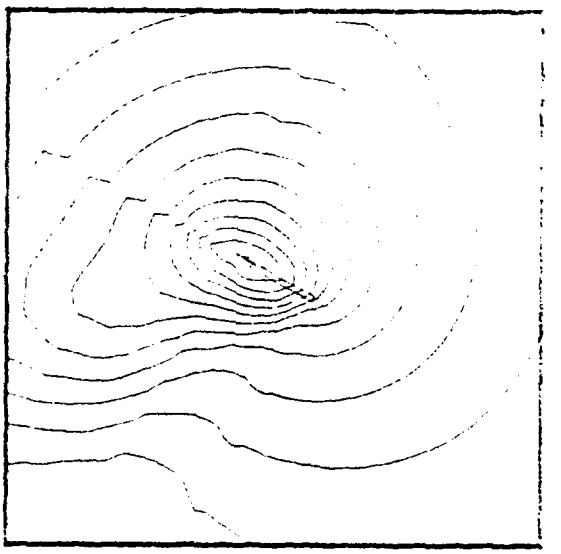

d) Frame 4

Figure C2 (cont.)

APPENDIX D

ADAM-BASHFORTH FORMULAE

The Adam's multistep formulae have been used in efficient computer routines to obtain the solution of ordinary differential equations. The Adam's formulae fall into two general categories: open formulae and closed formulae. The Adam's open formulae, also known as the Adams-Bashforth formulae, were the only formulae used to solve ordinary differential equations in this study.

The open formulae were derived by performing a forward Taylor series expansion about an arbitrary value of time. The derivatives in the expansion were replaced by various numbers of backward differences depending on the order of the formula. The coefficients of different order Adam-Bashforth formulae are shown in Table D.I.

These formulae are called open formulae since the next value in time of the function could be solved for explicitly in terms of the present and past values of the function. However, during start-up of the second order and higher order methods, the previous values of the function were not known. The previous values of the function were obtained by linearly extrapolating back in time. These extrapolated values made the Adam's formulae self starting regardless of the order.

Table D.I. Coefficients of the Adams Formulae

n \ k	0	1	2	3	4	5	Order of Method
0	1						1
1	3/2	−1/2					2
2	23/12	−16/12	5/12				3
3	55/24	−59/24	37/24	−9/24			4
4	1901/720	−2774/720	2616/720	−1274/720	251/720		5
5	4277/1440	−7923/1440	9982/1440	−7298/1440	2877/1440	−475/1440	6

VITA

Charles Ray Callaway was born on July 7, 1953 in Houston, Texas. Most of his childhood was spent living abroad culminating with his high school graduation in Kabul, Afghanistan, class of 1970. Charles attended Texas A&M University receiving a Bachelor of Science degree in 1973. He was commissioned in the U.S. Air Force but remained in school under an educational delay to obtain a Master of Science degree in 1974. Charles married Deborah VanSickle in Tegucigalpa, Honduras in December 1974.

Charles began his professional career as a high lift aerodynamics engineer with the Air Force Flight Dynamics Laboratory in January 1975. In 1977 he was transferred to the Foreign Technology Division as an intelligence analyst investigating foreign aerodynamic research. Upon separation from the Air Force in 1979 Charles remained with the Foreign Technology Division as a civil servant. He attended the Air Force Institute of Technology between September 1980 and March 1982 under the Long Term Full Time Training program.

UNCLASSIFIED

SECURITY CLASSIFICATION OF THIS PAGE (When Data Entered)

REPORT DOCUMENTATION PAGE

READ INSTRUCTIONS BEFORE COMPLETING FORM

1. REPORT NUMBER	2. GOVT ACCESSION NO	3. RECIPIENT'S CATALOG NUMBER
AFIT/DS/AA/83-2	AD-A128 700	

4. TITLE (and Subtitle)	5. TYPE OF REPORT & PERIOD COVERED
NUMERICAL AERODYNAMIC ANALYSIS OF A FREE FALLING AUTOROTATING PLATE	PhD Dissertation
	6. PERFORMING ORG. REPORT NUMBER
7. AUTHOR(s)	8. CONTRACT OR GRANT NUMBER(s)
Charles R. Gallaway	
9. PERFORMING ORGANIZATION NAME AND ADDRESS AIR FORCE INSTITUTE OF TECHNOLOGY (AFIT-EN) WRIGHT-PATTERSON AFB, OH 45433	10. PROGRAM ELEMENT, PROJECT, TASK AREA & WORK UNIT NUMBERS 2307N603
11. CONTROLLING OFFICE NAME AND ADDRESS FLIGHT DYNAMICS LABORATORY AIR FORCE WRIGHT AERONAUTICAL LABORATORIES WRIGHT-PATTERSON AFB, OH 45433	12. REPORT DATE October 1983 13. NUMBER OF PAGES 142
14. MONITORING AGENCY NAME & ADDRESS(if different from Controlling Office)	15. SECURITY CLASS. (of this report) UNCLASSIFIED 15a. DECLASSIFICATION/DOWNGRADING SCHEDULE

16. DISTRIBUTION STATEMENT (of this Report)

Approved for public release; distribution unlimited.

17. DISTRIBUTION STATEMENT (of the abstract entered in Block 20, if different from Report)

18. SUPPLEMENTARY NOTES

Approved for public release: IAW AFR 190-17

LYNN E. WOLAVER 9 Feb 84
Dean for Research and Professional Development
Air Force Institute of Technology (AIC)
Wright-Patterson AFB OH 45433

Approved for public release; IAW AFR 190-17

J.F. Dalby, Major, USAF
Director, Public Affairs

19. KEY WORDS (Continue on reverse side if necessary and identify by block number)

Aerodynamics	Equations of Motion
Rotating	Autorotation
Navier-Stokes Equations	Flat Plate
Numerical Methods	
Coupled Systems	

20. ABSTRACT (Continue on reverse side if necessary and identify by block number)

A computational method coupling the three degrees of freedom flight mechanics equations and the two dimensional Navier-Stokes equations was developed which could be used to predict the flight path of a free falling, autorotating, two dimensional flat plate. The two dimensional incompressible Navier-Stokes equations were cast in a body fixed coordinate system. The corresponding velocities were cast in an inertial reference system. The equations were represented by

DD FORM 1 JAN 73 1473 EDITION OF 1 NOV 65 IS OBSOLETE

UNCLASSIFIED

SECURITY CLASSIFICATION OF THIS PAGE (When Data Entered)

backward-time-central-space finite differences and solved using a successive-over-relaxation iteration technique. The resulting aerodynamic coefficients were entered into the three degrees of freedom flight mechanics equations. The system of ordinary differential equations was solved using an Adams open formula to predict the movement of the plate. New boundary conditions for the Navier-Stokes equations solver were derived from the movement of the plate. The process was repeated to advance the solution in time.

The computational method was used to calculate the flow field around a flat plate forced to rotate at nondimensional angular velocities of 1.0, 2.0, and 4.0. A calculation was performed for a plate with one degree of freedom (rotation) which simulated a plate mounted on a frictionless bearing in a wind tunnel. The plate was found to undergo pinned autorotation at a mean nondimensional rotational velocity of 1.58. Finally, the flight path of a free falling autorotating plate was predicted using the computational procedure. The validity of the overall approach was demonstrated by comparison with experiment.

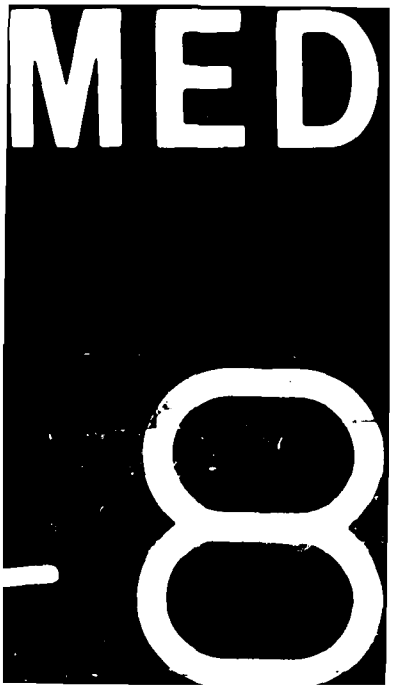
MED
8